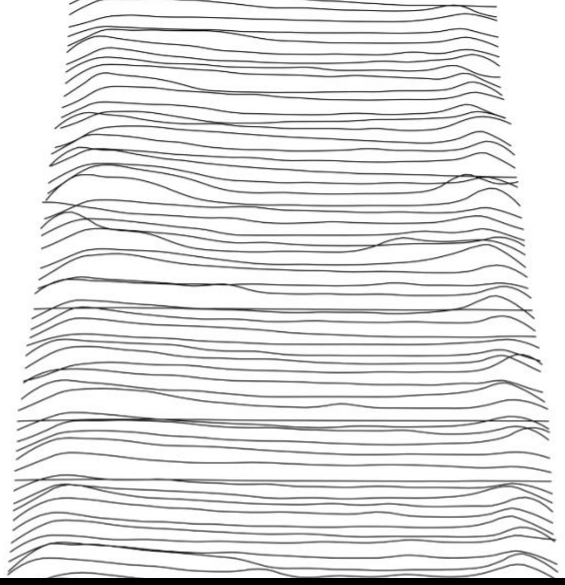

CATCHING A GLIMPSE: THE VISUALIZATION OF *MYCOBACTERIUM TUBERCULOSIS* FROM TB PATIENT BIOAEROSOLS

RYAN DINKELE

OCTOBER 2022

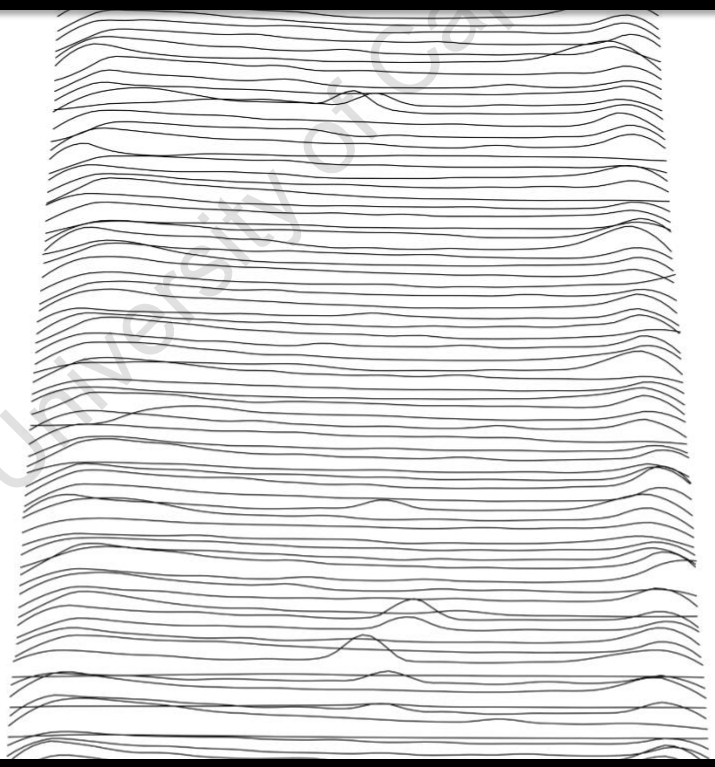

THESIS PRESENTED FOR THE DEGREE OF DOCTOR OF PHILOSOPHY
IN THE DEPARTMENT OF PATHOLOGY AT THE UNIVERSITY OF CAPE TOWN

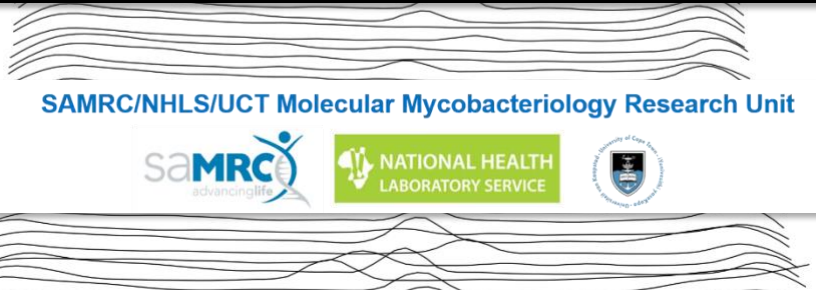

IDM INSTITUTE OF INFECTIOUS DISEASE AND MOLECULAR MEDICINE

SAMRC/NHLS/UCT Molecular Mycobacteriology Research Unit

saMRC advancinglife NATIONAL HEALTH LABORATORY SERVICE

DESMOND TUTU HEALTH FOUNDATION

ABSTRACT

Transmission between hosts is crucial for the success and survival of the obligate human pathogen and aetiological agent of tuberculosis (TB), *Mycobacterium tuberculosis* (*Mtb*). Despite this, little is known about how and when *Mtb* is aerosolized nor the key metabolic and morphological determinants driving successful transmission.

To address these knowledge gaps, my doctoral research sought to develop a microscopic method for the detection of aerosolized *Mtb* following liquid-capture within the respiratory aerosol sampling chamber (RASC). This was achieved through the combination of the mycobacterial cell wall probe, 4-*N*,*N*-dimethylamino-1,8-naphthalimide-trehalose (DMN-tre), with the arraying of bioaerosol samples on bespoke nanowell devices amenable to fluorescence microscopy. With this method, a median of 14 live *Mtb* bacilli (range 0-36) were detected in 90% of confirmed TB patients following 60 minutes of bioaerosol sampling. Three distinct DMN-tre staining patterns were identified among aerosolized *Mtb*, strongly suggestive of metabolic heterogeneity. Moreover, a low proportion of patients produced *Mtb* in small clumps. These observations highlight the advantages of using microscopy over conventional culture- or molecular-based techniques for probing the metabolic and morphological characteristics of aerosolized *Mtb*.

Applying this method in a second study, we sought to understand how and when *Mtb* is aerosolized. To this end, we aimed to compare the aerosolization of *Mtb* and total particulate matter from patients with TB during three respiratory manoeuvres: tidal breathing (TiBr), forced vital capacity (FVC), and cough. Although total particle counts were 4.8-fold greater in cough samples than either TiBr or FVC, all three manoeuvres returned similar rates of positivity for *Mtb*. No correlation was observed between total particle production and *Mtb* count. Instead, for total *Mtb* counts, the variability between individuals was greater than the variability between sampling manoeuvres. Finally, when modelled using 24-hour breath and cough frequencies, our data indicate that TiBr might contribute more than 90% of the daily aerosolized *Mtb* among symptomatic TB patients. Assuming the number of viable *Mtb* organisms detected provides a proxy measure of patient infectiousness, this method suggests that TiBr is a significant contributor to TB transmission.

In developing a novel platform for the detection of aerosolized *Mtb*, this work has suggested the need to re-examine old assumptions about *Mtb* transmission.

DECLARATION OF ORIGINALITY

I, ***Ryan Dinkele***, hereby declare that the work on which this thesis is based is my original work (except where acknowledgements indicate otherwise) and that neither the whole work nor any part of it has been, is being, or is to be submitted for another degree in this or any other university.

I empower the university to reproduce for the purpose of research either the whole or any portion of the contents in any manner whatsoever.

Signature:_____ **Date: 07 October 2022**

Acknowledgements

A PhD is not completed in isolation. It requires input and assistance from many people. My PhD journey was neither brief nor linear, and I owe a debt of gratitude to the many people who supported me along the way, enabling me to (finally!) cross the finish line.

To my supervisor, ***Digby Warner***, thank you for guiding me along this journey. Your constant endeavour to bring out the best in young scientists is inspiring. I have truly appreciated your patience with me along this journey, allowing me to extract every ounce possible from this degree.

To my co-supervisors, thank you for all the time and effort that you have so willingly invested into my PhD. ***Valerie Mizrahi,*** your hard work and dedication to the MMRU have been fundamental for so many young scientists lucky enough to follow in your footsteps. Thank you for the guidance and wisdom that you bring to the group. ***Robin Wood***, your passion for *Mycobacterium tuberculosis* transmission research is *infectious*. I started my PhD knowing almost nothing about this field and have been fortunate enough to spend several years learning it from one of the best. Thank you. ***Sophia Gessner***, I literally could not have done much of this work without you. I appreciate your love for the laboratory and your attention to detail. Thank you for all your blood, sweat, and tears in the BSL3 and for your input into this work!

To all the members of the ***MMRU***, thank you for your assistance and for making this PhD journey such a memorable experience. ***Anastasia***, thank you for your support and academic input over the years. ***Ditshego*** and ***Atica***, thank you for your assistance processing bioaerosol samples in the BSL3. To everyone based at the ***Aerobiology Research Centre***, thank you. Thank you to ***Ronnett*** for holding the team together, and to ***Andrea, Bryan***, ***Zeenat***, ***Venessa***, ***Andiswa***, and ***Juane*** for your hard work and dedication: from working with participants to your efforts in sample collection and preparation.

I would also like to thank our collaborators at **Edge Embossing** for their assistance in fabricating the nanowell devices used throughout this thesis, **Zeteo Tech** for the constant R&D improving the way that we capture bioaerosols, and **Carolyn Bertozzi** and **Mireille Kamariza** for their willingness to collaborate and supply us with DMN-tre as we got this project off the ground.

I would like to express my deepest gratitude to all ***the participants*** who agreed to partake in this study. Without your willingness to assist, even while you were unwell, this research would not be possible.

To my family. Thank you for always believing in me and for the unwavering support, year after year. It is thanks to your love and sacrifice that I am where I am today.

To my wife. Elizabeth, words cannot express the joy you bring to me. I am so grateful to have you by my side. Thank you for your willingness to listen to my endless ramblings, providing invaluable comment and critique, and helping to shape and refine many of my thoughts and ideas.

MANUSCRIPTS DERIVING FROM THIS THESIS

Dinkele R., Gessner S., McKerry A., Leonard B., Leukes J., Seldon R., Warner D.F., Wood R. (2022). **Aerosolization of *Mycobacterium tuberculosis* by Tidal Breathing**. *Am J Respir Crit Care Med.* 15;206(2):206-216. doi: 10.1164/rccm.202110-2378OC.

Barr D.A., Schutz C., Balfour A., Shey M., Kamariza M., Bertozzi C.R., de Wet T.J., Dinkele R., Ward A., Haigh K.A., Kanyik J.P., Mizrahi V., Nicol M.P., Wilkinson R.J., Lalloo D.G., Warner D.F., Meintjes G., Davies G. (2022) **Serial measurement of *M. tuberculosis* in blood from critically-ill patients with HIV-associated tuberculosis**. *EBioMedicine*. 78:103949. doi: 10.1016/j.ebiom.2022.103949.

Dinkele R., Gessner S., McKerry A., Leonard B., Seldon R., Koch A.S., Morrow C., Gqada M., Kamariza M., Bertozzi C.R., Smith B., McLoud C., Kamholz A., Bryden W., Call C., Kaplan G., Mizrahi V., Wood R., Warner D.F. (2021). **Capture and visualization of live *Mycobacterium tuberculosis* bacilli from tuberculosis patient bioaerosols**. *PLOS Pathogens* 17(2): e1009262. doi: 10.1371/journal.ppat.1009262.

Patterson B., Bryden W., Call C., McKerry A., Leonard B., Seldon R., Gqada M., Dinkele R., Gessner S., Warner D.F., Wood R. (2021). **Cough-independent production of viable *Mycobacterium tuberculosis* in bioaerosol**. *Tuberculosis (Edinb)* 126:102038. doi: 10.1016/j.tube.2020.102038.

Patterson B., Dinkele R., Gessner S., Morrow C., Kamariza M., Bertozzi C.R., Kamholz A., Bryden W., Charles C., Warner D.F., Wood R. (2020). **Sensitivity optimization of tuberculosis bioaerosol sampling**. *PLOS ONE* 15(9): e0238193. doi: 10.1371/journal.pone.0238193.

Patterson B., Koch A.S., Gessner S., Dinkele R., Gqada M., Bryden W., Cobelens F., Little F., Warner D.F., Wood R. (2020). **Bioaerosol sampling of patients with suspected pulmonary tuberculosis: a study protocol**. *BMC Infect Dis*. 20, 587. doi: 10.1186/s12879-020-05278-y.

List of abbreviations

AFB	Acid-fast bacilli
Ag85	Antigen 85
AO	Auramine-O
BBM	Bronchiole burst manoeuvre
BCG	Bacille Calmette-Guérin
BSL	Biosafety level
CASS	Cough aerosol sampling system
CFU	Colony forming units
CO_2	Carbon dioxide
COC	Cyclic olefin copolymer
Csi	*Corynebacterium striatum*
ddPCR	Droplet digital PCR
DMN	4-N,N-dimethylamino-1,8-napthalimide
DprE1	Decaprenylphosphoryl-β-d-ribose 2′-epimerase
DR	Drug resistant
ETH	Ethambutol
FITC	Fluorescein isothiocyanate
FVC	Forced vital capacity
GDP	Gross domestic product
HEPA	High-efficiency particulate arrestance
HIV	Human immunodeficiency virus
INH	Isoniazid
IRR	Incident rate ratio
LED	Light-emitting diode
MDR	Multi-drug resistant
Msm	*M. smegmatis*
Mtb	*M. tuberculosis*
MTBC	*Mycobacterium tuberculosis* complex
NS	Not significant
OD_{600}	Optical density at 600nm
OR	Odds ratio
PANTA	Polymyxin B, Amphotericin B, Nalidixic acid, Trimethoprim and Azilocillin
PAS	Para-aminosalicyclic acid
PBS	Phosphate buffered saline
PCR	Polymerase chain reaction

PCTE	Polycarbonate
PS	Particle sizer
PTID	Participant identification
PZA	Pyrazinamide
QTF	Quencher trehalose fluorophore
RASC	Respiratory aerosol sampling chamber
RAV	Rebreathed air volume
RIF	Rifampicin
SEM	Scanning electron microscopy
TB	Tuberculosis
TDM	Trehalose dimycolate
TDR	Totally drug resistant
TiBr	Tidal breathing
TMM	Trehalose monomycolate
Tre	Trehalose
v/v	Volume/volume
w/v	Weight/volume
WHO	World Health Organization
XDR	Extensively drug resistant
ZN	Ziehl-Neelsen

TABLE OF CONTENTS

LIST OF MAIN FIGURES

LIST OF SUPPORTING FIGURES

CHAPTER ONE – *MYCOBACTERIUM TUBERCULOSIS* TRANSMISSION

"…**a disease in which death and life are so strangely blended**, that death takes the glow and hue of life, and life the gaunt and grisly form of death; a disease which medicine never cured, wealth never warded off, or poverty could boast exemption from; which sometimes moves in giant strides, and sometimes at a tardy sluggish pace, but, slow or quick, is ever sure and certain."

The Life and Adventures of Nicholas Nickleby, Charles Dickens[1]

TUBERCULOSIS

BACKGROUND

Tuberculosis (TB) is an infectious disease transmitted via droplet aerosols[2] and has been a significant cause of human morbidity and mortality for millennia[3]. In the pre-antibiotic era, less than one third of TB sufferers survived TB, earning it the moniker, "Captain Among these Men of Death."[4,5]

Mycobacterium tuberculosis (*Mtb*) was discovered as the aetiological agent of TB in the 1880s[6]. This revolutionised our understanding of communicable diseases and led to several scientific discoveries and public health interventions. Among these were the widespread implementation of the first vaccine against TB, Bacille Calmette-Guérin (BCG), and the discovery of streptomycin in 1944[5]. However, drug-resistant strains of *Mtb* began to emerge shortly after the introduction of streptomycin[7,8].

Following the limited success of monotherapy, researchers began investigating the applicability of treating with combinations of antibiotics – a long-standing strategy in TB treatment[5]. "Triple therapy", a combination of para-aminosalicyclic acid (PAS), isoniazid (INH), and streptomycin, was among the first of these combinations[8]. Since then, further advances in combination chemotherapy have significantly increased the chances of surviving TB, with the modern treatment regimen reducing the case fatality rate to below 10%[9-11]. However, controlling TB incidence required additional developments in public health and social equality[11,12], leading to a global divide in the distribution of TB between developed and developing countries and a strong correlation between TB incidence and a country's GDP[11,13,14].

The introduction of antibiotics, therefore, failed to curb the high force of *Mtb* transmission in TB endemic communities[15]. This is exemplified in South Africa, with well over 500 cases of TB per 100,000 population[14]. Consequently, TB remains a leading cause of death owing to an infectious agent globally, claiming 1.4 million lives in 2020[14]. As such, cost-effective and creative approaches targeted at reducing *Mtb* transmission may represent key ancillary strategies to support the current use of antibiotics to eradicate TB[16].

MYCOBACTERIUM TUBERCULOSIS

Mtb is an obligate human pathogen whose life cycle is fully contained within its human host[3]. The only exception is during transmission, where *Mtb*-containing aerosols are exhaled from an infected individual and inhaled deep within the peripheral lung of a naïve host[17]. Here, alveolar macrophages

phagocytose *Mtb*, which survives by preventing the fusion of lysosomes to the phagosome in which they are encapsulated[18]. Surviving bacilli then replicate freely within the phagosome[19], while infected macrophages are transported to regional lymph nodes[20] resulting in the eventual activation of the adaptive immune response[21]. This leads to a unique TB pathology, whereby the recruitment of immune cells to the site of infection leads to the formation of a granuloma, which is aimed at containing and preventing bacterial replication[22-24]. In most cases, the host successfully contains the infection, even if *Mtb* bacilli are not eliminated. As such, developing active TB after infection represents a relatively rare event[25,26]. Despite this, 10 million people fell ill with TB in 2020 suggesting that improvements in the control of *Mtb* infection are desperately required[14,15].

Tuberculosis control

The current paradigm for TB control hasn't changed significantly for several decades, relying heavily on combination chemotherapy of ill individuals with four antibiotics over six months[14]. The standard regimen – which consists of an intensive phase comprising Rifampicin (RIF), INH, Ethambutol (EMB) and Pyrazinamide (PZA) treatment for two months, followed by a four-month continuation phase utilizing only RIF and INH[14] – has only recently been matched in efficacy by a four-month alternative[27]. This six-month regimen performs well in clinical trials, with an efficacy of 95%[28,29], however its effectiveness in real-world settings is more varied, with an average of 86% of individuals successfully completing treatment in 2019[14].

TB control is predicated on the use of antibiotics both for the curative treatment of ill individuals as well as the disruption of *Mtb* transmission[30]. Although antibiotic treatment of TB patients dramatically reduces the case fatality rate and supresses patient infectiousness within two weeks[31] to two months[32], it has been unsuccessful in achieving its ancillary goal of reducing *Mtb* transmission in high-burden settings[14]. Broadly, this limited ability to control the spread of TB can be attributed to three main categories: factors that delay treatment initiation, reduce treatment adherence, and facilitate the development of drug resistance.

Treatment initiation

TB control is heavily predicated on treatment of passively identified individuals with active disease, rendering it vulnerable to factors delaying the initiation of treatment[9,33]. In low-resource settings with high rates of TB, treatment-seeking delays of more than 10 weeks from symptom onset are common[34,35], with some estimates suggesting patients could delay treatment-

seeking for up to a year[36]. This is due to the personal and financial costs of treatment initiation as well as an inability to recognize symptoms as indicative of TB[34,35]. In general, the barriers to treatment initiation are greater for poorer individuals[37] and include large travelling distances to attend clinics[38,39] and social stigma[37,40,41], which have contributed greatly to the global divide in the distribution of the burden of TB[14].

Once at a health facility, patients require a rapid and accurate diagnosis to begin treatment. However, the lack of a definitive diagnostic further exaggerates the time between symptom onset and treatment initiation, with incorrect diagnoses leading to improperly treated patients[9,42,43].

Treatment adherence

Retaining patients for the duration of treatment (four to six months) is difficult; with fewer than 50% completing treatment in some settings[9,44]. The significant loss of patients on treatment represents, in part, a failure of health systems to appropriately manage patients with TB[44]. Similar to treatment initiation, the relative cost burden of continued treatment seeking is exaggerated for the most severely socio-economically disadvantaged[37]. This imposes a great financial and personal burden on poorer individuals who wish to receive treatment. Exacerbating this problem, patients feel better within the first two weeks of a six month treatment regimen with toxic side-effects[9,40]. As such, the perceived need for treatment decreases while the personal burden persists.

Treatment shortening, therefore, represents a major goal in TB drug discovery[45]. Although, in principle, combination therapy is simple, it is complicated by the existence of antagonistic drug-drug interactions[46] and the complex pathology associated with TB[47]. This pathology prevents the uniform distribution of antibiotics throughout the lungs, reducing the effectiveness of the combination as a whole and necessitating extended treatment durations[47-49].

Even in situations where bacteria are uniformly susceptible to an antibiotic, suboptimal drug concentrations at sites of infection are problematic[50]. This is further complicated by the presence of antibiotic persistent or tolerant *Mtb* cells that exhibit temporary, phenotypic resistance to antibiotics and are thought to contribute to the extended duration of treatment[51,52]. These resistant phenotypes are distinguishable from resistant genotypes as they are typically considered non-heritable and arise in a sub-population of bacilli through stochastic variation between cells or as a consequence of an environmental stimulus (*e.g.*, low pH, hypoxia, *etc.*)[52,53]. This is exemplified in the differential susceptibility to antibiotics arising from asymmetric binary

fission[54], or epigenic alterations in DNA organization[55]. In some instances, the genetic and molecular mechanisms yielding increased proportions of tolerant phenotypes have been determined, for example altered propionate metabolism as a result of mutations in the *prpR* gene[56]. The occurrence of phenotypic resistance, the formation of antibiotic concentration gradients, and limited antibiotic adherence together contribute to the development of drug resistance, significantly undermining efforts to control TB[50,57-59].

Drug resistance

Complete cure of patients is key to the success of the current TB control strategy and the development and transmission of antibiotic resistant strains of *Mtb* is fuelling an even more challenging epidemic[9,60,61]. The severity of drug-resistant (DR)-TB cannot be understated, with some mortality rate estimates as high as 40%[9], while the WHO suggest that only 59% of individuals successfully complete treatment for DR-TB, compared to 86% for drug-sensitive TB[14]. Moreover, RIF-resistant strains alone account for one quarter of the deaths among all antimicrobial resistant infections globally[62].

DR-TB is classified according to five categories by the WHO[14]: INH-resistant, RIF-resistant, multidrug-resistant (MDR), pre-extensively drug-resistant (pre-XDR), and extensively drug-resistant (XDR). RIF and INH are key frontline drugs, resistance to which complicates treatment even in mono-resistant strains[14]. A strain is defined as MDR if it is resistant to both INH and RIF, and as pre-XDR if it carries RIF resistance plus resistance to any fluoroquinolone (a class of second-line antibiotics). XDR strains of *Mtb* are resistant to RIF, any fluoroquinolone, and either bedaquiline or linezolid[14]. In addition to these categories, many researchers have recognised strains resistant to all first- and second-line antibiotics, termed totally drug-resistant TB (TDR-TB)[63,64].

Unlike many other pathogenic bacterial species, *Mtb* lacks classical resistance-conferring adaptations, such as horizontal gene transfer[65,66] and episomally encoded resistance[67]. As such, the primary method of resistance acquisition in *Mtb* is through the accumulation of resistance-conferring mutations[67,68]. Despite the high degree of sequence similarity in the *Mtb* complex (*MTB*C) and their relatively low mutations rates[3,66], strains that are resistant to multiple antibiotics continue to arise. Problematically, the current treatment regimens for resistant strains are longer, less effective, and impose a greater cost on both the health system and patient[9,14,69].

Despite the undeniable impact that the introduction of antibiotics has had on controlling TB[11], they have failed to perform their ancillary task of reducing TB transmission in high burden settings[11,30]. Improved antibiotics and a

shorter treatment regimen may aid in reducing TB incidence, however factors that reduce or delay access to antibiotics or which promote non-adherence, and the looming threat of antibiotic resistance, threaten to perpetually undermine this approach by allowing for the continued transmission of *Mtb*[9,61]. This has focussed significant attention on TB transmission research, as this may provide valuable insights and potentially novel interventions targeted at strengthening the current TB control paradigm by reducing the ongoing transmission of *Mtb*[16].

Tuberculosis transmission

Koch's demonstration of the infection of guinea pigs by *Mtb* isolated from the sputum of TB patients revolutionised our understanding of communicable diseases and unequivocally demonstrated that TB was infectious[6]. Moreover, it established *Mtb* as the necessary cause of TB. Koch proposed that *Mtb* was released from coughing individuals within droplets too large to support their bulk within the air, which would rapidly fall to the ground. He suggested that transmission occurred once these droplets were desiccated or disturbed sufficiently to release *Mtb* into the air, freeing them for inhalation by healthy individuals[6]. This led to the shunning of spitting in public and motivated for the shift from chewing to smoking tobacco[70]. At this point, the nature of *Mtb* transmission was purely speculative, however Koch's discovery prompted more than 140 years of research into how *Mtb* bacilli are transmitted from infected individuals to susceptible hosts[70]. Donald *et al*. recently provided a thorough review of the modern history of TB transmission research that will be used as a reference throughout this section, as many of the original manuscripts are difficult to access and/or not written in English[70].

A brief history of TB transmission research

Following on from Koch's work in the late 1800s, two facts were readily apparent: 1) TB patients produced sputum containing *Mtb* and 2) they coughed. As such, much of the early research focused on smear-positive, coughing TB patients[70].

Initially, the experimental setup for investigating *Mtb* aerosolization was very simple: a glass slide was placed several centimetres in front of a coughing TB patient for a set amount of time, after which the slide was viewed under a microscope[70-72]. Remarkably, within one to two hours *Mtb* bacilli were detectable in 20%–40% of pulmonary TB patients[70]. Moreover, in some cases, the slide contents could be washed off and used to infect guinea pigs[72]. This was among the first evidence demonstrating that viable *Mtb* was released by TB patients during coughing.

The impaction of *Mtb* onto glass slides, although an important observation, was insufficient to suggest that these droplets could remain suspended in the air for any length of time. This question required a more complex experimental setup. For this purpose, a TB patient would sit in a closed booth surrounded by sealed, liquid-filled glass bowls[71]. Periodically, researchers would open these bowls via ropes entering the system, hypothesising that *Mtb* would slowly settle and become suspended within the liquid[70]. After the experiment, the content of these bowls was concentrated and injected into guinea pigs. These experiments revealed that *Mtb* could remain suspended in the air for up to 30 minutes after the patient had left the booth[70,71,73].

The detection of *Mtb* released from coughing TB patients was a crucial first step in elucidating the mechanism of *Mtb* transmission. Next was to demonstrate the direct infection of an uninfected host. For this purpose, Chaussè developed a sampling apparatus that enabled TB patients to cough directly onto guinea pigs[70,74]. In two experiments which included slight modifications to the cough sampling system, he demonstrated that TB patients could infect guinea pigs by coughing and that the airflow within the system was an important determinant of infection risk[70].

Thus, within 30 years of Koch's discovery of *Mtb* as aetiological agent of TB, several important observations were made regarding the nature of *Mtb* transmission: 1) *Mtb* was released by coughing TB patients, 2) these bacilli could remain suspended in the air for several minutes, and 3) non-infected, susceptible animals could inhale *Mtb* and develop TB[70]. These continue to inform our understanding of TB transmission today[75,76]. However, upon closer inspection of the infectious droplets and the patients who produced them, a more nuanced understanding began to develop and significant interpatient variation was observed in the production of infectious droplets[70]. Healthier patients with less viscous sputum coughed more forcefully and produced smaller droplets; these patients seemed to be more infectious[70,72,74,77]. Despite this broad understanding of *Mtb* transmission and the observation that infectious droplets could remain suspended in the air for several minutes[70,72], the exact manner in which these infectious droplets travelled through the air would not be described for several years.

Aerosol transmission

Establishing how respiratory pathogens travel from infected individual to naïve host is challenging and often contentious[78,79]. However, the discrimination between fomite (droplet) and aerosol transmission is important for the implementation of appropriate public health interventions[78]. Fomites are large droplets, typically >100 µm, that remain

airborne for under five seconds and travel <1 m [78,80]. Interventions targeted at social distancing and hand sanitization are typically considered effective at reducing fomite transmission, as individuals are infected through droplet spray or touching contaminated surfaces[79]. However, these interventions will not prevent the transmission of respiratory aerosols, which can infect individuals within and beyond 1 m and remain suspended in the air for several minutes[79].

Wells and Riley definitively demonstrated the aerosol route of transmission of *Mtb* in 1959[2]. Their pioneering research utilized the remote infection of guinea pigs by air vented from the wards of TB patients. These guinea pigs were in bespoke housing units placed on the roof of the facility, several meters away from the TB patients. Through these experiments, Wells and Riley proposed that *Mtb* bacilli are transmitted within droplet nuclei that are formed as particle-bearing droplets leave the high humidity of respiratory system and rapidly evaporate[2,81,82]. Similar to much of the early work investigating the transmission of *Mtb*, significant interpatient heterogeneity in the propensity to produce infectious droplet nuclei was observed. Most infections arose from a minority (3%) of patients[2]. Interestingly, an individual with TB laryngitis was shown to be significantly more infectious than other TB patients, infecting a similar number of guinea pigs to a typical measles patient. This unexpected observation indicated that the site of *Mtb* infection significantly contributed to the aerosolization of *Mtb*[81]. This work supported a model suggesting that infectiousness is heterogenous and that small, rather than large, particles are responsible for remote transmission.

This work led to the definition of the infectious quantum[2]. A single quantum is the minimum infectious dose required to infect a new host and can be determined without knowing exactly how many infectious particles (discussed below) were released or inhaled[83]. The transmission of an infectious agent (including pathogen aerosolization, aerosol transmission, inhalation, and infection), is a probabilistic process, which Wells proposed followed a Poisson distribution. Therefore, the average probability of infection after exposure to one infectious quantum is 63.2%[82-84]. This solution circumvented the challenges in detecting very low numbers of *Mtb* in the air when understanding the probability of transmission.

The dependence of *Mtb* on aerosol transmission and the description of the infectious quantum ultimately led to the formulation of the Wells-Riley equation. This equation describes the probability of being infected by an airborne respiratory pathogen in a well-mixed airspace under steady-state conditions[85].

$$P = 1 - e^{\frac{-Iqpt}{Q}}$$

In this model, the probability of infection (P) is related to the number of infectious individuals present (I), the rate (L/s) of pulmonary ventilation (p), the time interval (t), the ventilation rate (L/s) of the room (Q), and the rate of infectious quanta production (q). As such, this equation linked the environment and the infectiousness of TB patients to the probability of a susceptible individual being infected.

Expanding on this work, Rudnick & Milton modified the equation to increase its applicability in non-steady-state conditions[84].

$$P = 1 - e^{\frac{-fIqt}{n}}$$

Key to this model was the replacement of breathing rate (p) and ventilation rate (Q) with the concept of the 'rebreathed fraction' (f). That is, the probability of infection is related to the amount of air that a certain number of individuals (n) share, while coexisting in a space. Fundamental to this model is the assumption that any increase in carbon dioxide (CO_2) within a closed space is derived from the respiratory activity of the people occupying the space[84]. The experimental and mathematical models developed to this point shaped our understanding of the probability of being infected by an airborne pathogen. Specifically, these models linked this probability to three key facets: social mixing and the environment (*i.e.*, the number of people in a space and the extent that the air is rebreathed), the number of infectious individuals within a space, and the 'infectiousness' of those patients in the form of the infectious quanta[84,85].

Limitations of the guinea pig infection model

The remote infection of guinea pigs unequivocally demonstrated the aerosol transmission of *Mtb*. Although this model was first developed in the 1950s, several researchers still promote its use for understanding patient infectiousness[86-90]. Problematically, the assessment of patient infectiousness through the remote infection of guinea pigs suffers from a lack of sensitivity and generalisability, owing to the inherent presence of bias confounding this model.

Selection bias

The complex apparatus required for the guinea pig infection model and the extended duration required for sampling (owing to the limited sensitivity of the system) restricts its use to a hospital setting, limiting the sample to the most severely ill individuals who are on TB treatment[86-90]. As such, patients

with less severe or subclinical TB are excluded from the sample, however, these categories represent important contributors to *Mtb* transmission[33,91,92]. Moreover, the use of TB treatment for differing durations confounds the estimation of patient infectiousness[81], and many of the guinea pig infections in the early experiments were attributable to drug-resistant strains of *Mtb*[93].

Poor sampling efficiency

The high ventilation rate of hospital wards designed to protect healthcare workers, and the poor respiratory sampling efficiency of guinea pigs, further confound the assessment of patient infectiousness, as many potentially infectious bacilli remain unsampled[94]. This biases the model to the detection of the most infectious patients[94]. Moreover, this model hinges on the assumption that guinea pigs are equally sensitive to *Mtb* infection compared to humans, which has not been directly assessed.

The use of the infectious quantum as a metric for patient infectiousness has guided our understanding of *Mtb* transmission for years[83]. However, owing to the lack of sensitivity and generalisability of the infectious quantum in understanding patient infectiousness, some researchers have proposed the use of an alternative metric: the infectious particle[94].

Infectious particles

Humans constantly produce respiratory aerosols, even during normal breathing[95,96]. These aerosols, commonly referred to as bioaerosols, originate from the length of the respiratory tract as small particle-bearing droplets[97,98]. Upon exhalation, droplets leave the high-humidity environment of the respiratory tract, allowing for the rapid evaporation of their liquid component and the formation of droplet nuclei[2]. In the context of infectious diseases, a small proportion of these bioaerosols are known as infectious particles, as they carry the pathogenic agent[94].

The enumeration of total infectious particles aerosolized by sick individuals provides a higher-resolution understanding of disease transmission relative to the pooling-method of the infectious quanta; however, direct study of aerosolized *Mtb* is complicated[99]. Issues such as bioaerosol collection, the small numbers of bacilli aerosolized, and the presence of environmental and patient-derived contaminating microorganisms and particulate matter, impose profound technical and analytical challenges[99,100]. When interpreting *Mtb* transmission research, it is important to determine which measure was used[83].

Issarow and colleagues adapted the previous models of *Mtb* transmission to include the number of infectious particles (β) released by a TB patient, rather

than the infectious quanta[94]. This model is applicable in both steady-state and non-steady-state conditions[84], while the assessment of infectious particles is not limited to an experimental setup or to hospitalised participants[101]. Broadly, this model assigns the annual risk of *Mtb* infection in a community into three categories: the number of infectious individuals in a community (ΔM), the degree of social mixing (ftp), and the infectiousness of TB cases (θ[β − μ]).

$$P = 1 - e^{-\Delta M \times \theta(\beta - \mu) \times ftp}$$

The number of infectious individuals in a community (*i.e.*, the prevalence of TB) is calculated by multiplying the incidence of TB (M) by the average duration of infectiousness (Δ)[101]. Regions with a high TB prevalence tend to have higher degrees of social mixing, further contributing to the rate of aerosol transmission[84]. Specifically, factors that increase the daily rebreathed air volume (RAV) are critical determinants of transmission risk[101]. Fundamental to understanding RAV (RAV = ftp) is the concept of the rebreathed fraction (f), which is inversely related to ventilation rate (Q). For example, in a poorly ventilated space with multiple individuals, a high proportion of bioaerosols are rebreathed. For infectious individuals, a certain proportion of their bioaerosols contain respiratory pathogens. Therefore, a higher rebreathed fraction (f), longer duration (t), or higher breathing rate (p) all determine the probability of rebreathing infectious particles. In contexts with high daily RAVs, such as prisons, the probability of infection is very high[101]. In the general public, daily RAVs are higher for individuals sharing public transport, workspaces, and schools[102].

TB patient infectiousness is an important, yet difficult to quantify, component when modelling transmission risk. Early work indicated significant interpatient heterogeneity in infectiousness related to disease state and sputum viscosity[70], with more recent observations concluding that the site of infection is also an important contributor[81]. Issarow and colleagues sought to increase the resolution with which we understand infectious quanta by breaking this term down into three components (Figure 1.1): the total number of infectious particles produced (β), the mortality rate of infectious particles (μ), and the deposition fraction (θ) of infectious particles within the peripheral lung[94,101].

The mortality of particles is the extent to which infectious agents are rendered non-infectious, either by removal (air filtration/ventilation) or through the death of the pathogen, whereas the deposition fraction is the proportion of infectious bioaerosols likely to deposit in the peripheral lung[101,103,104]. The total number of infectious particles produced is challenging

to measure and is likely determined by the host-pathogen interaction at a given time. Various methods have been applied in the estimation of the number of infectious particles released by TB patients.

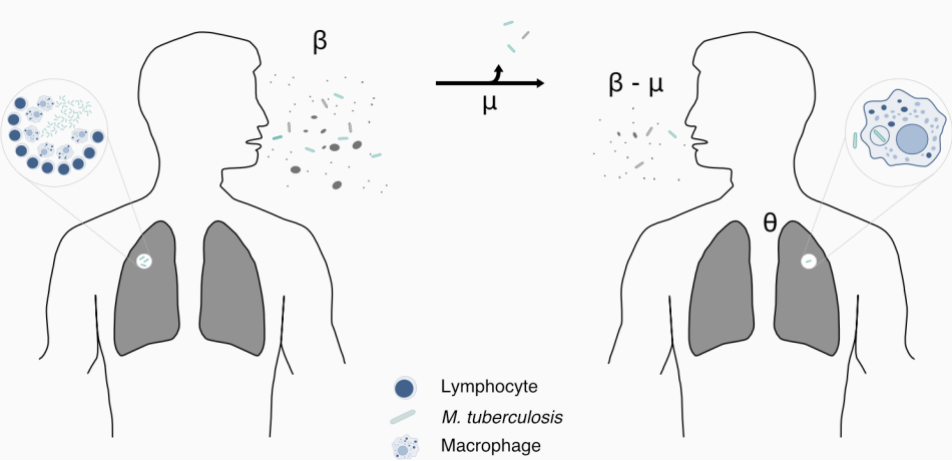

Figure 1.1: Mtb transmission from an infected individual to a naïve host. *Mtb infects the peripheral lung and alveolar spaces when phagocytosed by alveolar macrophages. This interaction leads to the formation of a granuloma, broadly characterised by an outer layer of lymphocytes surrounding an inner layer of macrophages and Mtb[105]. Collapse of granulomas can occur, and enables Mtb to be shed into the airways and aerosolized[75]. A portion of these aerosolized Mtb are inhaled by a susceptible host and deposited into the peripheral lung, initiating infection[101].*

Bioaerosol sampling techniques

Understanding *Mtb* transmission in a community setting is often done by molecular epidemiology and/or contact tracing[106-110]; however, linking incident cases to source patients is challenging[111]. This highlights the importance of knowing when, by whom, and how many *Mtb* bacilli are aerosolized in a community. Investigating the number of infectious particles aerosolized by TB patients therefore requires sensitive and specific methods capable of detecting very few bacilli in large volumes of expired air.

Molecular detection and face-mask sampling

One of the first methods to detect infectious particles directly relied on the filtration of air from hospital wards. This method showed a markedly improved sensitivity over guinea pig infection models, with molecular detection of *Mtb* DNA in six of the seven (86%), and 12 of the 16 (75%) TB patients across two separate studies[112,113]. Although this method exhibited an improved sensitivity over the guinea pig infection model, it suffered several

of the same limitations: for example, these studies were restricted to hospitalised patients, while patient-derived bioaerosols were sampled with limited efficiency.

Face-mask sampling of bioaerosols was recently introduced in an attempt to increase the efficiency of bioaerosol capture[114]. Notably, this method is scalable and can be implemented to better understand the community-dynamics of *Mtb* transmission. In the study by Williams and colleagues, the detection of *Mtb* in bioaerosols was based on two assays: phage infection and GeneXpert detected *Mtb* in the face masks of 11 of the 17 (65%) and 13 of the 20 (65%) TB positive participants, respectively. Although phage infection revealed viability information, this method was not pursued further in future research; rather, detection of DNA was selected as the primary method of *Mtb* identification (discussed below).

Molecular techniques have a high specificity for the target organism, a key feature when attempting to detect pathogens in complex, biological samples that may contain several contaminating microorganisms. PCR-based techniques provide accurate counts down to extremely low DNA concentrations[115], however, inefficient methods for cell lysis and DNA extraction in *Mtb* significantly impede the sensitivity of PCR-based techniques[116].

A key limitation inherent in the use of DNA as a proxy measure of infectiousness, is the assumption that each bacillus detected can initiate an infection in a susceptible host. This is analogous to the assumption that one infected guinea pig is equivalent to an infected human. Moreover, using PCR-based techniques for the detection of specific sequences of DNA does not provide evidence of bacillary viability, as DNA is stable and may represent dead bacilli[117]. Protocols that target RNA may provide information regarding cellular viability[118], however, they too suffer from the limited nucleic acid extraction efficiency of *Mtb*. Regardless, these bioaerosol sampling techniques highlighted the possibility that more patients may be infectious than previously suspected.

The cough aerosol sampling system

The cough aerosol sampling system (CASS) was designed to measure *Mtb* in cough-generated aerosols through the enumeration of colony forming units (CFUs) on solid media[119]. The CASS provides additional information over molecular-based techniques as bacillary viability is a prerequisite for colony formation. With this system, *Mtb* CFUs were detected in 25% (4 of 16), 27.7% (28 of 101) and 43% (43 of 95) of TB patients after 5–10 minutes of coughing[119-121], with an estimated rate of *Mtb* production ranging from 18–

3798 CFU/hour. Although the sensitivity of this technique was lower than that of techniques implementing PCR-based detection of *Mtb* DNA, infectious particles were detected in a higher proportion of TB patients and at a considerably higher rate than reported by the remote guinea pig model, which estimated an average of 30 infectious quanta per day[2]. This discrepancy has two possible interpretations: a single infectious quantum consists of several infectious particles, or it reinforces the limited sensitivity of the remote guinea pig model.

Although the CASS was conceptually similar to the Chaussé cough box[74], the substitution of guinea pigs for Andersen viable impactors[119] – which separate airborne particles according to aerodynamic radius – enabled the measurement of particle size prior to colony formation[122]. This is critical given the likelihood that size determines aerosol longevity and ability to access lung alveoli[103,104], key elements of infectiousness[123]. Most of the *Mtb*-containing particles were in the respirable range (1–5 µm). However, the slow rate of sampling (28.3 L/minute) appears inadequate to capture bioaerosols from coughs which are associated with rapid release (>240 L/min) and expansion[80,124]. Therefore, inefficient bioaerosol sampling likely reduced the sensitivity of this system.

The respiratory aerosol sampling chamber

The respiratory aerosol sampling chamber (RASC) was developed as a small (1.4 m^3) personal clean room for the efficient capture of bioaerosols[99]. Additionally, the RASC was fitted with several additional monitors and sensors, such as a particle sizer and CO_2 monitor, which enabled detailed quantification of respiratory outputs[100]. Although these adaptations increase the resolution with which bioaerosols can be analyzed, they increase the complexity of the system as a whole and necessitate specialised personnel to operate the RASC. However, this system is installed in a community with a high burden of TB[125], enabling the potential investigation of the transmission dynamics of *Mtb*.

The RASC was designed to collect aged bioaerosols produced by participants through tidal breathing and spontaneous coughing over approximately 30–60 minutes[99]. After the bioaerosol production phase, samples were collected utilizing physical impactors, liquid impingers, and filters at flow rates ranging from 12–300 L/min. *Mtb* detection was achieved utilising either culture or droplet digital (dd)PCR. Overall, 27 of the 35 (77%) participants had detectable levels of *Mtb* in their bioaerosol sample[100]. When comparing culture to ddPCR, these detection methods identified *Mtb* in 15 of the 35 (43%) and 25 of the 27 (93%) samples tested, respectively.

Culture is the gold standard for bacterial identification[126] and is commonly used in bioaerosol studies for the detection of *Mtb*[121,127]. Culture on solid media is capable of identifying as few as 10–100 CFU[128], while also providing a clear indication of viability. Problematically, the link between culturability and viability is confounded by the existence of differentially culturable states of *Mtb*, such as 'differentially detectable'[129] and viable but non culturable (VBNC)[130] bacilli. Differentially detectable *Mtb* can only be cultured in liquid media supplemented with resuscitation promoting factors (Rpfs) and are thought to arise as a result of the sudden transition to laboratory media coupled with sampling stresses[131,132]. As such, microbiological culture often underestimates the true size of the viable bacillary population, while also precluding any analysis of the physiological state of transmitted bacilli[133], as colony formation requires several rounds of cell division in artificial culture medium.

The slow formation of CFU on solid media (four to eight weeks)[134] creates an extremely slow turnaround time for culture-based assays and renders them susceptible to contamination by faster-growing organisms[100]. Decontamination further undermines assessments of bacillary load and physiological state: where excessive, it depletes the number and viability of *Mtb* bacilli in the sample[135], where inadequate, it risks overgrowth by contaminants, obscuring the signal. Molecular methods for the detection of *Mtb* offer an increased sensitivity of detection when compared to culture-based techniques[100], however similarly to culture, nucleic acid extraction obviates the potential to investigate the physiological and metabolic state(s) of aerosolized bacilli. For these reasons, a novel approach was required for the capture and detection of aerosolized *Mtb* that enabled the preservation of the bacterial physiological state during transmission. This motivated for considerable effort in updating the RASC for a shift from solid to liquid capture of bioaerosols[99,100]. Unlike air filtration, which resulted in bacterial desiccation, or impaction onto solid media, where detection proceeded weeks of culture, liquid capture was thought to collect bioaerosols in a manner compatible with physiological preservation and direct detection.

The visualization of *Mtb*-like rods within foil-impacted bioaerosols utilizing scanning electron microscopy (SEM) catalyzed efforts for the specific, microscopic detection of *Mtb* in paucibacillary samples[99,100]. However, no protocol existed for the detection of viable *Mtb* in liquid-captured TB-patient bioaerosols. Therefore, this thesis sought to develop a method for culture-independent, microscopic visualization of live *Mtb* bacilli in liquid-captured bioaerosols. This was done by utilising 4-N,N-dimethylamino-1,8-

napthalimide-trehalose (DMN-tre) for the specific detection of *Mtb* on nanowell arrayed devices using fluorescence microscopy.

Aims and objectives

This thesis sought to investigate key aspects of *Mtb* transmission, including the metabolic and morphological characteristics associated with bacterial aerosolization and the respiratory manoeuvres that produce them. This was done according to two aims:

1) This thesis aimed to develop a novel, microscopy-based methodology for the detection of *Mtb* captured in liquid from TB-patient derived bioaerosols, according to the following objectives:

    a. Identify a probe suitable for the detection of *Mtb* in paucibacillary, biological samples.

    b. Compare sample concentration strategies to facilitate the detection of *Mtb* in paucibacillary samples.

    c. Design an identikit to aid in the identification and characterization of *Mtb* in bioaerosol samples.

    d. Develop a sample processing pipeline, including sample capture, concentration, and imaging for implementation in a clinical research setting.

    e. Utilizing (a-d), apply the pipeline to patient bioaerosol samples for the detection and characterization of aerosolized *Mtb*.

    f. Determine the applicability of the pipeline for the long-term, serial imaging of *Mtb* within bioaerosol samples.

2) This thesis aimed to investigate the propensity for the aerosolization of *Mtb* and particulate matter from three respiratory manoeuvres, namely, forced vital capacity, tidal breathing, and induced cough, according to the following objectives:

    a. Design a sampling algorithm for each of the three experimental respiratory manoeuvres.

    b. Develop an analytical pipeline for the comparison of the three experimental manoeuvres based on a combination of particle count and CO_2 data.

    c. Compare the number of *Mtb* bacilli aerosolized by each of the three respiratory manoeuvres.

    d. Estimate the daily contribution of the respiratory manoeuvres to the aerosolization of *Mtb*.

1

Chapter two – The microscopic detection and characterization of live *Mycobacterium tuberculosis* captured from TB patient bioaerosols

This chapter contains excerpts from the following publication:

Dinkele R., Gessner S., McKerry A., Leonard B., Seldon R., Koch A.S., Morrow C., Gqada M., Kamariza M., Bertozzi C.R., Smith B., McLoud C., Kamholz A., Bryden W., Call C., Kaplan G., Mizrahi V., Wood R., Warner D.F. (2021). **Capture and visualization of live *Mycobacterium tuberculosis* bacilli from tuberculosis patient bioaerosols**. PLOS Pathogens 17(2): e1009262.

Introduction

Contrast in microscopy

Microscopy has been used for the detection and characterization of bacteria since Antonie van Leeuwenhoek first described 'living animalcules' in 1676 and was fundamental in the establishment of microbiology as a discipline[136]. The ability to magnify minute organisms enabled an unprecedented view of the world, inspiring the development of microscopes with ever-increasing resolution. The importance of resolution in microscopy cannot be understated, with the development of techniques such as electron microscopy[137] and super-resolution fluorescence microscopy[138] both leading to Nobel Prizes for their inventors.

Contrast is similarly of undeniable importance in microscopy, with the developer of the phase contrast microscope earning a Nobel Prize in 1953[139]. Enhanced contrast aids in the ability to detect and resolve minute structures[140,141]. Phase contrast microscopy converts phase shifts in light into brightness information in the final image, aiding in the ability to see fine details[139]. As an alternative to the manipulation of light, contrast can be enhanced chemically by the addition of stains and dyes, further facilitating the detection of specific cell types or structures.

The Gram stain has been a cornerstone of microbiology since its development in 1884, and is based on the differential ability of bacteria to retain the purple crystal violet dye after alcohol decolouration[142,143]. Gram staining broadly categorises bacteria as either gram-positive (purple) or gram-negative (pink) based on structural differences in their cell walls, primarily peptidoglycan content. Both gram-positive and gram-negative bacteria initially appear purple following exposure to the crystal violet dye; however, after dye fixation and alcohol decolourization, gram-negative bacteria are decolourized and stained pink during the safranin counter stain[142,143]. Gram-positive bacteria are typically characterised by a thick layer of peptidoglycan that is resistant to alcohol decolourization. In contrast, gram-negative bacteria have a significantly thinner cell wall encased in an external membrane. During the staining procedure, this membrane is lost and the thin peptidoglycan layer is rendered leaky, resulting in a loss of the crystal violet dye[142].

Microscopy as a TB diagnostic technique

Mtb is peculiar in that, like gram-negative bacteria, it has an outer membrane[144]; however, like gram-positive bacteria, it is not susceptible to the safranin counter stain, and therefore appears purple after gram staining. As such, *Mtb* is classified as gram positive[142,145]. This discrepancy is due to the

unique architecture of the outer membrane of *Mtb* (or mycomembrane), which is waxy in nature, consisting predominantly of mycolic acids, covalently bound to the peptidoglycan cell wall by a layer of arabinogalactan[144].

The unique *Mtb* cell wall architecture was exploited in the development of the Ziehl-Neelsen (ZN) staining technique for acid-fast bacteria (AFB)[146,147]. Carbol fuchsin, the primary dye in ZN staining, provides AFB with the characteristic pink-red appearance[148] while also partially solubilising the lipid content of the mycobacterial cell wall. This lipid solubilization, combined with a heat treatment, drives carbol fuchsin into the mycobacterial cytoplasm[147]. Once excess carbol fuchsin is removed and the heat treatment is ended, the dye becomes trapped within the cytoplasm of AFB. Non-AFB are susceptible to the acid alcohol decolourization step, and therefore appear purple-blue once stained with methylene blue[146]. Unlike the Gram-stain, which broadly categorises cells based on commonly shared cell wall properties, ZN staining targets a cell wall architecture unique to the genera of nocardia and mycobacteria[146,147]. This is important clinically as it enables the use of ZN staining in TB diagnostics and research[70,128,146,149,150], with sputum-smear microscopy remaining a commonly used tool for the diagnosis of TB[14] and capable of same-day results in the right settings[14,146,147,151].

ZN staining was eventually modified to allow for the replacement of carbol fuchsin with the fluorescent stain, Auramine-O (AO). AO exhibited improved sensitivity in both sputum and tissue samples[148,152,153] and was shown to be more cost effective, even in low resource settings[148]. Unlike ZN staining, where the carbol fuchsin penetrates into the cytoplasm of the AFB, AO directly binds to the mycolic acid within the cell wall[154]. Therefore, ZN positivity is based on the structural integrity of the mycomembrane, whereas positivity for AO is dependent on the presence of mycolic acids.

Requirements for microscopy in *Mtb* aerobiology research

Microscopy has provided several significant insights into the morphological and metabolic states of *Mtb* bacilli in clinically relevant settings[149,150,155,156]. However, the physiological and morphological requirements enabling the successful transmission of *Mtb* are unknown, as conventional culture, PCR, and infection-based models lack the resolution to address these complex questions. As microscopy has yielded valuable insights into the morphology and physiology of *Mtb* within sputum samples, with a historical precedent for applications in *Mtb* transmission research[70], we reasoned that a microscopy-based method for the detection and characterization of *Mtb* in bioaerosol samples was not only possible, but necessary.

The detection of *Mtb* by traditional acid-fast staining relies on the passive ability of the mycomembrane to resist acid alcohol decolourization; this necessitates several wash steps and renders it unable to distinguish live from dead *Mtb*[147,157]. Moreover, only a small volume of the total sample can be smeared onto the slide, reducing the chances of detecting *Mtb* in paucibacillary samples[146,147]. Together, these factors reduce the sensitivity of this method relative to culture and restrict its limit of detection to around 10,000 CFU/mL[128,152,158], well above the estimated hourly aerosolization rate of *Mtb* (18–3798 CFU/hour)[121].

More recently, several fluorescent probes have been designed to exploit the unique architecture and chemical composition of the mycomembrane, requiring enzymatic activity for their incorporation. Although limited information exists regarding the metabolic state of aerosolized *Mtb* capable of initiating infection, it can reasonably be assumed that the transmitted bacilli must be viable. Therefore, probes that are actively incorporated into the mycomembrane are advantageous over passively staining dyes in that enzymatic activity is suggestive of viability[151]. Moreover, a 'decolourization' step is not required as these probes are only incorporated into bacteria that poses the specific enzymatic activity required for probe activation, reducing the number of processing steps required[151].

Trehalose-based probes

One of the first probe designs, FITC-trehalose (-tre), targeted the metabolic pathway for trehalose incorporation into the mycobacterial cell envelope as either trehalose mono- (TMM) or dimycolates (TDM)[144,159]. This incorporation is catalyzed by the antigen 85 complex (Ag85), which shares homologs among the actinomycetales order[151]. Although FITC-tre showed promise as a molecular tool for investigating mycomembrane metabolism *in vivo*, FITC lacks a mechanism for fluorescence activation, necessitating several wash steps to minimize background (non-specific) fluorescence signal, thereby limiting its applicability in complex and potentially paucibacillary clinical samples.

In a subsequent design, FITC was replaced by the solvatochromic probe, DMN[151,160]. Solvatochromic fluorophores undergo a shift either in the spectrum or intensity of their fluorescence under specific conditions[151]. DMN, for example, undergoes a 1,000-fold increase in fluorescence intensity in a hydrophobic environment[151,160], thereby enhancing the specific signal of DMN-tre post incorporation into the mycomembrane and limiting background noise attributable to unmetabolized probe, circumventing the need for multiple washes[151]. The ability of DMN-tre to facilitate the detection

of *Mtb* in sputum samples, the enhanced signal-to-noise ratio owing to its solvatochromic nature, and its specificity for viable bacilli, positioned DMN-tre as prime candidate for viable *Mtb* detection in bioaerosol samples[151].

The quencher-trehalose-fluorophore (QTF) probe is similar to DMN-tre in that it also requires Ag85-mediated incorporation into the mycomembrane[161]. Unlike DMN-tre, however, QTF mimics a TMM molecule and is cleaved by Ag85, releasing the quencher and initiating fluorescence. This reduces non-specific fluorescence of unmetabolized probe and limits the requirement for wash steps. However, QTF was not initially intended for the detection of *Mtb* in sputum and its utility in this context requires further investigation. The availability of multiple probes exploiting Ag85 enzymatic activity nevertheless identifies this complex and the mycomembrane more broadly as flexible targets for the design of fluorescent probes.

Arabinogalactan-targeting probes

CDG-DNB3 was designed to target the arabinogalactan layer of the cell envelope[144,162]. Similar to QTF, CDG-DNB3 is based on a fluorophore and matching quencher design. For CDG-DNB3, the quencher is released from the probe after catalytic cleavage by the class A β-lactamase, BlaC. The liberation of the quencher enables probe fluorescence and allows for the specific interaction between CDG-DNB3 and decaprenylphosphoryl-β-D-ribose 2′-epimerase (DprE1), an enzyme that is required for the synthesis of cell wall arabinans and is conserved among actinobacteria[162]. As with DMN-tre, CDG-DNB3 was intended for use in sputum samples and showed promise for the detection of *Mtb* in complex samples[162].

Since none of the probes described above had been utilized for the detection of *Mtb* in bioaerosol samples, we sought in this study to test their applicability for the detection of *Mtb* in TB patient bioaerosols captured within the RASC.

Results

Selection of a fluorescent probe for the detection of Mycobacterium tuberculosis

The detection of *Mtb*-like bacilli in foil-impacted bioaerosols using SEM reinvigorated interest in the application of microscopy for the detection of aerosolized *Mtb*[99,100]. Although SEM is a high-resolution microscopy technique, it is time-consuming, expensive, and lacks the specificity required to reliably identify *Mtb*. Moreover, the approach is destructive, with all imaged material lost through the SEM process. We therefore aimed to develop a method applicable to widefield fluorescence microscopy, a simpler, more

cost-effective technique that benefits from several unique staining procedures and fluorescent probes, enabling the specific detection of certain cell types or structures while potentially retaining sample viability.

As expected, DMN-tre only stained viable mycobacteria, which could be imaged without removing excess probe (Figure S2.1). When tested in bioaerosol samples, fluorescing mycobacteria were readily observable over background, although an increase in non-specific fluorescence was observed in these samples relative to culture media (Figure 2.1 & S2.4). Despite this, a key limitation remained: Ag85 incorporation of trehalose into the mycobacterial cell envelope, the key mechanism by which DMN-tre facilitates the detection of *Mtb*, is common to other bacteria in the actinomycetales order. That is, DMN-tre possesses limited specificity.

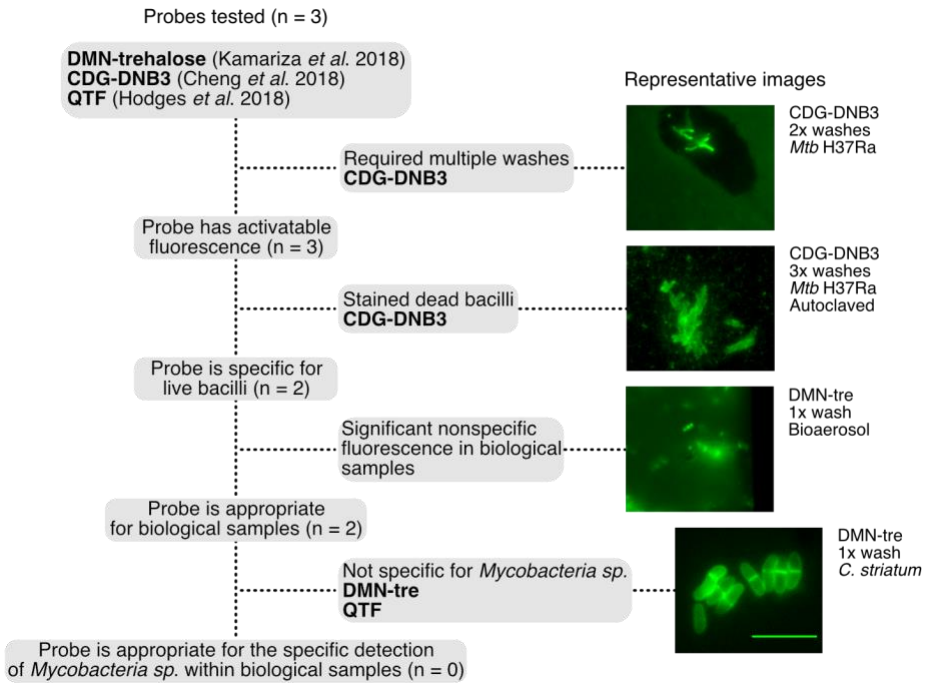

Figure 2.1: A workflow to test the utility of a fluorescent probe for the detection of Mtb in extremely paucibacillary clinical samples. *(i) A probe should have a robust mechanism for activatable fluorescence such that wash steps are not required. (ii) The mechanism of probe incorporation should be specific for viable bacilli. (iii) The background and/or non-specific fluorescence in clinical samples should not inhibit the detection of the organism of interest. (iv) The probe should be specific for the organism of interest.*

During the course of this thesis, alternative fluorescent probes became available, namely QTF[161] and CDG-DNB3[162]. When staining lab-grown mycobacteria, QTF performed comparably with DMN-tre. However, its

reliance on Ag85 for cell envelope incorporation left it similarly vulnerable to false-positive identification of other acinomycetales as putative *Mtb*. Since CDG-DNB3 stains *Mtb* independently of Ag85, exploiting both BlaC and DprE1 for incorporation into the mycobacterial cell envelope[162], it appeared to offer some advantages over both DMN-tre and QTF. Disappointingly, our preliminary in vitro assays revealed a number of unexpected flaws with CDG-DNB3 that were not disclosed in the original publication describing its development. These included high levels of background fluorescence *in vitro*, the staining of heat-killed (autoclaved) *Mtb* H37Ra, and the staining of *Corynebacterium striatum* (*Csi*) (Figure 2.1), all of which eliminated this probe as candidate. Instead, DMN-tre remained the preferred option for the identification of putative *Mtb* in paucibacillary clinical samples owing to its requirement for minimal wash steps, its selectivity for viable bacilli, its limited specificity, and its propensity for low background fluorescence in clinical samples (Figure 2.1).

Towards an identikit of DMN-trehalose-positive *Mtb* bacilli

Owing to the limited specificity of DMN-tre for *Mtb* and the possibility of detecting all actinobacteria possessing homologs of the mycobacterial Ag85 complex, we proposed the development of a framework (or "identikit") based on cell morphology to aid in the identification of putative *Mtb* organisms. To this end, both exponentially growing (log phase) and aged cultures (stationary phase) of *Mtb* H37Rv were processed and stained with DMN-tre to determine the morphological and cytological characteristics of different *Mtb* growth states (Figure 2.2).

The median length of *Mtb* H37Rv (Figure 2.2A) did not vary between exponential growth and early stationary phase. However, *Mtb* cell length is a commonly reported feature of morphological heterogeneity in clinical samples, even between regions of the lungs[156], which can be exacerbated by DNA damage-induced filamentation[163,164]. For this reason, we placed less emphasis on cell length as an identifier of *Mtb*, instead expecting bacilli to range between 0.5–9 μm in length[156]. Despite largely overlapping distributions, bacilli entering early stationary phase were very slightly thinner than exponentially growing organisms (Figure 2.2B). This observation was consistent with previous reports that the cell width of *Mtb* ranges from 0.4–0.8 μm, even during exposure to several antibiotics[165]. Cell width in *Mtb* therefore appeared to be subject to significantly less variation than length, so was prioritized as identifying feature.

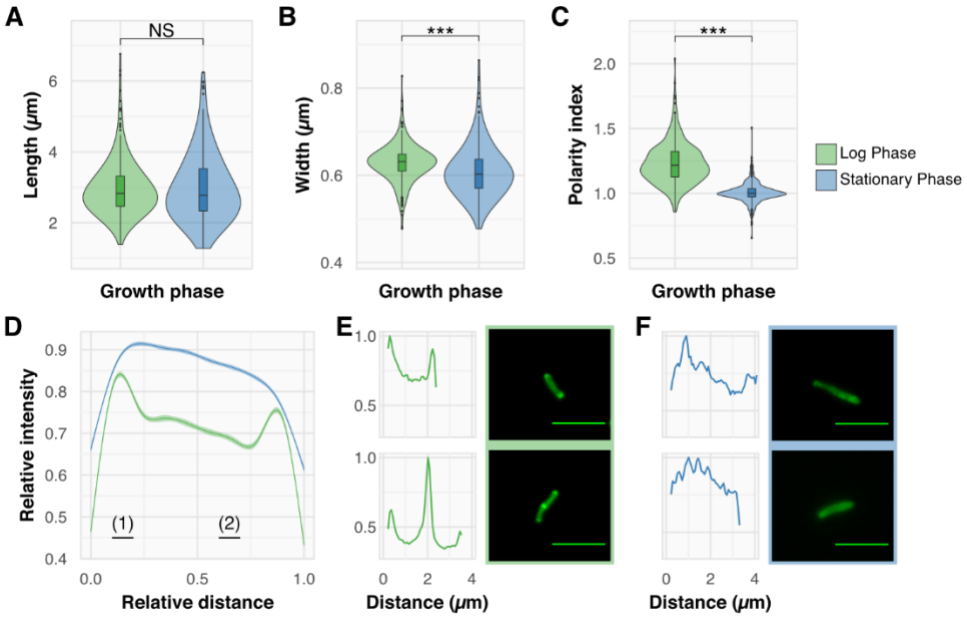

Figure 2.2: The differentiation of growth states in Mtb using DMN-tre and cell morphology. *Comparisons between log (green) and stationary (blue) phase Mtb according to (**A**) cell length, (**B**) width, and (**C**) polarity index. (**D**) Average DMN-tre profile for log and stationary phase bacilli, with single-cell examples in both (**E**) log and (**F**) stationary phase. Polarity index for each cell was calculated as the median fluorescence intensity at region (1) divided by the median fluorescence intensity at region (2) in panel (D). Wilcoxon signed-rank test performed, p < 0.001 = ***, NS = not significant.*

Corynebacteria are among those actinobacteria that possess homologs of the mycobacterial Ag85 complex and, therefore, the capacity to incorporate DMN-tre. Moreover, they are a common constituent of the oral microbiome and have previously been identified in TB sputum samples[166]. To expand our database of potential DMN-tre-positive organisms, we included the opportunistic pathogen, *Csi*[167], in the *in vitro* analyses (Figure S2.2A). Although *Csi* and *Mtb* were similar in length (Figure S2.2C), they could be easily differentiated based on cell width and DMN-tre staining profiles (Figure S2.2D-F). This reinforced the utility of width and DMN-tre positivity as primary markers for the identification of "putative *Mtb*" in bioaerosol samples.

Differentiating between mycobacterial growth phases by DMN-tre cytological profiling

The metabolic state of aerosolized *Mtb* remains unknown. Hodges and colleagues demonstrated the ability of QTF to differentiate between the old and new poles at cell division[161]. Therefore, we reasoned that probes

targeting mycolic acids might provide information regarding metabolic state in mycobacteria. To test this, we investigated the utility of cytological profiling via DMN-trehalose staining to differentiate bacilli broadly as either slow or fast growers based on their growth phase.

Differences in DMN-tre uptake and distribution along the cell length were observed between log and stationary phase bacilli (Figure 2.2C–F). Polarity index, a previously used summary metric for cytological profile information[168], is calculated as the relative brightness of the old pole compared to the mid cell. A polarity index much greater than one is indicative of rapidly elongating cells, as trehalose incorporation is greatest at the cell poles. In contrast, a polarity index closer to one suggests that cells are not rapidly extending at the poles.

In our experiments, the polarity index was greater in log phase (1.21, IQR = 0.242) compared to stationary phase cells (0.948, IQR = 0.112) (Figure 2.2C). Thus, cells identified as putative *Mtb* based on cell width and DMN-trehalose positivity could be characterised broadly into at least two growth categories based on DMN-tre incorporation.

Filtration of dilute culture facilitates the detection of mycobacteria

The sampling of TB patient bioaerosols required capture and concentration of all particulate matter in 5–7 mL liquid in a Bertin® cyclone collector, thereby resulting in the extreme dilution of an already paucibacillary sample[2,100,119,121]. We therefore required a sample preparation pipeline involving minimal processing steps and ready amenability to fluorescence microscopy.

For our first approach, we attempted to concentrate dilute cultures of *Mycobacterium smegmatis (Msm)* and *Mtb* by filtration onto polycarbonate (PCTE) filters. The filters were placed bacteria-side up on 7H10 media supplemented with 100 µM DMN-tre and incubated at 37°C for three hours (*Msm*) or overnight (*Mtb*). After incubation, the filters were placed between a coverslip and glass slide and visualized. *Msm* bacilli could be detected at numbers as low as 40 CFU/mL (Figure 2.3A), with similar results obtained for *Mtb* (Figure 2.3B). Although this method showed promise for the detection of mycobacteria in paucibacillary samples, it was limited in its utility in a clinical setting owing to a low sample throughput, the challenges of working with PCTE filters in biosafety cabinets, difficulty finding bacilli due to a low signal-to-noise ratio, and the requirement for incubation of samples on solid media for dye incorporation.

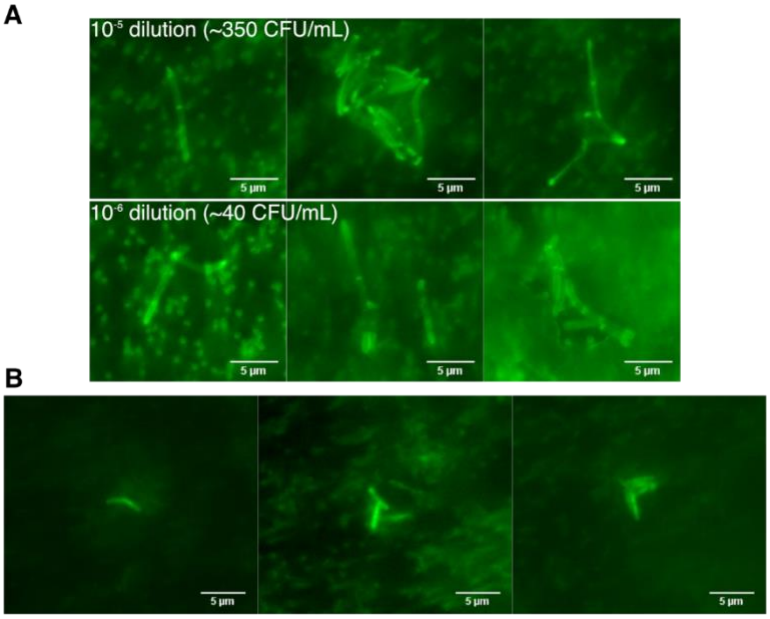

Figure 2.3: The combination of sample filtration and DMN-tre staining to facilitate the detection of mycobacteria in paucibacillary samples. *(**A**) Msm was grown to mid-log phase, after which, serial tenfold dilutions were performed. Diluted samples were filtered through PCTE membranes and incubated on 7H10 agar containing 100 µM DMN-tre for three hours (**B**) Dilute mid-log phase Mtb culture was passed through a PCTE filter. This filter was incubated overnight (bacteria-side up) on 7H10 agar containing 100 µM DMN.*

A CUSTOM-BUILT NANOWELL DEVICE FOR MICROSCOPIC ANALYSIS

To enhance our capacity for the isolation and microscopic detection of single *Mtb* cells captured from TB patient bioaerosols, we shifted to nanowell-arrayed microscopy devices. Several iterations of these devices were designed and tested, with the best performance in image quality and bacterial detection obtained from devices fabricated from cyclic olefin copolymer (COC) film with 50 × 50 µm nanowells arrayed ~140 µm apart centre-to-centre (Figure 2.4). The superstructure of each device consisted of two rows of eight microwells (16 total), each arrayed with approximately 1600 nanowells with a total volume capacity of 20 µL. This allowed an entire bioaerosol sample to be concentrated and loaded into a single microwell.

This improved upon the use of filters as it simplified sample processing and allowed for the maintenance of cells in liquid media. Moreover, the physical separation of the sample across thousands of individual nanowells was considered beneficial in several ways: firstly, the dispersion of any contaminating fluorescent particulate matter across the nanowells enhanced our ability to detect *Mtb*, while also limiting overgrowth of faster growing

organisms during overnight labelling; secondly, the ability to assign a physical address based on the *x-y* coordinates of the specific nanowell facilitated the re-identification of the same organism in serial imaging experiments (outlined below).

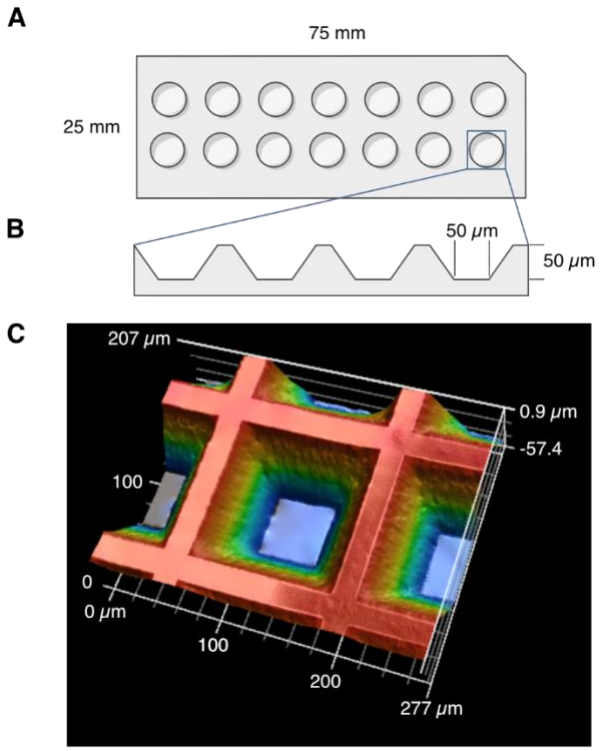

Figure 2.4: The design and fabrication of nanowell-arrayed microscope slides for the compartmentalization and visualization of TB patient bioaerosols. *Schematics depicting (**A**) the overall slide layout and (**B**) nanowell design. (**C**) 3D scan of a 207.840 × 277.029 μm section of the slide. Each device (25 mm × 75 mm) consists of two rows of round microwells machined from cast acrylic. The microwells are 6 mm in diameter and 2 mm deep. The nanowell film, which is bonded to the superstructure with UV-curing adhesive, is made from embossed COC film. The nanowells have side-wall angles of 35˚ and are 50 μm deep. The distance through the bottom of each well to the back of the film is~170 μm, equivalent to a number 1.5 coverslip.*

Microscopic identification and characterization of DMN-tre positive *Mtb* in TB bioaerosols

Having established the utility and limitations of using DMN-tre in combination with the nanowell devices for the detection of *Mtb* in paucibacillary samples (Figure 2.1, 2.2 & S2.4), we sought to develop a sample processing pipeline that could be applied in a pilot study for the capture and detection of live *Mtb* bacilli from TB patient bioaerosols (Figure 2.5). For the

pilot study, 31 individuals with GeneXpert-positive, drug-susceptible TB were recruited from TB clinics in Masiphumelele and Ocean View, peri-urban communities in Cape Town, South Africa. Aged bioaerosols produced by participants over a 30–60-minute sampling window were then captured using the RASC. Prior to participant sampling, the same bioaerosol sampling algorithm was run on an empty booth as a baseline comparison.

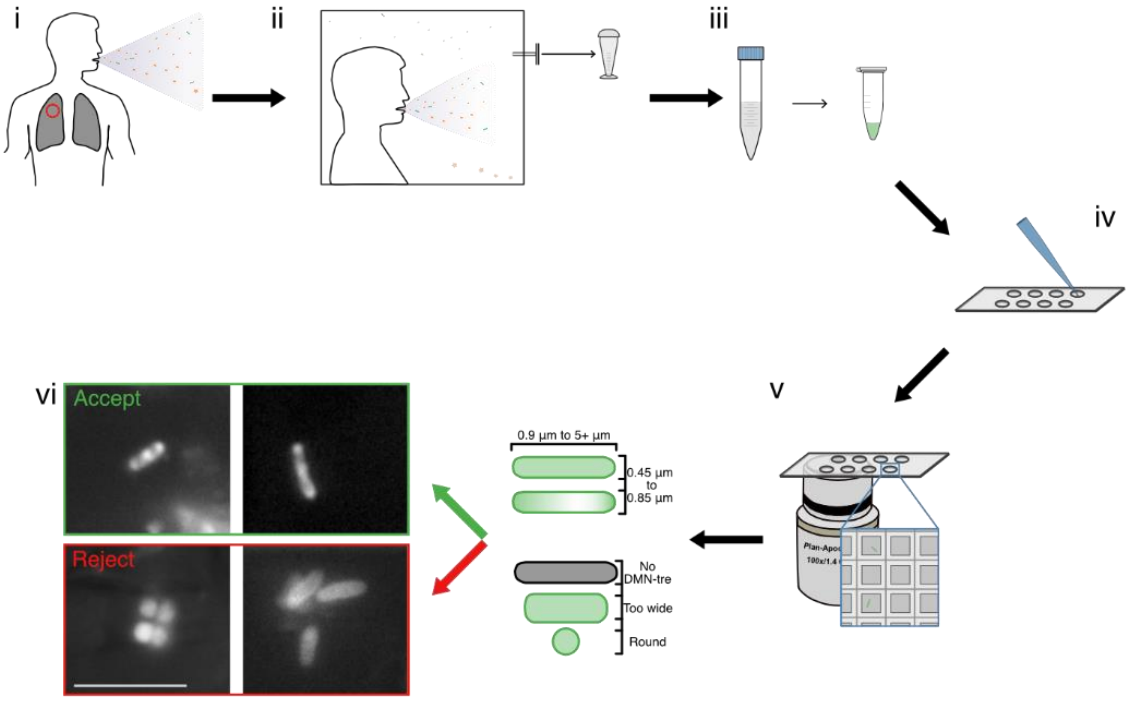

Figure 2.5: The workflow from participant recruitment to image analysis. *(i) Recruitment of GeneXpert-positive TB patients. (ii) One hour of bioaerosol production during tidal breathing and non-induced cough within the RASC, followed by liquid capture of patient bioaerosols using a Bertin Coriolis µ Biological Air Sampler. (iii) Bioaerosol concentration and staining with 100 µM DMN-tre during overnight (~16 hours) incubation at 37 ℃. (iv) Sample arraying within the nanowell device. (v) Manual sample scanning and bacillary detection according to the "identikit" established for Mtb. (vi) Nanowell imaging. Bacilli not matching inclusion criteria were excluded from subsequent analyses. Scale bar, 5 µm.*

Liquid-captured bioaerosols were concentrated to 200 µL in complete 7H9 liquid media supplemented with 100 µM of DMN-tre and incubated overnight at 37°C. Stained samples were centrifuged and resuspended in 20 µL PBS to minimize background fluorescence when imaging, after which the entire sample was loaded into a single microwell well of the nanowell device, followed by a final centrifugation step before imaging. Differing forms of particulate matter were observed in the bioaerosol samples, with large

crystalline debris being the most prevalent (Figure S2.5A). Putative *Mtb* were identified based on cell width and DMN-tre positivity in 90% (28/31) of the TB patient bioaerosols. The median count in the captured air from TB-positive patients was 14 (range 0-36), *versus* 1.5 (range 0-10) in the air analyzed from the empty booths, suggesting low-level carry over/contamination of the booth between individuals (Figure 2.6A). When comparing the basic morphological characteristics of aerosolized *Mtb* to those organisms observed during log-phase growth *in vitro*, it was apparent that the aerosol-derived bacilli were significantly shorter than log-phase bacilli (Figure 2.6B), with an average length closely resembling cells described previously from cavity caseum[156]. In contrast, bacillary width was, on average, equivalent between cells from bioaerosols or log-phase culture, however a greater degree of width variation was observed in clinical samples (Figure 2.6C).

Further investigation into the profiles of DMN-tre incorporation led to the observation of three distinct labelling patterns (Figure 2.6D-F, S2.4B), namely polar labelling (sample TRDS182, top row), diffuse labelling (sample TRDS174, middle row), and a patchy labelling pattern (sample 180801JM9, bottom row). Both polar and diffuse labelling have been previously observed in log and stationary phase bacilli, respectively (Figure 2.2D). Interestingly, the patchy labelling pattern wasn't common in our *in vitro* experiments. Like the *in vitro* cultured organisms, no significant differences in cell length were observed for the different labelling patterns in the bioaerosol samples (Figure 2.6G). However, more prominent differences were seen in labelling patterns of DMN-tre (Figure 2.6H), highlighting the potential utility of trehalose probes in indicating underlying metabolic states of aerosolized bacilli. Additional surprising results were the observation of clumps and small clusters of organisms; however, these were not common and were observed in only a fraction (2/31) of patients (Figure 2.6I).

Numerous organisms were detected with features closely matching those observed with laboratory grown *Csi* (Figure S2.5A), suggesting they were likely to be corynebacteria. We also observed multiple DMN-tre-positive organisms of possible bacterial and/or fungal origin – despite the expectation that the ability to metabolise the fluorescent trehalose analogue should be limited to the actinomycetales order (Figure S2.5B). Utilising the morphologic exclusion criteria developed above, all of these were eliminated from "putative *Mtb*" classification despite showing a DMN-tre-positive phenotype (Figure S2.5B) and were consequently not considered in downstream analyses.

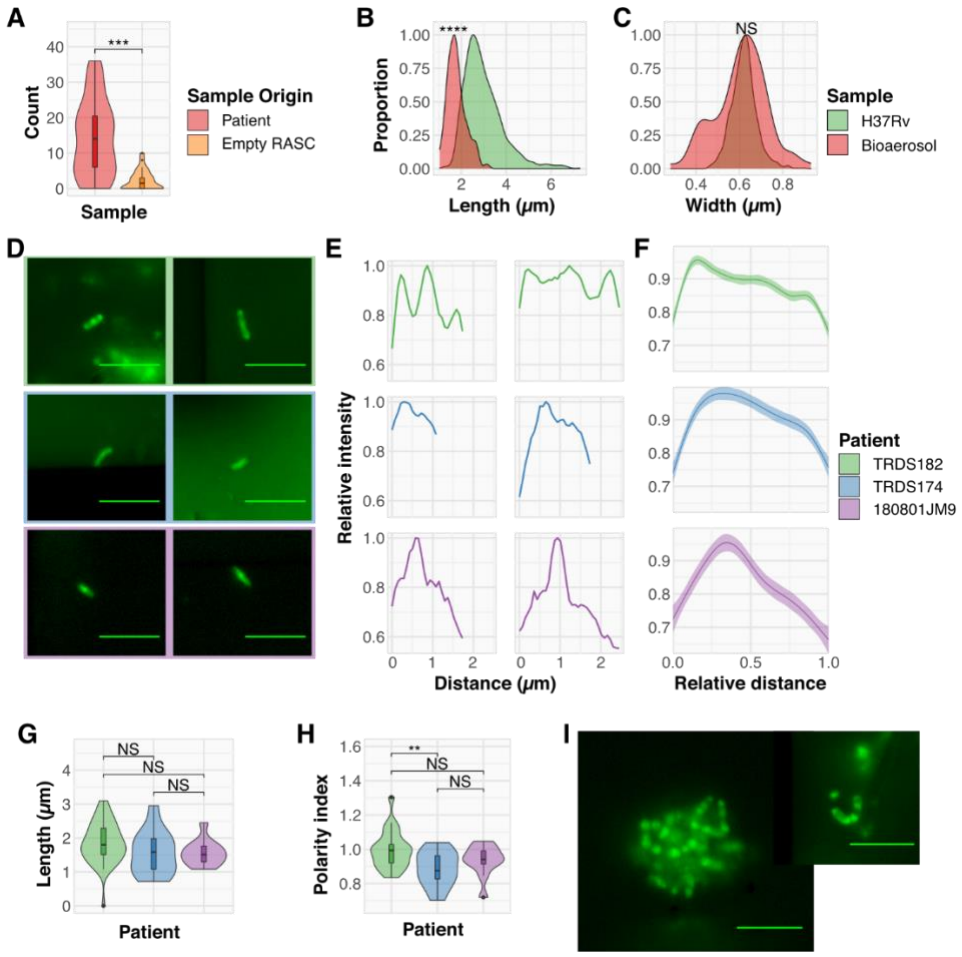

Figure 2.6: The detection and characterization of putative Mtb within bioaerosols of confirmed TB patients. *(**A**) Plot comparing the number of putative Mtb detected within TB-positive participants (red, n = 31) and empty RASC controls (orange, n = 27). Comparing distributions of (**B**) cell lengths and (**C**) cell widths in putative Mtb bacilli detected within bioaerosols of TB patients (red) to Mtb H37Rv cultured within the lab (green). Representative (**D**) images and (**E**) plots of the three distinct, exemplar cytological profiles from three patients in which putative Mtb were detected. (**F**) Average plots indicating the different staining patterns of all bacilli detected in these three patients. (**G**) Polarity indices and (**H**) cell lengths of bacilli detected within these patients. (**I**) Representative images of clumps of putative Mtb detected within bioaerosol samples (TRDS182). Scale bar, 5 μm. Wilcoxon Rank-Sum test performed, p < 0.01 = **, < 0·001 = ***, p < 0,0001 = ****, NS = not significant.*

Serial imaging of captured, DMN-tre-positive *Mtb* bacilli in the arrayed nanowells

A key motivation informing the development of the RASC platform was the need to capture live, aerosol-derived *Mtb* for analysis and propagation as part

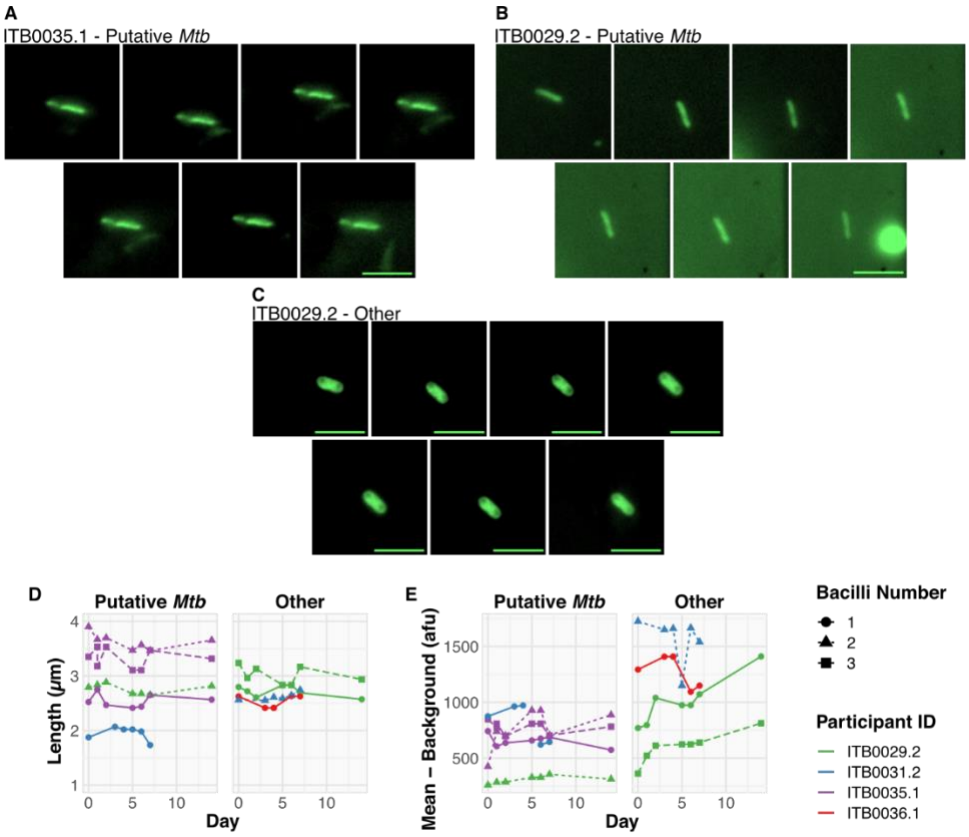

Figure 2.7: Serial imaging of putative Mtb bacilli captured directly from patient bioaerosol for up to two weeks. *Single bacilli identified from four separate patients were serially imaged daily for the first seven days (except weekends) and weekly thereafter. Up to three bacilli were tracked per patient (bacilli number – represented by shape and dashed lines) in four patients (represented by colour) and identified as either "Putative Mtb" or "Other". (**A–C**) Representative bacilli from two separate patients imaged on days zero, one, two, five, six, seven, and 14. (**A**) and (**B**) represent putative Mtb, whereas (**C**) represents other organisms with a low probability of being Mtb based on the applied inclusion criteria. Summary of bacterial changes in (**D**) length and (**E**) mean fluorescence intensity minus the average background intensity. Scale bar, 5 µm.*

of a larger research program in TB transmission and *Mtb* aerobiology. This required the capacity not only to isolate and detect individual bacilli, but also to maintain the viability of organisms in a format amenable to extended analysis and cultivation. To investigate the suitability of the nanowell array for this purpose, we prepared a small subset of bioaerosol samples for extended incubation *in vitro*. The samples were processed according to the

standard DMN-tre staining protocol but, after the final wash step, were resuspended in fresh Middlebrook 7H9 culture medium before arraying on the nanowell slide and incubating at 37°C without shaking. Following initial identification of putative DMN-tre-positive *Mtb* bacilli (Day 0), images were captured every 24 hours for the first week (excluding weekends) and again on day 14 post isolation. This was done using the *x-y* coordinates of the specific nanowell to enable re-location of the same organisms for serial imaging (Figure 2.7). Alterations in metabolic or replicative state were expected to manifest in changes to bacillary morphology and/or DMN-tre profile.

Over the two-week incubation period, no changes in length were observed for any of the cells, whether classified as "Putative *Mtb*" or "Other". Similarly, the fluorescence intensities over background for individual cells displayed only minor increases for some of the "Other" organisms. It was possible that the incubation time was too short to allow for adaptation of the bioaerosol-derived bacilli to the culture medium and/or solid substrate. Therefore, subsequent work included exploring different culture media and extending the analysis from weeks to months, as well as investigating the possibility that the COC nanowell substrate might be growth inhibitory. We were nevertheless encouraged by the ability to obtain serial images of the same organisms, supporting the utility of the nanowell array in enabling re-imaging of DMN-tre-positive bacilli identified immediately post capture and assigned a unique "address" to allow for re-location.

Discussion

Since the 1990s, the direct detection of *Mtb* in TB patient bioaerosols has been carried out using PCR or culture[112,114,119], each with its own advantages; however, the discordant sensitivities of these methods and their limited ability to probe bacterial metabolic state support the need for an alternative approach.

Microscopy was fundamental in the founding and development of microbiology as a discipline[136] with current applications proving vital in understanding mycobacterial cell biology[54,164,165,169]. Moreover, microscopy remains a commonly used tool in both TB diagnostic and clinical research laboratories, elucidating key aspects of bacterial morphological and metabolic states within the lungs[150,156], while also having a historic precedent in transmission studies[70,149]. Given the gaps that exist in understanding the aerobiology of *Mtb* and the benefits of microscopy in microbiology, we sought to establish a pipeline for the microscopic detection of *Mtb* in bioaerosol samples captured in liquid.

Fluorescence microscopy of bioaerosol samples enabled the detection of putative live *Mtb* in 90% of GeneXpert-confirmed TB patients at a median of 14 bacilli per sample (maximum = 36). The high sensitivity of this technique is in line with that of a recent face-mask sampling study, which detected *Mtb* in 86% of participants[170]. Together, these methods exhibit a marked improvement in the sensitivity of *Mtb* detection over culture-based techniques, with two recent studies finding *Mtb* in 45%[171] and 31%[172] of participants. Interestingly, the agreement between these methodologies is reversed when examining the number of bacilli detected during sampling. In this study, aged bioaerosols produced through normal breathing and spontaneous coughing during the 60-minute sampling window were collected, thus representing a natural rate of *Mtb* aerosolization. Consequently, simple extrapolation of the 14 bacilli median would suggest the release of around 336 viable bacilli per day. Cough-sampling consistently identifies fewer than 100 CFU in 5–10 minutes of sampling, however this technique necessitates that each participant coughs as frequently and forcefully as possible during the sampling window[171,172]. This is difficult to standardise or relate to natural rates of *Mtb* aerosolization; however, if the same extrapolation is applied to the median count of 14 CFU per sample, cough sampling estimates a rate of aerosolization of ~2000 CFU per day[171].

Face-mask sampling can be performed for extended durations and multiple times a day, agnostically of respiratory manoeuvre, lending it to the non-invasive collection of naturally aerosolized *Mtb*. For *Mtb* quantification Williams and colleagues used PCR for the detection of the multicopy *Mtb* gene, *IS*6110, detecting 10^4–10^9 *IS*6110 copies per day (median = 340,000). Based on their estimated median number of *IS*6110 copies per genome (median = 4, range = 1–36), face-mask sampling suggests that 85,000 *Mtb* bacilli are aerosolized per day. This is significantly higher than estimates based on either culture or microscopy[170]. However, direct comparison of these methods is difficult owing to the differing techniques utilized for bioaerosol collection and *Mtb* detection and enumeration. Regardless, we were encouraged to see commonalities between these techniques.

The benefit of utilising microscopy for the purpose of detecting *Mtb* in bioaerosols extends beyond attempting to optimize the sensitivity of detection. Notably, there is strong evidence that DMN-tre incorporation is indicative of viability, which cannot currently be assessed via PCR and takes six to eight weeks to assess via culture. Moreover, the observation of clumps of putative *Mtb* in bioaerosol samples resonates with *in vitro* evidence demonstrating the enhanced capacity of *Mtb* aggregates to subvert macrophage antimicrobial defences[173]. Although, in principle, only a single

bacillus is required to initiate a new infection[24], the precise events – and numbers – which allow colonization of a new host following exposure to *Mtb*-infected bioaerosols, remain unknown.

The aerobiology of *Mtb* remains an elusive part of its lifecycle. We determined that DMN-tre staining could be used to broadly distinguish bacilli based on metabolic states. Interestingly, three distinct cytological profiles were observed in bioaerosol-derived bacilli, two of which bore a close resemblance to those observed in log- and stationary-phase. Although this observation suggests metabolic heterogeneity in aerosolized bacilli, the implications of these observations remain uncertain and many questions remain, such as if these organisms are actively replicating, or if aerosolized bacilli contain defining alterations in cell envelope[174] or other macromolecular compositions and/or inclusions[150]. Fully addressing these questions will require continued research with the incorporation of more than one spectrally compatible fluorescent probe[175].

The potential exists to extend this work beyond investigating metabolic state, focusing on drug resistance, for example. Previous work has shown differences in probe incorporation profiles in response to antibiotic treatment[168]. At a quantitative level, imaging organisms from diagnosed TB patients before and after treatment initiation, as well as serially over the course of standard chemotherapy, might therefore offer a more rapid indication of drug efficacy, in effect affording the sensitivity of broncho-alveolar lavage without the invasiveness of that procedure.

Considerable effort was made to minimize the acquisition of "contaminating" debris during RASC sampling – for example, by working in a clean-room and requiring that all patients wore disposable biohazard suits to reduce release of non-respiratory particles. This is because the cleanliness of samples is critical for microscopic visualization: auto- and/or nonspecific-fluorescence represent major confounders in environmental samples, while debris can obscure *Mtb* bacilli under microscopic investigation. Our "empty booth" controls – in which sampling was performed in the empty RASC in the absence of an incumbent individual and was therefore expected to be *Mtb* free – returned 54% (14/26) positivity; however, the difference in median count compared to the TB-positive patients suggested that these organisms were carried over from the cyclone collection system or RASC. Moreover, improvements to the collection system subsequent to this study ensured higher efficiency bioaerosol capture and complete sterilization, eliminating carryover as confounder[176,177].

Sample concentration, too, impacted on the ease with which *Mtb* could be detected within samples. Although the filtration of samples was sensitive and has since been applied in the detection of bloodstream *Mtb* infection[178], the challenges of working with filters under biosafety level (BSL) 3 containment conditions and the slow nature of sample scanning led us to develop the nanowell-arrayed microscope slides. The nanowell device was designed to maximize *Mtb* detection by increasing the likelihood of separating debris and bacilli through sample dispersal across thousands of nanowell chambers. It is possible that the composition and origin of the particulate matter will prove invaluable in future in determining the anatomical origin of aerosolized bacilli. In this work, though, raising the signal from putative *Mtb* above background noise was our priority.

The nanowell array provided a unique address to each DMN-tre-positive bacterium, allowing these organisms to be serially imaged for the purposes of monitoring their growth and fluorescence profile. Although we did not detect any clear alterations in morphology or DMN-tre incorporation profile, the incubation period was limited to two weeks, which might be too short to allow for metabolic and/or replicative adaptation in the captured organisms; subsequent work has extended the duration of incubation (to ~50 days) and has shifted to the use of other compartmentalised capture devices (*i.e.*, multi-well glass microtitre plates) as alternatives to the COC-embossed nanowell format. At the very least, these initial results supported the ability to capture and maintain single *Mtb* cells in an arrayed format for serial imaging, and hinted at the potential to exploit the physical separation of cells into nanowell compartments for clonal propagation of bacilli downstream for genomic and other analyses which require biomass[179].

The amplification of fluorescence consequent on incorporation into the mycomembrane facilitated the DMN-tre-based detection of *Mtb* within untreated and decontaminated sputum[151]. Unlike sputum, which routinely harbours >10,000 bacilli[180], bioaerosols typically contain tens of *Mtb* organisms. To minimize loss, we deliberately omitted a decontamination step, risking the potential for a proportionally larger numbers of non-*Mtb* DMN-tre-positive organisms to be present in the bioaerosol samples than in decontaminated sputum. This complicates the use of this probe on its own to classify aerosol samples as "*Mtb* positive", leading us to develop an "identikit" based on cell morphology to aid in the identification of *Mtb*. We reasoned that, although morphological plasticity is a common survival strategy in bacteria[181], large-scale phenotypic screens of mycobacteria under diverse conditions tend to report a greater degree of variation in cell length rather than width[164,165]. This is exemplified in the typical lack of reporting of cell

width in studies investigating mycobacterial morphology[182], even in clinical samples[156,178]. Although we saw no significant difference in average cell length between log and stationary phase *Mtb*, Eum *et al*. (2009) reported significant differences in the length of bacilli from sputum, bronchoalveolar lavage samples, and cavities. For that reason, we identified cell width as the morphological characteristic of *Mtb* that was likely subject to the least variation under several conditions[165]; therefore, we considered it reasonable and conservative to only consider a bacillus 'putative *Mtb*' if it was both DMN-tre positive and between 0.4–0.8 μm in width.

An alternative approach to improving the specify of our method would be the application of another fluorescent probe. When this work was initiated, there was a lack of ancillary mycobacterium-specific probes that could be applied to increase the specificity of the microscopic detection while retaining sample viability (thus excluding standard approaches including auramine and acid-fast staining which involve inactivation steps). However, as this work progressed, additional fluorescent probes became available which we were able to test, including QTF[161] and CDG-DNB3[162]. In our brief experience with QTF, it performed similarly to DMN-tre on lab samples and was considerably brighter; however, owing to its reliance on Ag85 and limitations to its availability, we did not pursue it further in clinical samples. CDG-DNB3 represented an enticing alternative as it did not require Ag85 for incorporation, rather utilising a dual mechanism guiding its specificity. Disappointingly, this probe produced significant background fluorescence in axenic culture and stained both heat-killed (autoclaved) *Mtb* H37Ra and *Csi*, suggesting that the initial report had overstated its specificity. As such, DMN-tre represented the best option as it had been shown to readily detect *Mtb* in sputum samples and was capable of distinguishing between growth phases on cultured organisms.

Limitations

As for any study describing the development of technologies to investigate a previously occult stage of the infectious disease cycle, the approach detailed here inevitably carries inherent limitations which must be considered when interpreting the data. Orthogonal data confirming the identity of the "putative *Mtb*" identified microscopically have not yet been presented. The presumptive evidence, however, was strong: the bioaerosol samples were obtained from GeneXpert-positive TB patients immediately after diagnosis and before treatment initiation, and our previous work had demonstrated the isolation in the RASC platform of PCR-confirmed *Mtb* colony forming units in bioaerosol samples[99,100]. Moreover, ongoing work in which two samples collected from the same individual are analyzed via DMN-tre probing and

either auramine staining or RD9 PCR detection have confirmed 100% positivity correlation, with significant advances including the ability to extract whole genome sequence (WGS) data from bioaerosol samples following 50 days laboratory culture.

The bacillary counts and morphological phenotypes presented here are not augmented with clinical metadata (chest radiography scores, HIV status, *etc*.). The intention of this study was to establish the technological platform for bioaerosol sample capture and analysis that could be applied in more rigorously defined clinical cohorts aimed at examining the effect of treatment on bioaerosol bacillary load, the production of *Mtb* by individuals clinically diagnosed as TB-negative, and the relative contribution of various respiratory manoeuvres to the aerosolization of *Mtb*[177].

The criteria used to classify DMN-tre-positive organisms as "putative *Mtb*" are potentially restrictive, especially given that prevailing assumptions about the size and shape of clinical *Mtb* isolates are heavily influenced by the commonly applied staining methods (almost never supported by confirmatory molecular or microbiological data) as well as knowledge of *Mtb* morphology from growth *in vitro* in defined culture, in some cases in intracellular infection models or under applied stress conditions. There is a strong likelihood that we are failing to detect *Mtb* which do not conform to these criteria; moreover, our use of fluorescence positivity necessarily excludes organism which might be transiently inactive or quiescent[129]. We are exploring the incorporation of automated image detection software to facilitate machine-driven detection of "interesting" structures following capture of microscopy images for all particulate matter (organic and inorganic) arrayed on the nanowell slides. This development is proposed to address a further limitation of our approach, namely that our method relies on detecting then imaging cells (including microscope focusing) based on DMN-tre fluorescence. The noise in some samples means finding an optimal focus can be a challenge, which may artifactually increase or decrease the width (and to some degree the length) of the bacilli we measure.

Conclusion

This chapter outlines the development of a novel, microscopy-based method for the rapid detection of *Mtb* in TB patient bioaerosols. However, this work was conducted exclusively on GeneXpert-positive TB patients and without any requirement for specific respiratory manoeuvre, such as induced cough. Our priority in subsequent work has therefore been to expand our sampling strategies – both the participants we recruit and the number and type of

respiratory manoeuvres they perform – to better understand how *Mtb* is aerosolized, and by whom.

Materials and methods

Bacterial culture and staining conditions

Mtb H37Rv (MA)[183], *Mtb* H37Ra, and *Msm* mc²155 were grown at 37°C in Middlebrook 7H9 (Difco) liquid broth supplemented with 0.2% (v/v) glycerol, 10% (v/v) Middlebrook OADC enrichment and 0.05% (w/v) Tween80 (Sigma-Aldrich). *Csi* was cultured in LB broth (Sigma-Aldrich) at 37°C.

For staining of exponentially replicating and stationary-phase bacilli, *Mtb* H37Rv (MA) cultures were grown to an OD_{600} ~0.5 and ~1.2, respectively, before staining with 100 μM DMN-tre for two hours. Thereafter, cells were harvested by centrifugation at 13,000 × *g* (Allegra X-15R, Beckman Coulter) for five minutes before resuspending in PBS prior to visualization.

Whole cell staining with CDG-DNB3[162], and QTF[161] were performed as described previously. Briefly, *Mtb* H37Ra and *Csi* grown to early log-phase were incubated at 37°C in complete 7H9 (Difco) liquid broth supplemented with 5 μM, 10 μM, or 20 μM CDG-DNB3 for one hour. The same staining procedure was repeated on an autoclaved culture of *Mtb* H37Ra. Samples were left unwashed or washed up to four times in fresh PBS before imaging. For QTF, *Msm* mc²155 cells grown to early log-phase were incubated at 37°C in complete 7H9 (Difco) liquid broth supplemented with 1 μM or 5 μM QTF for five, 10, or 60 minutes. Samples were left unwashed or washed in fresh PBS before imaging.

Fluorescence microscopy

Imaging was done on a Zeiss Axio Observer 7 equipped with a 100× plan-apochromatic phase 3 oil immersion objective with a numerical aperture of 1.4. Epifluorescent illumination was provided by a 475 nm LED and non-specific fluorescence was removed with a Zeiss 38 HE filter set. Images were acquired using the Zeiss Zen software, and quantitative data extracted using MicrobeJ[184]. For serial imaging of bioaerosol samples, re-identification of putative bacilli detected at day zero was done by determining the *x-y* coordinates of the specific nanowell relative to the top-most, centre nanowell in the macro well.

Staining on polycarbonate membrane filters

Log-phase *Msm* mc²155 cells were filtered through a 13 mm white polycarbonate (PCTE) filter (Sterlitech Corporation). The filter was then incubated, bacilli-side facing upwards, for three hours on a 1.5% low-melt agarose (Sigma-Aldrich) pad containing 7H9 (Difco) media and 100 µM DMN-trehalose. Log-phase *Mtb* H37Rv (MA) bacilli were similarly filtered and stained for 24 hours to maximize staining efficiency and fluorescence intensity. PCTE filters were placed between a coverslip and microscope slide that was sealed using clear nail varnish. Fluorescence microscopy was performed as outlined above.

Staining of bioaerosol samples for nanowell slides

The 5–10 mL bioaerosol samples were concentrated by centrifugation at 3000 × *g* for 10 min (Allegra X-15R, Beckman Coulter). The pellet was resuspended in 200 µL fresh Middlebrook 7H9 medium and stained overnight (12–16 hours), following which, the stained sample was concentrated at 13000 × *g* (Allegra X-15R, Beckman Coulter) for five minutes and resuspended in 20 µL sterile filtered PBS.

Nanowell arraying

Stained bioaerosol samples were arrayed in a custom-designed nanowell device (Edge Embossing) (Figure 2.4). Prior to inoculation, the device was plasma coated (Novascan) to counteract hydrophobicity. Following DMN-tre staining, the concentrated aerosol sample was added to a single microwell. Samples (20 µL) were loaded, and plates sealed using an adhesive film (ThermoFischer Scientific) before centrifuging at 3000 × *g* (Allegra X-15R, Beckman Coulter) for 10 minutes to disperse the sample for imaging.

Ethics and patient recruitment

Ethics approval was obtained from the Human Research Ethics Committee, University of Cape Town (HREC 529/2019). Patients were recruited from primary healthcare facilities in Masiphumelele and Ocean View, peri-urban townships located outside Cape Town, South Africa. Informed consent was obtained from all participants and criteria for inclusion were (i) 18 years or older, (ii) GeneXpert-positive TB, and (iii) no evidence of drug resistant TB. All participants were recruited prior to initiation of standard anti-TB chemotherapy; following routine diagnosis, participants were transferred for RASC sampling, ethical approval having sanctioned a two-hour delay to initiation of standard TB chemotherapy to enable bioaerosol collection.

Liquid collection of aged bioaerosols within the RASC

The liquid collection of aged bioaerosols was conducted utilising the RASC (Figure S2.6) according to a slightly modified version of a previously described protocol[99,100]. Prior to participant sampling, the RASC was purged for 10 minutes with ambient air entering the system via a high-efficiency particulate arrestance (HEPA) filter. After purging, air from an empty booth was liquid-captured in a Coriolis μ Biological Air Sampler (Bertin Technologies SAS, France). This was followed by patient-driven contamination of the booth until the CO_2 concentration of the booth was 4,000 ppm above the ambient level, or after 30 minutes. Bioaerosols produced during 30 minutes of patient respiratory activity (primarily consisting of tidal breathing, with occasional spontaneous coughing and sneezing events) were then liquid-captured in 5–10 mL of sterile PBS.

Serial imaging of putative *Mtb* in bioaerosols

For serial imaging experiments, bioaerosol samples were processed as above, however, after imaging these samples were placed back into an incubator and kept at 37°C without shaking. Images were captured every 24 hours for the first week (excluding weekends) and again on day 14 post isolation.

Statistical analysis

Data were exported from MicrobeJ and analyses performed using R, version 3.5.1[185]. Data normality was assessed visually and, where applicable, a Wilcoxon Rank-Sum test was performed.

CHAPTER THREE - AEROSOLIZATION OF *MYCOBACTERIUM TUBERCULOSIS* BY TIDAL BREATHING

THIS CHAPTER CONTAINS EXCERPTS FROM THE FOLLOWING PUBLICATION:

Dinkele R., Gessner S., McKerry A., Leonard B., Leukes J., Seldon R., Warner D.F., Wood R. (2022). **Aerosolization of *Mycobacterium tuberculosis* by Tidal Breathing**. Am J Respir Crit Care Med. 15;206(2):206-216.

Introduction

Who aerosolizes *Mtb*?

Chronic cough is pathognomonic of TB and is commonly considered to be the dominant source of *Mtb* aerosols[70,75,76], placing it at the centre of TB transmission research for over a century[70]. This assumption is reasonable, given that coughing aids in the clearance of *Mtb*-containing sputum from the lungs in violent respiratory events, generating both droplets and aerosols[80,96,186,187]. There are multiple lines of evidence, however, which suggest that the focus on cough risks ignoring other important contributing mechanisms, undermining the implementation of new approaches to reduce TB transmission, especially in TB endemic settings.

A recent national TB prevalence survey in South Africa reported that nearly 60% of individuals with bacteriologically confirmed pulmonary TB were asymptomatic[26]. Given the relative rarity of progression to active disease[25,26] and the overwhelming force of infection in TB endemic settings[15], it is conceivable that *Mtb* transmission from symptomatic individuals, and therefore cough, is efficient. However, cough-based transmission studies identify aerosolized *Mtb* in a minority of participants (<30%) and in extremely small quantities[121,127,172]. Moreover, the lack of association between *Mtb* aerosolization and cough frequency[170], and the observation of *Mtb* transmission from sputum smear-negative individuals[188,189] are indicative of cough-independent aerosolization of *Mtb* separately from sputum. This has led to a growing appreciation for the role of subclinical TB in *Mtb* transmission[33,92] and may explain the challenges faced when trying to identify *Mtb* transmitters[33,108].

When are *Mtb* bacilli aerosolized?

Humans constantly produce respiratory droplets and aerosols from the length of the respiratory tract[97], even during normal (tidal) breathing[95,96]. Bioaerosols are generated in the peripheral lung, the site of *Mtb* infection and disease[190], as the alveoli and terminal bronchioles reopen during inspiration and released during expiration: this mechanism is known as fluid film rupture (Figure 3.1)[95]. The rate of inspiration and depth of expiration determine the extent to which bioaerosols are generated and released, respectively[95]. Importantly, the alveoli and terminal bronchioles do not experience turbulence during exhalation[104], suggesting that violent respiratory events (such as cough) have little impact on bioaerosol generation from the peripheral lung. This has led some to speculate that cough may not be the only source of aerosolized *Mtb*[191,192].

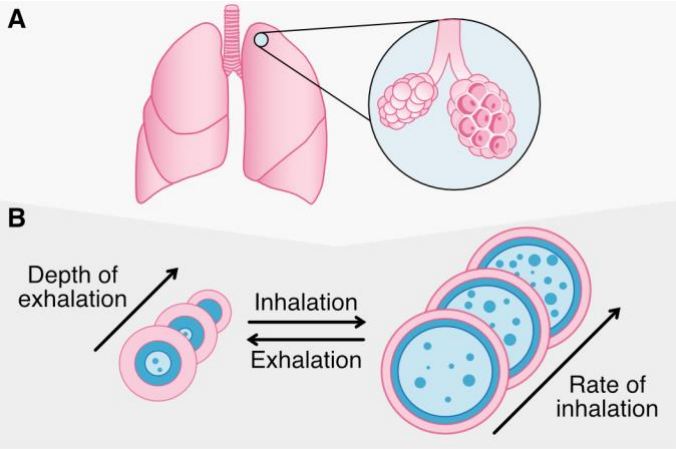

Figure 3.1: The generation of aerosols in the peripheral lung by fluid film rupture. *(**A**) An illustration of alveolar sacs (comprised of several alveoli) and terminal bronchioles in the peripheral lung. (**B**) Schematic representation of the effects of inhalation and exhalation on a single alveolus. The alveolar epithelium (pink) is lined by a layer of surfactant (blue). A proportion of the alveoli collapse during exhalation (determined by the depth of exhalation), which then burst open during inhalation, generating small droplets. The number of droplets formed depends on the rate of inhalation and the depth of the preceding exhalation, whereas the number of droplets released depends on the depth of exhalation. The fluid component of the droplets rapidly evaporates as they leave the high-humidity environment of the respiratory tract. The resulting droplet nuclei (the particulate matter released within the fluid droplet) become aerosolized (thereafter referred to as bioaerosols) at a rate determined by their size and aerodynamic properties.*

Chapter two of this thesis outlined the development of a rapid, highly-sensitive microscopic method for the detection of *Mtb* in bioaerosols, without considering the impact, if any, of the type of respiratory manoeuvre performed[193]. Subsequent work reporting additional applications of this method demonstrated the aerosolization of equivalent numbers of *Mtb* bacilli during induced cough and via a bronchiole-burst (deep breathing) manoeuvre (BBM)[194]. There, the BBM consisted of two deep breaths, ensuring full exhalation. The cumulative results of those two studies, as well as the lack of correlation between *Mtb* detection and cough frequency during face-mask sampling[170], prompted the hypothesis that tidal breathing (TiBr) might be capable of aerosolizing *Mtb*. Therefore, the aim of the work presented in this chapter was to investigate the capacity for *Mtb* and total particle aerosolization from three distinct respiratory manoeuvres: forced vital capacity (FVC), TiBr, and induced cough. For this work, we replaced BBM with FVC (a spirometry measure during which a participant forcefully exhales the

maximum volume of air from the lungs) as FVC is more commonly used and easier to standardise in clinical settings.

Materials and methods

Participant recruitment

Participants over 13 years of age presenting with TB symptoms and returning a GeneXpert-positive sputum result were recruited from March 2020 to June 2021 at primary healthcare facilities in Ocean View and Masiphumelele, periurban townships in Cape Town, South Africa. Recruitment and sampling occurred before the initiation of standard anti-TB chemotherapy. Ethical approval was obtained from the Human Research Ethics Committee of the University of Cape Town (HREC 529/2019).

Sample collection

Bioaerosols from three respiratory manoeuvres, FVC, TiBr, and cough, were captured in liquid cyclone collectors within the RASC (Figure S3.1) using a direct sampling strategy (Figure 3.2A)[194]. A unidirectional airflow forced exhaled air via a CO_2 monitor and a high-flow cyclone collector at a maximum flow rate of 300 L/min, trapping particulate matter in the collection medium (sterilised phosphate-buffered saline supplemented with Polymyxin B, Amphotericin B, Nalidixic acid, Trimethoprim and Azilocillin (PANTA) [Becton Dickinson]). During TiBr sampling, each participant placed their head within the elliptical cone and breathed normally for five minutes for an average of 92 breaths. Bioaerosols were captured within the cyclone collector at 200 L/min, whereas 100 L/min of exhaled air was diverted to a particle sizer (PS). During FVC and cough sampling, each participant performed 15 manoeuvres directly into the elliptical cone every 15 seconds. These samples were conducted as three sets of five, with longer rest periods between each set. Bioaerosols were captured within the cyclone collector at 300 L/min for the first five and last five manoeuvres. During the middle five manoeuvres, 100 L/min of exhaled air was diverted via the particle sizer. New cyclone collectors were attached after each sampling to allow for the independent enumeration of *Mtb* for each respiratory manoeuvre.

Staining and visualization of bioaerosol samples

Bioaerosols were stained with DMN-tre (Olilux Biosciences Inc.) and visualised as outlined in chapter two, facilitating the detection of viable *Mtb* bacilli. Briefly, liquid-captured bioaerosols (5–10 mL) were centrifuged for 10 minutes at 3,000 × *g* (Allegra X-15R, Beckman Coulter) and resuspended in 200 µL of Middlebrook 7H9 medium supplemented with 100 µM DMN-tre.

Staining was done overnight, after which, samples were concentrated at 13,000 × *g* for five minutes and resuspended in 20 µL filtered PBS. Stained samples were loaded on nanowell-arrayed microscope slides and viewed on a Zeiss Axio Observer 7 with widefield illumination from a 475 nm LED and a Zeiss 38 HE filter-set. A 100× plan-apochromatic phase 3 oil immersion objective (Numerical aperture = 1.4) was used.

Particle and CO_2 data handling and variable calculations

Manoeuvre and peak detection

CO_2 and particle data collection were contiguous throughout participant sampling, as such, manoeuvre detection algorithms were written for each dataset to distinguish between FVC, TiBr and Cough samples. Although particle data were outputted in a single file, gaps in sampling occurred as the PS was only utilized periodically for the different respiratory manoeuvres (Figure 3.2A). Distinguishing between the respiratory manoeuvres in the particle dataset was based on the detection of the two large time gaps that occurred post FVC and TiBr sampling (Figure S3.2A). In contrast, CO_2 measurements were taken at consistent intervals throughout sampling (Figure 3.2A & S3.2B). To separate the CO_2 measurements according to respiratory manoeuvre, the data were smoothed, and the lowest minima were detected in the first and last half of the data, which corresponded to the end of FVC and TiBr sampling, respectively. These positions were readily detectable, as the breaks between manoeuvres were longer than within manoeuvre samples, generating long, contiguous zero measures for CO_2 concentration, thereby lowering the smoothed average detected for these sections (Figure S3.2B).

Once the CO_2 and particle count data could be assigned to a particular manoeuvre, we sought to identify individual peaks (corresponding to individual FVC or cough manoeuvres) occurring during FVC and cough sampling. A localised smoothing algorithm was written to facilitate the peak detection (Figure S3.3) with a peak finding package in R[195]. Peaks were checked visually for FVC and cough samples to ensure all manoeuvres were assessed. In 12 participants, peaks were manually adjusted. For FVC and cough samples, peak identification was critical, as only particles that fell within these peaks were considered (Figure 3.2B). This was because participants removed their heads from the sampling apparatus between manoeuvres. For TiBr, the participants' heads remained in the cone for the duration of sampling; therefore, all particles were considered for TiBr samples.

Volume calculation for bioaerosol particles

The PS enumerated particles in five size categories, designated C.1 to C.5. The diameter ranges for these categories were 0.5–1 µm (C.1), 1–1.5 µm (C.2), 1.5–2 µm (C.3), 2–5 µm (C.4) and >5 µm (C.5) (Figure 3.5A). Particles were assumed to be spherical and the mean diameter from each size category was estimated without curve fitting according to the following equation:

$$bioaerosol\ volume\ (nL)_{C.x} = \frac{\frac{4}{3} \times \pi \times \left(\frac{diameter_{C.x}}{2}\right)^3 \times\ count_{C.x}}{10^6}$$

The diameter for particles defined as C.1 was assumed to be 0.5 µm, the lower bound of the size category, as counts in this category were on average 0.892 $\log_{10}$-units higher than in C.2. This suggested a greater proportion of smaller particles and is consistent with previous observations[96]. The differences in C.2–C.4 were smaller; therefore, the mid-point of each bin was used to estimate the average diameter. A diameter of 5 µm was used for C.5. To estimate the total volume of bioaerosol released, the volume of each particle was summed together for each respiratory manoeuvre.

Estimation of per manoeuvre particle counts and volumes

The flowrate via the PS was one-third that of the total bioaerosol sample and was constant for all manoeuvres (Figure 3.2A). Therefore, to estimate the total number of particles released during particle sampling, the count for each sample was multiplied by three. This gave the overall particle count for each manoeuvre (Figure 3.2B). The sample count was divided by the number of manoeuvres detected within the particle data to determine the average number of particles per manoeuvre (particles/manoeuvre). The particles/manoeuvre variable was then multiplied by the total number of peaks detected in the CO_2 data for each participant to obtain the estimated total particles for both FVC and cough samples. For TiBr, particle enumeration continued for the full duration of bioaerosol sampling, as such, particle count was equivalent to total particles for this manoeuvre. This led to a better comparison of the total number of particles produced across the three manoeuvres.

Estimation of the total number of *Mtb* bacilli

For TiBr, only two-thirds of the bioaerosol was collected versus eight-ninths for both FVC and cough. To estimate the total number of Mtb bacilli in each sample, the microscope counts were multiplied by 3/2 for TiBr and 9/8 for FVC and cough.

STATISTICAL ANALYSES

Individual participants each produced bioaerosol samples from three respiratory manoeuvres, violating the assumption of independence and necessitating an alternative analytical approach. Various linear mixed-effects models were applied as the addition of the random effect for slope enabled the average difference between manoeuvres to be determined while accounting for variation between participants. All linear mixed models outlined below contained manoeuvre (sample type) as the "fixed effect" and participant ID (PTID) as the "random effect". This was done using the lme4 package in R[196]. Where indicated, additional fixed effects were added. Data were analyzed in R studio[197] with R version 4.0.3[185].

LINEAR MIXED EFFECTS MODELS

To determine manoeuvre differences in average particle count, particle volume, *Mtb*/particle and *Mtb*/manoeuvre, these outcome variables were $\log_{10}$-transformed and linearity, normality of residuals, and homoskedasticity assessed. Next, they were regressed against sample type in separate univariate regression models. The simplified equation for a simple linear regression is:

$$y = \beta_0 + \beta_1 X_1$$

However, owing to the outcome variable being $\log_{10}$-transformed, the equation was modified to:

$$\log_{10}(y) = \beta_0 + \beta_1 X_1$$

In the raw form, the β coefficients are therefore interpretated as a unit change in X_1 leading to a β_1 change in $\log_{10}(y)$. Alternatively, the coefficients can be modified to provide a more intuitive interpretation:

$$y = 10^{\beta_0} + 10^{\beta_1 X_1}$$

Here, a unit change in β_1 relates to a fold change in y, relative to TiBr.

GENERALISED LINEAR MIXED MODELS

For the binary outcome of sample positivity for putative *Mtb*, logistic regression was performed with sample type as the fixed effect and variation in slope (random effects) accounted for with PTID. The odds ratio (OR) was determined by exponentiating the β_1 coefficient:

$$OR = e^{\beta 1}$$

Negative binomial regression

For count data obtained through enumerating *Mtb* in each sample, a negative binomial regression was applied using the MASS package in R[198]. Owing to the complexity of incorporating random effects into this model and the poor correlation between individual and *Mtb* count across the different manoeuvres, random effects were not considered, and statistical independence was assumed. Because overall sampling duration was set to about five minutes, no offset was applied for this analysis. As such, this regression model simply interrogated whether there were different rates of *Mtb* production within the different samples, not accounting for other potential differences. Exponentiating the β_1 coefficient gave the incident rate ratio (IRR):

$$IRR = e^{\beta 1}$$

Assessment of model appropriateness was tested with the deviance goodness of fit test, with a visual inspection done by plotting the mean and dispersion parameter calculated within the model overlayed on the data.

Correlation analysis

To assess the correlation between putative *Mtb* count and total particles, a correlation analysis was conducted with a $\log_{10}$-transformation of both variables. Negative counts (zero *Mtb* detected) were excluded. Linearity was visually assessed, and a Pearson correlation was performed.

Results

Detection and quantification of particles released during different respiratory manoeuvres

Direct bioaerosol sampling was performed on 38 GeneXpert-positive participants before initiation of standard TB chemotherapy. Each participant was required to perform three respiratory manoeuvres in the same sequence (FVC → TiBr → cough) (Figure 3.2A). During bioaerosol sampling, corresponding CO_2 concentration and particle count data were recorded for 32 and 33 participants, respectively. FVC and cough samples were excluded if fewer than two peaks (manoeuvres) in particle counts were detected above the background (Figure 3.3).

Spontaneous coughs occurred during TiBr sampling in a minority of participants (33%). The potential impact of spontaneous coughs on *Mtb* production during TiBr sampling was determined using particle count data (described below).

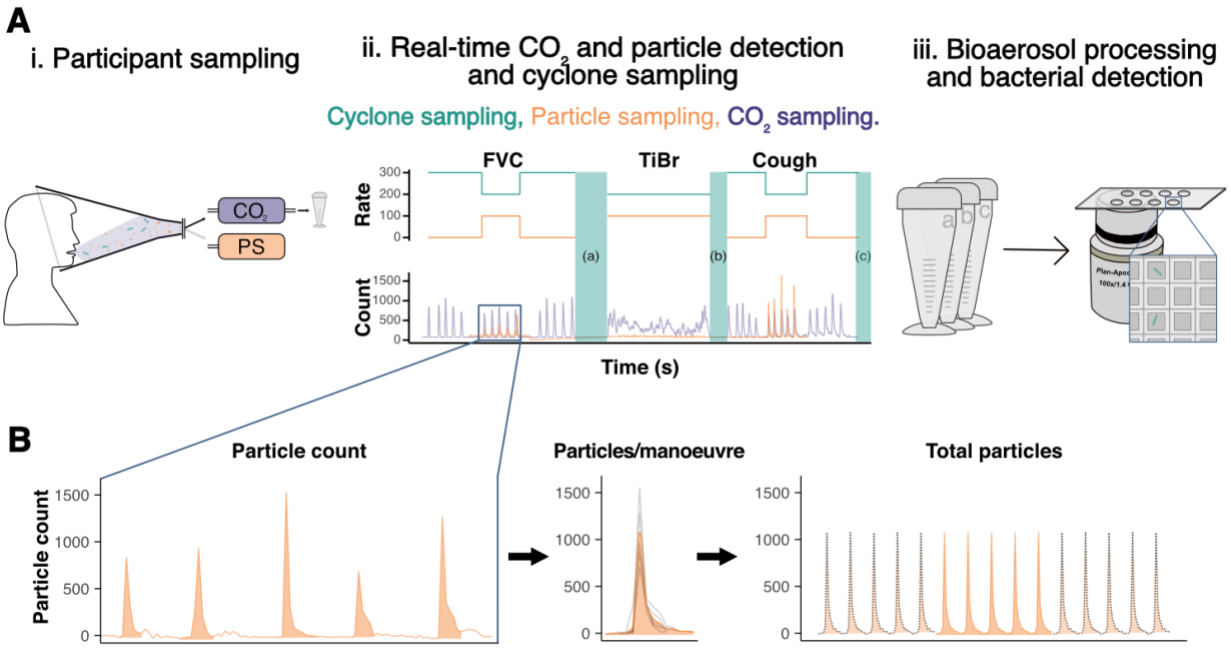

Figure 3.2: The participant sampling strategy utilized for the comparison of FVC, TiBr, and cough. *(A) (i) GeneXpert-positive participants were recruited from TB clinics in Masiphumelele and Ocean View. Bioaerosol samples were collected in the RASC from three respiratory manoeuvres: FVC, tidal breathing (TiBr), and coughing (cough). FVC and cough samples consisted of bioaerosols collected from 15 independent FVC and cough manoeuvres. These were conducted directly into the elliptical cone sampler every 15 seconds in three sets of five. Brief rest periods were taken between each set. For TiBr samples, patients breathed normally directly into the elliptical cone for five minutes, producing an average of 92 tidal breaths. (ii) During sampling, real-time data were collected for CO_2 concentration (purple) and particle counts (orange). Data are displayed in the lower section of the graph in panel ii. Measuring particles required diverting one-third (100 L/min) of the exhaled air into a PS. Particles were only counted for one-third of FVC and cough sampling and the full duration of TiBr sampling. Sampling flowrates are displayed in the upper section of the graph in panel ii. (iii) Three independent liquid cyclone collectors were attached for each manoeuvre, which were microscopically scanned for Mtb stained with DMN-tre (green columns labelled a, b, and c from the graph in panel ii indicate when cyclone collectors were removed). (B) Graphical representation of the variables used to compare the number of particles between manoeuvres, using FVC as an example. Manoeuvres were compared by particle count, particles/manoeuvre, and total particles. Particle count represents the total count of particles directly measured by the PS. Particles/manoeuvre represents the average count of particles per manoeuvre during particle sampling. Total particles represent the estimated total number of particles per sample, calculated by multiplying the average count per manoeuvre by the total number of manoeuvres during sampling (counted using CO_2 data).*

Owing to variations in sampling duration, samples were assessed in three ways (Figure 3.2B): 1) the total number of particles detected during sampling by the PS (particle count); 2) the average number of particles produced per manoeuvre (particles/manoeuvre); and 3) the estimated total number of particles produced overall (total particles). For this analysis, no attempt was made to ascertain the number of viable *Mtb* bacilli, which required fluorescence microscopy detection of putative organisms after incubation with the DMN-tre probe.

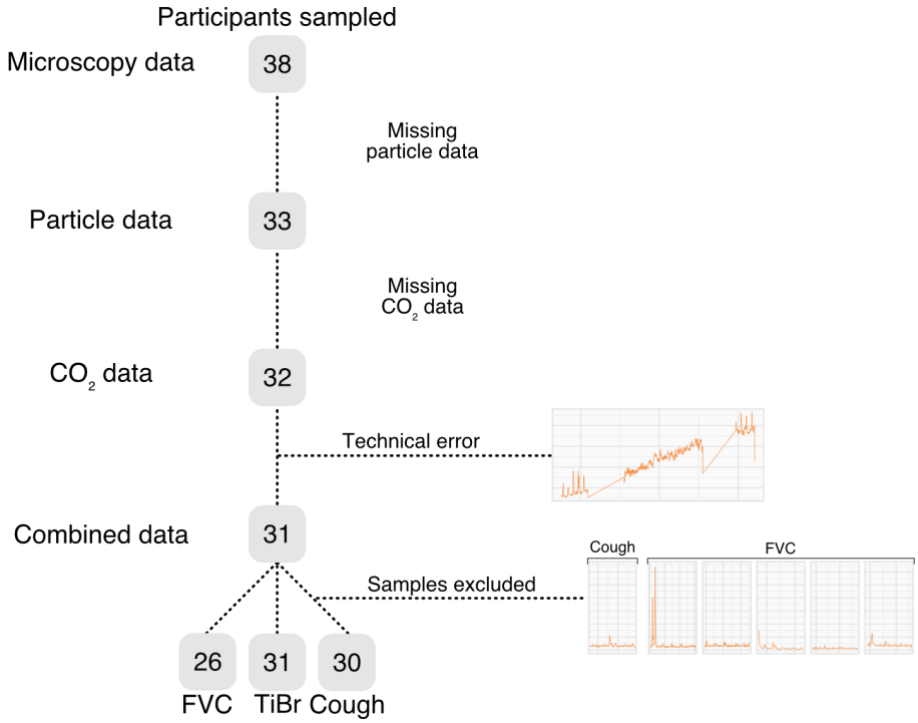

Figure 3.3: Participants and samples that were excluded. *A technical error occurred in one participant, whereby a constant increase in background particle counts was observed. The remaining six sample exclusions were based on the detection of fewer than two peaks in the particle data.*

During the particle sampling window, similar numbers (Figure 3.4A) and volumes (Figure S3.4A) of particles were collected for TiBr and cough, with FVC producing significantly fewer particles than TiBr. However, after averaging the number of particles per manoeuvre, it was clear that TiBr produced a significantly lower number (Figure 3.4B) and volume (Figure S3.4B) of particles compared to either FVC or cough. When considering the total number of manoeuvres performed, TiBr and FVC produced comparable numbers (Figure 3.4C) and volumes (Figure S3.4C) of particles, with cough producing 4.75-fold more particles than TiBr. Together, these data suggest that variation in particle production between the three respiratory

manoeuvres contributed to variation in the overall volume of bioaerosol collected after five minutes of sampling; moreover, no manoeuvre was significantly under-sampled.

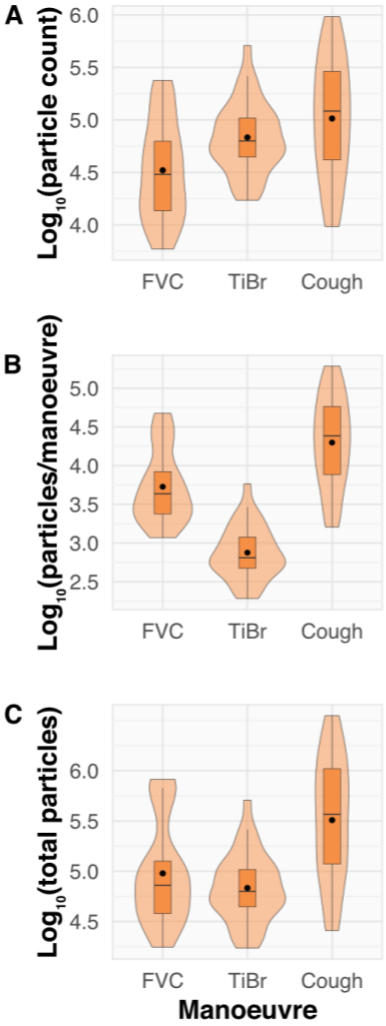

	Level	β	95% CI	Fold change	p
Manoeuvre	FVC	-0.314	-0.541, -0.086	0.48	**0.0086**
	Cough	0.181	-0.037, 0.399	1.52	0.1097

	Level	β	95% CI	Fold change	p
Manoeuvre	FVC	0.850	0.620, 1.080	7.1	**8.5e-10**
	Cough	1.423	1.202, 1.643	26.5	**< 2e-16**

	Level	β	95% CI	Fold change	p
Manoeuvre	FVC	0.145	-0.096, 0.386	1.40	0.243
	Cough	0.677	0.446, 0.908	4.75	**3.6e-07**

Figure 3.4: Variation in the number of particles produced by FVC, TiBr, and cough. *A comparison of the (**A**) particle count, (**B**) particles/manoeuvre, and (**C**) total particles produced during sampling, presented on a logarithmic scale. The adjacent tables contain the results of univariate linear mixed models for each. The β coefficients and 95% CIs are presented with fold-change relative to TiBr. CI = confidence interval.*

Size stratification of particles enables more specific comparisons of respiratory manoeuvres

Particles of various sizes (including, but not limited to, microorganisms such as *Mtb* bacilli) are aerosolized and may differ between respiratory manoeuvres[96]. The PS binned particles into size categories (Figure 3.5A);

therefore, we examined the effect of each manoeuvre on the distributions of particles across the categories measured: 0.5–1 µm (C.1), 1–1.5 µm (C.2), 1.5–2 µm (C.3), 2–5 µm (C.4), and .5 µm (C.5).

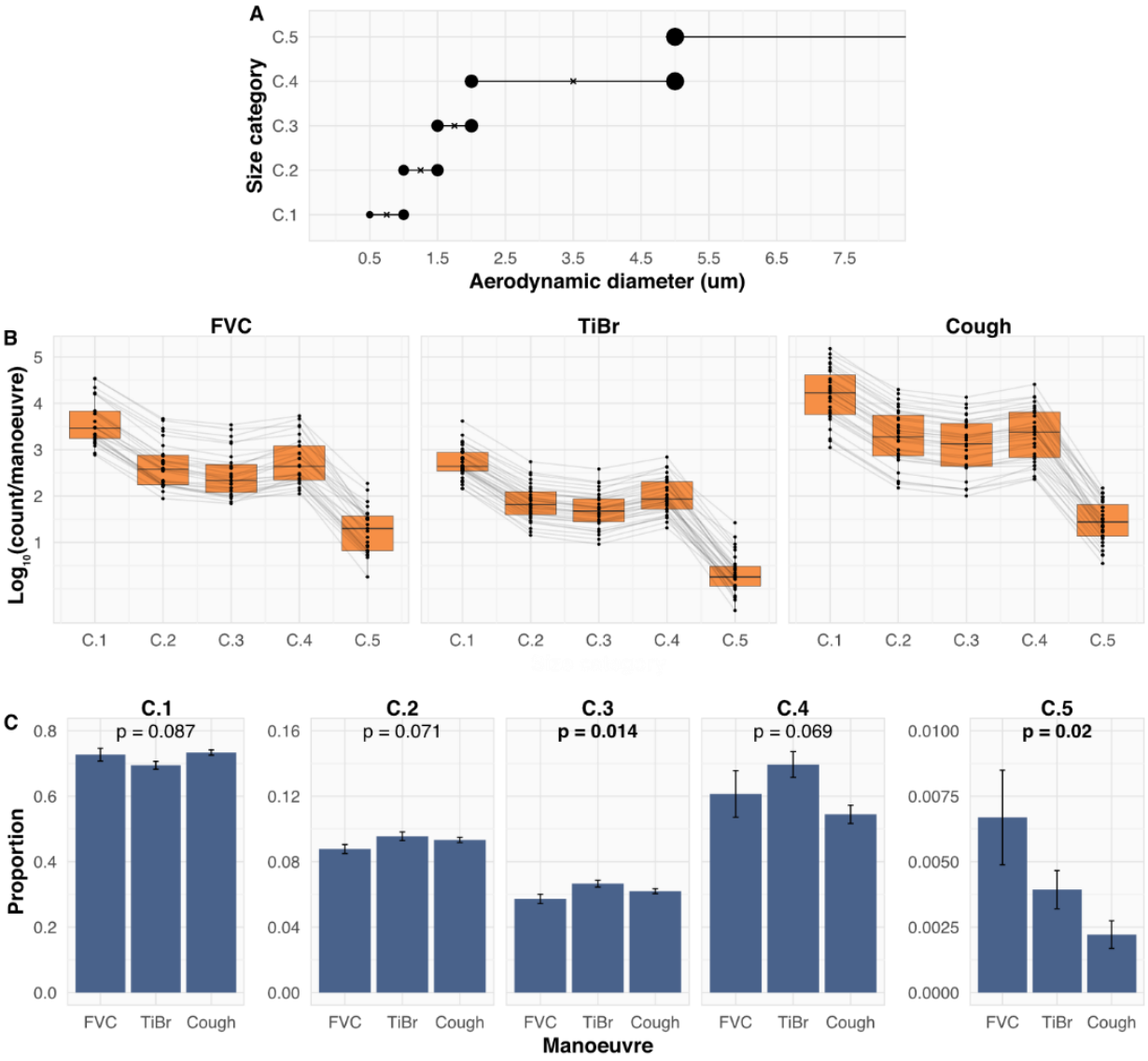

Figure 3.5: The relative contribution of particles of various sizes is consistent between FVC, TiBr and cough. *(**A**) Graphical representation of the size categories detected by the PS. The diameter ranges for these categories were 0.5–1 µm (C.1), 1–1.5 µm (C.2), 1.5–2 µm (C.3), 2–5 µm (C.4), and >5 µm (C.5). (**B**) A comparison of the average particle count per manoeuvre stratified by size category, presented on a logarithmic scale. Grey lines indicate the average number of particles per manoeuvre stratified by size category and participant ID. (**C**) A comparison between manoeuvres of the proportion composition of each size category per manoeuvre. The data in (**C**) are presented as the mean proportion ± SEM. A repeated measures ANOVA was performed; P values below 0.05 are represented in bold text.*

The average number (Figure 3.5B) and volume (Figure S3.5A) of particles per manoeuvre were stratified by size category and sample type, with the individual data from each participant overlayed. Two features were apparent: firstly, there was a consistent distribution in average count per size category across all three manoeuvres. Notably, this trend was recapitulated when the proportion of each size category relative to the total particle count per manoeuvre was compared for each size category (Figure 3C). Only minor variations were detected, with degrees of significance reached solely for C.3 (1.5–2 μm) and C.5 (.5 μm). This suggested that factors leading to increased bioaerosol generation did not affect the distribution of size categories aerosolized over the size range measured. The second observation was the per patient consistency in the relationship between the different size categories. These results indicate that intrinsic differences in the propensity for total particle production separate individuals and that these are conserved across particle sizes.

Use of three independent cyclone collectors to enable enumeration of *Mtb* bacilli

The relative contributions of different respiratory manoeuvres to the aerosolization of *Mtb* bacilli have been poorly studied, with most reports focusing on cough. We implemented a sampling strategy comprising 15 FVC and cough manoeuvres and five minutes of TiBr. This resulted in closely matching volumes of bioaerosol collected for TiBr and FVC samples, with a 3.7-fold greater volume collected during cough sampling (Figure S3.4C).

For microscopic detection and quantification of putative viable *Mtb* bacilli, bioaerosol samples were probed with DMN-tre, a fluorescent trehalose analogue that is incorporated into the mycomembrane of metabolically active organisms[151]. Given the increased volume of bioaerosol collected from cough and its assumed importance in TB transmission, we expected to find the greatest numbers of *Mtb* bacilli in the cough samples.

The incident rate ratio (IRR) of *Mtb* production between the three manoeuvres during five minutes of sampling was estimated using negative binomial regression. For both FVC (IRR = 0.53; p = 0.0971) and cough (IRR = 0.51;p = 0.0662), there was a trend to *Mtb* production at a lower rate compared to TiBr; however, neither of these was statistically significant (Figure 3.6A). The percent of positive samples was consistent for all three manoeuvres, with 66%, 70%, and 65% of the samples positive for *Mtb* in TiBr, FVC, and cough, respectively. In addition, no significant differences were detected in the odds ratio of detecting *Mtb* between TiBr and FVC or TiBr and cough (Figures 3.5B and S3.6).

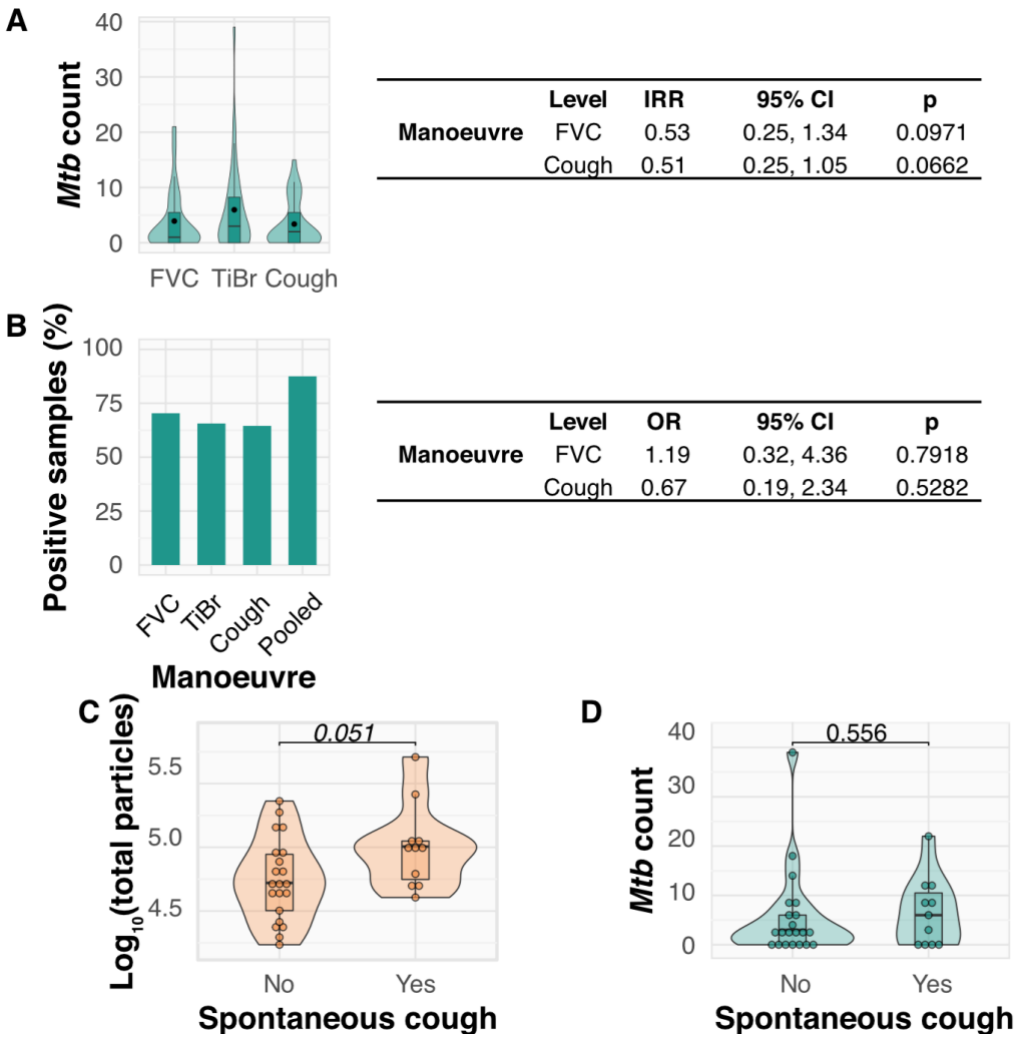

	Level	IRR	95% CI	p
Manoeuvre	FVC	0.53	0.25, 1.34	0.0971
	Cough	0.51	0.25, 1.05	0.0662

	Level	OR	95% CI	p
Manoeuvre	FVC	1.19	0.32, 4.36	0.7918
	Cough	0.67	0.19, 2.34	0.5282

Figure 3.6: The detection of putative Mtb within each respiratory manoeuvre sample. *(**A**) A comparison of the total number of Mtb detected in each sample, adjacent to the results from a negative binomial regression. (**B**) A comparison of the percent of samples that were positive for aerosolized Mtb, adjacent to the results of a generalised linear mixed model. The "pooled" variable in (**B**) represents the percentage of individuals who produced at least one positive sample. (**C**) A comparison of the total number of particles detected during tidal breathing (TiBr) sampling stratified by the detection of spontaneous coughs, presented on a logarithmic scale. (**D**) A comparison of the total number of Mtb detected during TiBr sampling stratified by the detection of spontaneous coughs. For (**C**) and (**D**), a Mann-Whitney U test was performed. CI = confidence interval; IRR = incident rate ratio; OR = odds ratio.*

The occurrence of spontaneous coughs during TiBr sampling might confound assessments of particle and *Mtb* aerosolization in these samples. To test this possibility, peaks in particle counts detected in TiBr that were greater than 1.5 times the average peak height in the corresponding cough sample were

detected and assumed to be spontaneous coughs (Figure S3.7A, right panel). When stratifying TiBr samples by the presence or absence of spontaneous coughs, a near-significant trend for increased particle production was observed in individuals who coughed (Figures 3.5C and S3.7B). In contrast, no association was observed between the occurrence of spontaneous coughs during TiBr sampling and the detection of *Mtb* (Figures 3.6D and E6C). A large range in the aerosolization of particles and *Mtb* with or without the occurrence of spontaneous cough was observed, highlighting interindividual variability in the propensity to generate bioaerosols.

To examine the relationship between particle numbers and the aerosolization of *Mtb*, the relative abundance of bacilli per particle was calculated for all three manoeuvres. Participants with a zero count for *Mtb* were excluded from this analysis. The average concentration of *Mtb* bacilli for TiBr was 70% and 90% higher than that of FVC and cough, respectively (Figure 3.7A). In addition, no correlation between total *Mtb* count and total particle count was observed for either FVC or cough (Figure 3.7B); that is, the increased overall particle count seemed to occur independently of an increase in aerosolization of *Mtb*. A slightly more apparent linear relationship was observed for TiBr (Figure 3.7B); however, this did not reach statistical significance. Together, these data imply a disconnect between the aerosolization of particles and the aerosolization of *Mtb*, at least for the three respiratory manoeuvres tested here.

The extent of aerosolization of *Mtb* depends predominantly on manoeuvre frequency

Knowing the concentration of *Mtb* per volume of bioaerosol suggested the potential to gain useful insight into the relative contributions of cough and TiBr to the daily production of *Mtb*. To this end, we first compared the numbers of bacilli produced per manoeuvre: on average, TiBr produced 2.6- and 3.2-fold fewer *Mtb* per manoeuvre compared to FVC and cough, respectively (Figure 3.8A). Next, we extrapolated the values for the average number of *Mtb* bacilli per manoeuvre and the average frequency of manoeuvres per day to estimate daily *Mtb* production. Because FVCs are artificial, directed manoeuvres that are performed only under specific instruction, we used TiBr and cough for this calculation.

Our data revealed that participant TiBr occurred at a rate of one breath every 3.9 seconds, suggesting approximately 22,047 tidal breaths over 24 hours. Because we did not directly measure the frequency of spontaneous coughs, we estimated 24-hour cough frequencies from published data[170], with a median of 466 coughs/day (first quartile, 234; last quartile, 551). We then

used a constant maximum number of breaths per day (22,047) and assumed that, for each cough, there would be one fewer breath. The average numbers of *Mtb* bacilli produced by TiBr and cough were then calculated, and the relative proportions determined by dividing the number per manoeuvre by the total. This enabled an estimation of the relative contribution per day for an average person with an increasing number of coughs (Figure 3.8B).

According to this estimation, cough contributed between 3% and 7% of the total number of *Mtb* bacilli released, with TiBr consistently producing over 93%. Together, these data suggest that coughing is likely to produce significantly fewer bacilli per day than TiBr. That is, whereas the higher per event number and velocity of bacillary release might ensure an important (perhaps critical) role for coughing in disease transmission in short contacts, for typical exposures in high-risk settings (on public transport, at workplaces, schools, *etc.*[102]), TiBr is expected to contribute significantly to TB prevalence.

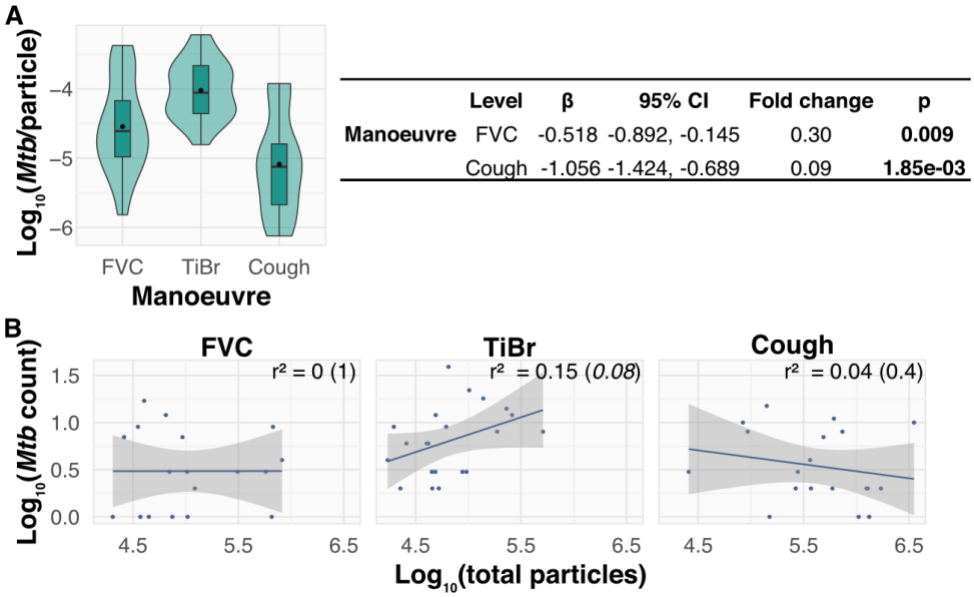

	Level	β	95% CI	Fold change	p
Manoeuvre	FVC	-0.518	-0.892, -0.145	0.30	**0.009**
	Cough	-1.056	-1.424, -0.689	0.09	**1.85e-03**

Figure 3.7: The concentration of Mtb relative to particle count for each respiratory manoeuvre. *(**A**) A comparison of the average number of Mtb per particle within the bioaerosol, presented on a logarithmic scale and adjacent to the results from a linear mixed model. The β coefficients and 95% CIs are presented with fold-change relative to TiBr. (**B**) Correlation assessment between log_{10}(particle count) and log_{10}(Mtb count), with the results of a Pearson's correlation (r^2 and p value in parentheses). CI = confidence interval.*

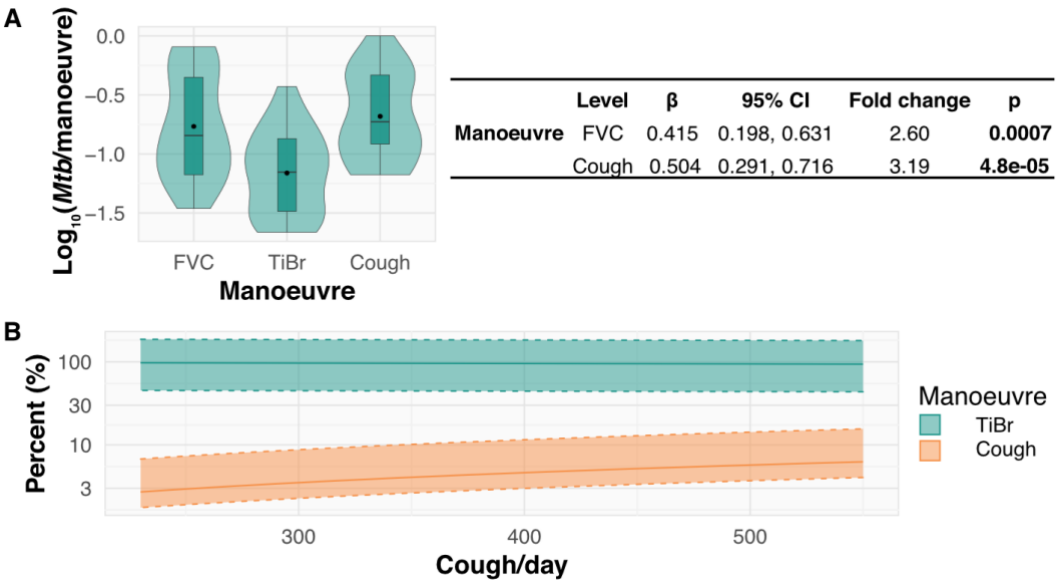

	Level	β	95% CI	Fold change	p
Manoeuvre	FVC	0.415	0.198, 0.631	2.60	**0.0007**
	Cough	0.504	0.291, 0.716	3.19	**4.8e-05**

Figure 3.8: The relative contribution of Mtb by each respiratory manoeuvre. *(**A**) A plot of the average number of Mtb per manoeuvre with the results of the linear mixed model. The β coefficients and 95% CIs are presented with fold-change relative to TiBr. (**B**) The relative contribution of bacteria per day (percent). We used the median frequency of breaths in five minutes to estimate an average of 22,047 breaths per day. We then assumed that for every cough, there would be one fewer breath over a range from 234–551 coughs. At each cough frequency, we determined the average number of bacilli per breath or per cough. We then estimated the percentage contribution of aerosolized Mtb that each manoeuvre made relative to the total. Therefore, the solid lines represent the percentage daily contribution to the aerosolization of Mtb made by an average person through breathing (green) or coughing (orange). To estimate the relative contribution of individuals with a higher or lower propensity for Mtb aerosolization per manoeuvre, the same procedure was followed for the Mtb concentrations corresponding to the upper and lower quartiles, respectively. These results are depicted by the dashed lines and indicate the percentage increase or decrease that could be expected from the upper and lower quartiles of Mtb aerosolization per manoeuvre, respectively. These results indicate that, even for an individual generating over 500 coughs per day with each cough producing numbers of Mtb in the upper quartile, breathing is likely to be the major contributor to Mtb aerosolization. CI = confidence interval.*

Discussion

Cough has traditionally been considered the primary means of TB transmission[75]. The result is that TB transmission research has predominately focused on factors including cough induction[199], frequency,

and the cough-borne *Mtb* bacillary load[70]. However, the absence in all studies of a comparator respiratory manoeuvre[119,127,172] has rendered impossible any assessment of alternative contributory mechanisms.

Transmission by aerosol requires the aerosolization of particles from the site of infection[200]. For *Mtb*, which infects the peripheral lung and alveolar spaces[201], the proposed mechanism of particle aerosolization is fluid film rupture[191]. According to this model, particles are produced during inspiration by alveolar reopening and released through expiration[95]. Factors impacting particle release are therefore the rate of inspiration and the depth of expiration[95], with a recent study comparing deep exhalation (analogous to FVC in this study) and cough finding no significant difference in the number of *Mtb* aerosolized between the two manoeuvres[194]. For these reasons, we hypothesised that TiBr might contribute to the aerosolization of *Mtb*. Therefore, we sought in this study to directly compare the capacity for particle and *Mtb* aerosolization via three defined respiratory manoeuvres: cough, FVC, and TiBr.

We sampled bioaerosols from 38 symptomatic, TB-positive participants before the onset of chemotherapy. Consistent with findings from similar studies, 88% of participants produced at least one bioaerosol sample that was positive for *Mtb*[170,193,194], a marked increase over culture-based cough-sampling techniques[172]. Our results also indicated that all three respiratory manoeuvres were equally likely to produce *Mtb*, with TiBr, FVC, and cough returning positive signals in 66%, 70%, and 65% of samples, respectively. If extrapolated on the basis of estimated daily manoeuvre frequency, these observations imply that TiBr could contribute more than 90% of the daily aerosolized *Mtb* across a range of cough frequencies, a conclusion consistent with the lack of correlation between *Mtb* aerosolization and cough frequency[170].

The cough-independent generation of bioaerosol from the peripheral lung is accentuated by deep exhalation. In a continuation of the work outlined in chapter two, Patterson *et. al.,* reported no significant difference in the propensity for *Mtb* aerosolization between forced exhalation and induced cough[194]. The BBM was used for the forced exhalation samples in that work. To ensure continuity, we have again included a manoeuvre involving forced exhalation; in this case, replacing the BBM with FVC. This change was motivated by the inherent difficulty in explaining the BBM to participants, undermining attempts to standardise. Like BBM, FVC ensures forced exhalation and, in addition, benefits from wider application in respiratory research and easier reproducibility in trial settings, making inter-manoeuvre comparisons more reliable.

Establishing a sampling algorithm appropriate for three distinct respiratory manoeuvres is challenging. However, the total number of particles produced during FVC and TiBr sampling were similar, with the cough producing approximately fourfold more particles. This suggested that, despite differences in sampling algorithms, the risk of under-sampling any manoeuvre was low. In addition, we saw significant variation between participants, spanning two orders of magnitude, consistent with previous observations[202].

Per manoeuvre, TiBr produced significantly fewer particles than both FVC and cough, with cough producing the most particles. Although it is tempting to speculate that the turbulence of the expired air played a role in the increased number of particles produced by cough, this interpretation seems unlikely given the similarity in particle counts for cough and FVC. Considering cough and FVC are quite different in the rate of expiration, it might be instructive that both these manoeuvres require deep inspiration: the inference, then, that the rate of expiration plays a minimal role in aerosol generation is consistent with a fluid-film rupture model of aerosol generation in the peripheral lung[95]. This is also consistent with the similarities in size distributions of particles between both participants and respiratory manoeuvres. Although the absolute counts per category varied between manoeuvres, the proportional compositions within each size category were conserved (an observation that supports the inference that the mechanism of particle production is consistent across the three respiratory manoeuvres)[96,202].

The average cumulative amount of *Mtb* aerosolized by each participant was 12.6 (max = 52), consistent with the results reported in the previous chapter. However, owing to continued enhancements of our bioaerosol collection system (Figure S2.1 → Figure S3.1) and the switch from indirect to direct bioaerosol capture[176], participants were sampled for approximately 15 minutes in this study versus the 60-minute sampling duration reported in chapter two. All three respiratory manoeuvres produced consistently low concentrations of *Mtb*, with a mean count of 3.9 (max = 21), 5.9 (max = 39), and 3.4 (max = 15) for FVC, TiBr, and cough, respectively. TiBr samples tended to have a twofold higher rate of *Mtb* aerosolization compared to both FVC and cough; however, these differences were not significant. As noted above, the probability of a sample returning a positive result was consistent for all respiratory manoeuvres. Notably, among the participants who generated at least one positive sample, most (96%) produced *Mtb* within their FVC and/or TiBr sample.

Contrary to our expectations, the concentration of *Mtb* bacilli per particle was 70% or 90% lower in FVC and cough, respectively, compared to TiBr. In addition, no correlation was observed between particle number and *Mtb* count, even when stratified by participant. Together, these data suggest that variation in particle production alone is insufficient evidence to identify infectious patients and that applications to reduce particle production seem unlikely to reduce infectiousness[98].

The occurrence of spontaneous cough events might be advanced as a potential confounder of any attempt to measure *Mtb* (and particle) release during TiBr sampling. The design of our collection platform ensures that we can rule out this possibility. During TiBr sampling, no adjustment or modification is made to the sampling method to accommodate (or account for) coughs. That is, particle detection (via the particle sizer) and collection are agnostic of cough events. This is important because it enables the identification, via retrospective analysis of the raw particle count data, of the occurrence and frequency of spontaneous coughs for each participant sampled and, consequently, the impact on *Mtb* (and particle) count. From this analysis (summarised in Figures 3.5C&D and S3.7), we determined that spontaneous coughing occurred in a minority (11/33) of participants sampled, with the majority (22/33) of participants showing no evidence of cough during TiBr sampling. Interestingly, we determined that, on average, these participants spontaneously coughed 1.55 times in five minutes of TiBr sampling. As such, by simple extrapolation (1.55 coughs * 24 hours * 12/minute [that is, the average number of coughs in five minutes multiplied by the number of five-minute windows during a day]), we calculated an average of 466.4 coughs/day. This reassured us both in our sampling methodology and by comparison to the cough-frequency data obtained from Williams and colleagues[170].

Consistent with our observations from induced cough, the occurrence of spontaneous coughs during TiBr sampling resulted in a trend toward increased particle counts but did not increase the number of *Mtb* detected within these samples. It was notable, too, that the participant who produced the greatest number of *Mtb* organisms during TiBr sampling did not cough. Together, these results imply the potential importance of interindividual variability in TB transmission and, at the same time, caution against the assumption that cough is the major determinant of *Mtb* release. In practical terms, they suggest that both induced and spontaneous cough may be unnecessary in studying *Mtb* transmission, a potentially important innovation given the strenuous nature of the induced cough, especially for unwell patients with underlying lung pathology.

Despite the apparent unlinking of particle count and *Mtb* aerosolization, the sizeable increase in aerosol production during FVC and cough manifest as a threefold increase in *Mtb* aerosolization for these manoeuvres compared to TiBr. However, when extrapolated to daily estimates, the relatively high frequency of breathing compared to coughing suggests that, over time, TiBr might represent a major source of *Mtb* aerosols, as suggested previously[191,192]. We calculated that during any single day, breathing could contribute more than 90% of the *Mtb* aerosolized by a TB-positive individual.

Limitations

Our study had several limitations that urge caution in interpreting these findings. The sample collection algorithm was not consistent for all respiratory manoeuvres (TiBr samples were primarily defined by time *versus* FVC and cough that were defined by event number), and the particle collection and measurement apparatus were connected in parallel and not in series. Consequently, extrapolations were required to estimate the total number of particles and organisms present in the entire bioaerosol. In addition, no work was done to determine the effect of the sequential order of manoeuvres on bioaerosol production; for example, the strict implementation of the FVC → TiBr → cough (Figure 3.2A) sequence could have impacted particle and *Mtb* production through participant exhaustion or particle clearance. That said, we did separate FVC and cough samples to ensure that TiBr provided a rest period between strenuous samples. In addition, the occurrence of spontaneous coughs during TiBr sampling did not impact the aerosolization of *Mtb,* and there was not a constant downwards trend in the numbers of *Mtb* between the three manoeuvres, further suggesting that manoeuvre order might not be a confounder of *Mtb* aerosolization.

Another limitation is that the participants in this study presented with TB symptoms and were diagnosed TB-positive via GeneXpert. Therefore, we cannot conclude the relative importance of TiBr to asymptomatic transmission. Although our data indicate that significant concentrations of *Mtb* are aerosolized daily independent of participant cough, further work is required to investigate this hypothesis in GeneXpert- negative, asymptomatic individuals. This is a challenging task that will require cross-sectional sampling in our study community. It is also important to note that, owing to technical challenges inherent in studying spontaneous cough over short sampling periods, we only studied induced cough, which may not be as infectious; for example, owing to the fact that specific pathological and/or signalling events might be required to precipitate natural expulsion of irritants[199]. Nevertheless, we were able to detect spontaneous coughs in a

proportion of TiBr samples, with no discernible effect on the overall production of *Mtb*. A further limitation is that, in estimating cough frequency per hour, we assumed that the rate was consistent throughout the day. This is a strong assumption, and it is more likely that coughs cluster into discrete events with multiple coughs occurring at a time, suggesting potential outbursts of infectious aerosol production. Finally, although it might reasonably be assumed that *Mtb* bioaerosol counts are directly linked to infectiousness, this has not been formally demonstrated.

Conclusion

Despite these limitations, we interpret our results as indicating that TiBr might be a significant contributor to *Mtb* transmission. This has significant ramifications for both transmission studies and intervention strategies. Firstly, bioaerosol capture lends itself to a non-invasive participant sampling. Although the impact of induced cough on a participant is relatively low, if a less invasive sampling algorithm can be applied, it should be. Secondly, standard interventions targeting disease transmission, such as active screening for symptomatic individuals, may not be effective. Because bioaerosol sampling offers the potential to identify infectious individuals well in advance of any typical screening regimen, it may provide a novel means to identify and treat infectious individuals irrespective of the presence or severity of symptoms.

A paradigm in which cough is the primary driver of TB transmission places disproportionate emphasis on lung pathology as essential for *Mtb* aerosolization. Moreover, it appears inconsistent with key epidemiological observations that increasingly recognise the likely role of subclinical TB as a source of TB transmission. Consequently, understanding how *Mtb* bacilli are aerosolized is of critical importance to curbing the epidemic, especially in high-burden settings

Chapter 4 - Concluding remarks

"**Such is hope**, Heaven's own gift to struggling mortals; pervading, like some subtle essence from the skies, all things, both good and bad; as universal as death, and more infectious than disease!"

The Life and Adventures of Nicholas Nickleby, Charles Dickens[1]

The RASC was developed as an efficient bioaerosol sampler, compatible with several methods for the capture and detection of *Mtb*[99,100]. The successful detection of *Mtb* DNA in liquid-captured samples combined with the visualization of whole bacilli on SEM motivated for the shift from solid to liquid capture and the development of a microscopy-based method for the specific detection of *Mtb*.

This thesis combined bespoke nanowell devices with the novel fluorescent probe, DMN-tre, to facilitate the microscopic detection of viable *Mtb* bacilli in TB patient bioaerosols following liquid capture within the RASC. This approach provided several advantages over previously utilized technologies for the detection of *Mtb* in bioaerosol samples.

The detection of *Mtb* in 90% of TB patients within 24 hours of bioaerosol collection was a considerable advancement over culture-based approaches, while providing a sensitivity equivalent to that of molecular techniques. Unlike both culture- and molecular-based approaches, however, the direct visualization of bacilli provided a first glimpse into the morphological and metabolic characteristics of aerosolized *Mtb*, with the noteworthy observation of bacterial clumps in some samples.

Despite these advances in our ability to enumerate aerosolized *Mtb*, an important question remained: how are *Mtb* bacilli aerosolized? Cough-based studies perpetuate the belief that cough is the dominant source of aerosolized *Mtb*; however, the lack of any comparative manoeuvre has rendered this conclusion impossible to prove, while face-mask sampling studies provide strong evidence that cough-frequency and *Mtb* aerosolization are not correlated. Although it constitutes a positive attribute of face-mask sampling (owing to the capacity for capture of maximum biomass), the collection of bioaerosols from all naturally occurring respiratory manoeuvres precludes understanding the number of bacilli released per manoeuvre.

The complexity of the RASC necessitates skilled personnel to facilitate its functioning, reducing its scalability and cost-effectiveness relative to face-mask sampling. However, advantageously, this complexity enables the real-time measurement of several important factors during participant sampling; most notably, particle counts and CO_2 concentration. As such, we compared the extent of *Mtb* aerosolization between three distinct respiratory manoeuvres; namely, FVC, TiBr, and cough. Based on the number of *Mtb* released per respiratory manoeuvre and the frequency at which each manoeuvre is likely to occur per day, we conclude that manoeuvre frequency is the primary driver of the rate of *Mtb* aerosolization, and not the per event number.

The sensitive microscopic method for the detection of *Mtb* in paucibacillary samples developed during this thesis worked synergistically with the technically advanced RASC, enabling the holistic investigation of *Mtb* aerobiology; from the bacillary size, shape, and metabolic state to the specific respiratory manoeuvres responsible for releasing them.

Despite these advances, further improvements are required to increase the utility of this method.

Sample capture and concentration

The current method for the liquid-capture of patient-derived bioaerosols results in a significant dilution of the sample, from 1 nL to 5 mL. Additionally, the current design of the nanowell-arrayed device is such that each microwell has a maximum capacity of 20 µL. Therefore, all sample processing steps, from initial concentration to DMN-tre staining, occur off the device, increasing the likelihood that *Mtb* bacilli are lost during manipulation.

Several iterations of the nanowell devices were fabricated and tested, with the primary goal being to compare alternative nanowell structures and plastic compositions. In addition, some iterations were designed such that the volume capacity of each well was increased to 200 µL, facilitating on-device processing after the initial concentration step. Typically, these designs weren't implemented, as the increased well capacity was combined with suboptimal nanowell layouts or plastic compositions. Although this suggested that the fabrication of an improved device was possible, the poor bacterial growth observed in serial imaging experiments stalled further development of these devices. Moreover, continued improvements to the RASC significantly reduced the extent to which background debris obscured the microscopy, reducing the need for the nanowell arraying of the sample. Currently, we are testing the applicability of 96-well imaging plates to improve sample processing and on-device culture.

An alternative to reducing the number of processing steps required, thereby increasing the sensitivity of this approach, is to reduce the dilution that occurs during bioaerosol capture. Although not yet implementable, significant advances have been made in the development of a 'virtual impactor'. This device captures patient-derived bioaerosols into a single drop, targetable to 1mm^2 area on the base of any compatible device. Switching to this technology would reduce the need for sample processing steps, thereby increasing the sensitivity of this method.

Mycobacterium tuberculosis detection

What we call *Mtb*

When this work was initiated, our intention was not to use DMN-tre as the definitive identifier of *Mtb* bacilli; rather, the DMN-tre signal (and incorporation/uptake profile) was intended to be part of a suite of tools used in conjunction for this purpose. However, the challenges of working with so few bacilli imposed technical limitations as to what techniques could be applied. For this reason, developing correlative techniques to increase the specificity of *Mtb* identification represents a crucial sphere for future research.

To aid in the identification of *Mtb* in bioaerosol samples, we determined that cell width was the morphological characteristic of *Mtb* subject to the least variation. Applying this criterion, bacilli were only identified as putative *Mtb* if they were both DMN-tre-positive and between 0.4–0.8 μm in width. Problematically, our understanding of *Mtb* morphology is primarily driven by experience of bacilli cultured in different media and under various laboratory conditions. As such, the possibility exists that we are overlooking non-canonical morphologies of *Mtb* in these samples. A correlative approach to *Mtb* detection will aid in the identification of novel *Mtb* morphologies in bioaerosol samples.

The application of a more specific fluorescent probe would aid greatly in the identification of *Mtb*. However, when this work initiated, DMN-tre was the only viable candidate for the specific detection of *Mtb* in extremely paucibacillary samples. As this work progressed, additional candidates were developed and available for testing. Unfortunately, none of the probes tested outperformed DMN-tre, supporting the need for continued design and development of novel probes specific for *Mtb*.

Automated imaging and image analysis

A current limitation of this work is the time-consuming nature of sample scanning. This has been a key motivator of switching back to glass-bottomed imaging devices, as hardware autofocus modules on the microscope do not work on plastic devices. However, imaging itself is not the only limitation. The relatively low contrast and high noise of the resulting images have impeded quantitative assessment of the images from all participants. As such, more work needs to be done in the imaging and image analysis component of this work.

PATIENTS WE RECRUIT

All bioaerosol sampling conducted in this thesis was performed on GeneXpert-positive participants, facilitating the establishment of a novel method for the detection of aerosolized *Mtb*. Although the resolution of this technique enabled a per-manoeuvre estimation of *Mtb* release, limiting participant sampling to TB-positive individuals provided insufficient evidence to understand the community dynamics of *Mtb* transmission or fully answer the questions of when *Mtb* are aerosolized, and by whom.

Our priority now is the deployment of the RASC to identify viable *Mtb* in bioaerosols collected from potentially infectious subclinical and/or asymptomatic cases. The capacity for non-invasive capture and isolation of viable *Mtb* from bioaerosol within 24 hours of collection also supports the potential utility of the RASC to measure the impact of TB treatment on the viability of *Mtb* bioaerosol release.

Two ongoing applications of the microscopic method developed in this thesis are intended to address these limitations. The first is a cohort study recruiting patients with suspected pulmonary TB from TB clinics in Ocean View and Masiphumelele[177]. Patients in this study are recruited directly following diagnosis as either GeneXpert-positive TB, GeneXpert-negative TB, and TB not diagnosed. Where required, participants are initiated onto standard TB chemotherapy directly after bioaerosol sampling. Participants are followed and resampled periodically for six months, giving insight into the differing capacity for *Mtb* aerosolization between the three groups, as well as the effect of treatment.

Chapter three of this thesis outlined the role of TiBr in the aerosolization of *Mtb* and proposed this as a mechanism by which asymptomatic *Mtb* transmission may be possible. However, that work sampled GeneXpert-positive, symptomatic TB patients exclusively. The second ongoing study is focussed on recruiting healthy Masiphumelele community members at a single time point. Through this study, it will be possible to conclude whether healthy individuals are capable of aerosolizing *Mtb*. Moreover, to increase the understanding of the community dynamics of *Mtb* transmission in this setting, captured bioaerosols are cultured for 50 days; where culture is successful, whole-genome sequencing of the *Mtb* bacilli is attempted.

So, although the work contained within this thesis cannot definitively conclude on the extent to which asymptomatic transmission contributes to TB incidence in South Africa, that question is being investigated using the technologies and techniques developed in this thesis.

Closing the loop

Finally, while this technology enables the detection of viable bacilli, like all aerosol capture methods it does not provide a measure of infectiousness. Ascertaining which *Mtb* isolates go on to infect new individuals and cause TB disease will require innovative approaches toward "closing the loop"; that is, demonstrating productive infection of a new host following release. Historically, this has been achieved primarily by demonstrating infection of animals[203], however, the application of genomic epidemiology or a macrophage infection model in combination with RASC-enabled bacillary capture, perhaps in closed community (or even household) settings, offers a modern alternative. For now, the planned modifications to our platform are primarily informed by the need to enable multi-omic analyses of the single-cell organisms isolated from patient aerosols to generate insights that can be pursued in the human host.

Conclusions

This thesis has detailed the development of a novel, microscopy-based technique for the identification of *Mtb* within liquid-captured bioaerosols. This technique showed an improved sensitivity and reduced turnaround time over culture, and an increased resolution for determining the aerobiology of *Mtb* over molecular-based techniques. The significance of this research was demonstrated in the per-manoeuvre quantification of *Mtb* release and the establishment of tidal breathing as potential major contributor to the aerosolization of *Mtb*. The methods developed and described here have been implemented in routine practice at the Aerobiology Research Centre (ARC) in Masiphumelele to facilitate ongoing research into the aerobiology of *Mtb*.

Supporting information

"'**It's very soon done**, sir, isn't it?'"

The Life and Adventures of Nicholas Nickleby, Charles Dickens[1]

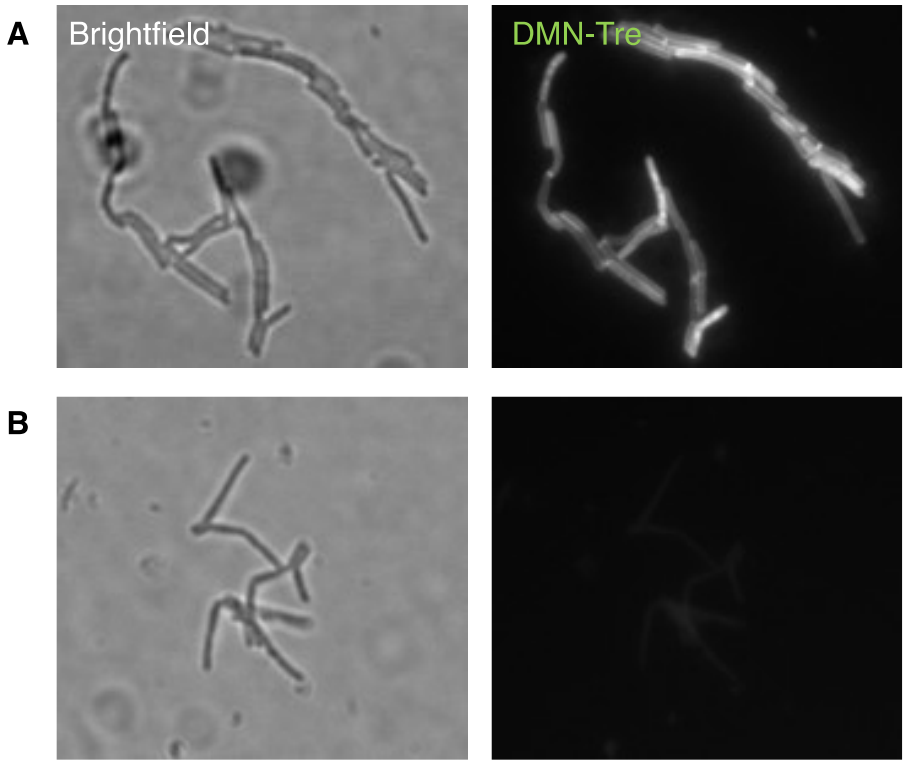

Figure S2.1: DMN-tre staining and visualization of Msm. *(**A**) Visualization of Msm stained with DMN-tre without any wash steps. (**B**) DMN-tre staining of heat-killed Msm.*

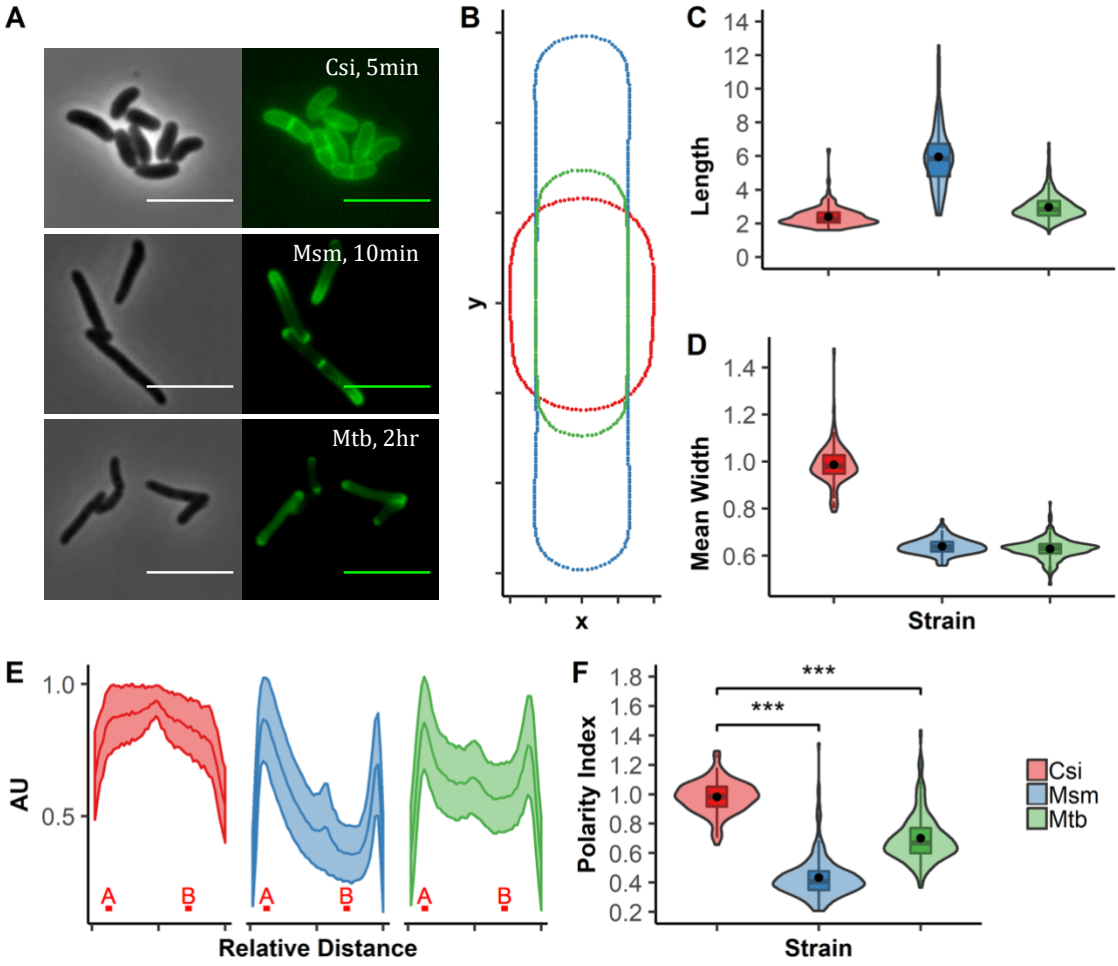

Figure S2.2: DMN-tre staining and cell morphology enable discrimination between Csi, Msm, and Mtb. *(**A**) Representative images of Csi Msm, and Mtb stained with DMN-tre for 5min, 10min and 2hours, respectively. (**B**) The average normalized shape of Csi (red), Msm (blue) and Mtb (green). (**C**) The length and (**D**) average width distributions of Csi (red), Msm (blue) and Mtb (green). (**E**) The relative fluorescence intensity profiles of DMN-tre for Csi (red), Msm (blue) and Mtb (green), indicating the relative positions which were used to calculate the polarity index: defined as the average relative intensity of B over A. (**F**) The polarity index for Csi (red), Msm (blue) and Mtb (green). Scale bars = 5μm. A Wilcoxon rank sum test was used, *** $p < 0.001$.*

SI

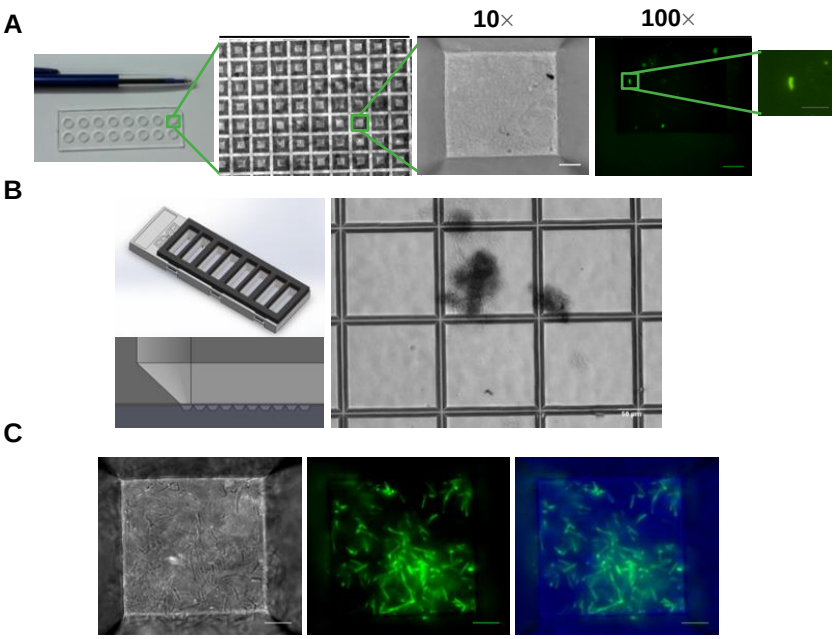

Figure S2.3: Custom-designed, nanowell-arrayed slides used in conjunction with DMN-tre pre-staining enables the immobilization and detection of mycobacteria. *(**A**) Images of the custom-designed slides used in this study, indicating the structure of the arrayed microwells at both 10× and 100× magnification, with a representative image of an immobilised Mtb bacillus stained with DMN-tre (100× scale bar = 10µm, and 5µm on enlarged image). (**B**) The latest design of the microwell-arrayed slide (10× magnification scale bar = 50µm). (**C**) A representative image (100× magnification) of patient sputum spiked with DMN-tre pre-stained Msm; Scale bar = 10µm.*

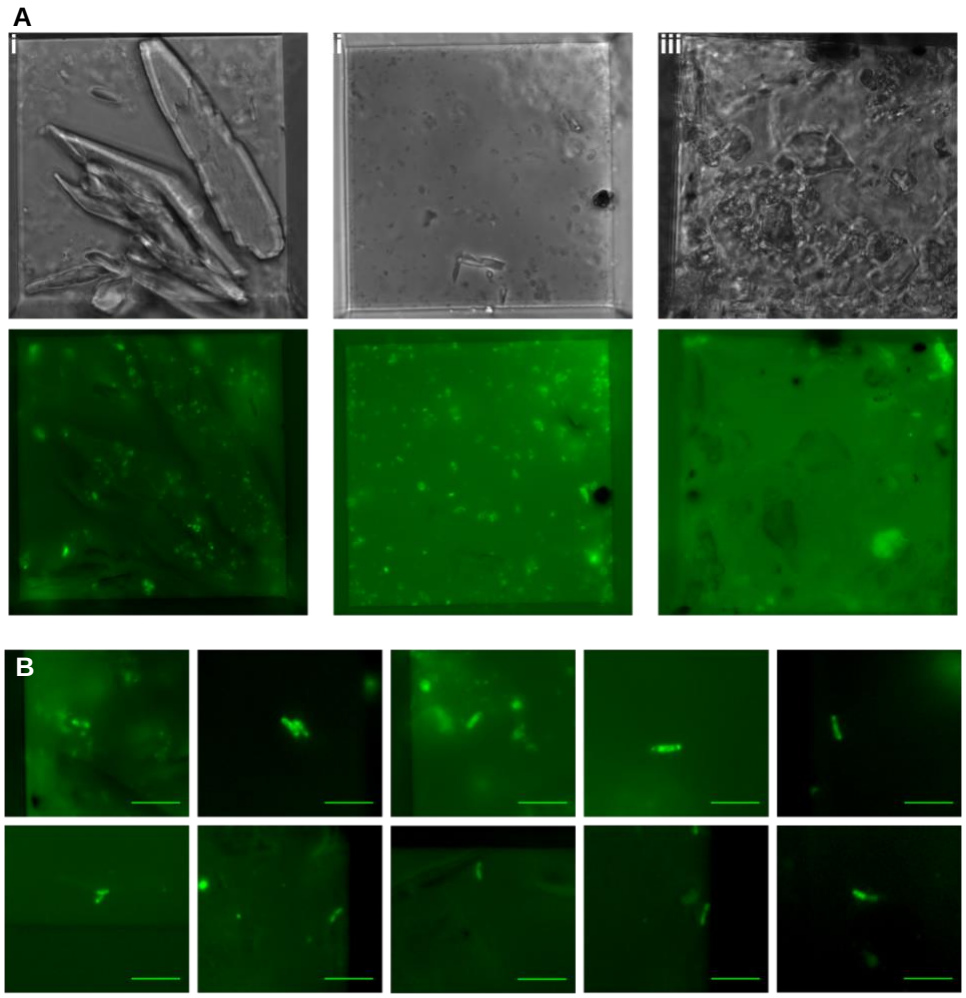

Figure S2.4: Debris and Mtb staining patterns commonly found within TB bioaerosols. *(**A**)Representative images of the three major categories of debris found within bioaerosol samples after overnight staining with 100 μM DMN-tre and visualization within a 50 × 50 μm nanowell. (i) Large, crystalline debris, (ii) small fluorescent debris, and (iii) granular debris. (**B**) Additional images of putatively identified Mtb.*

SI

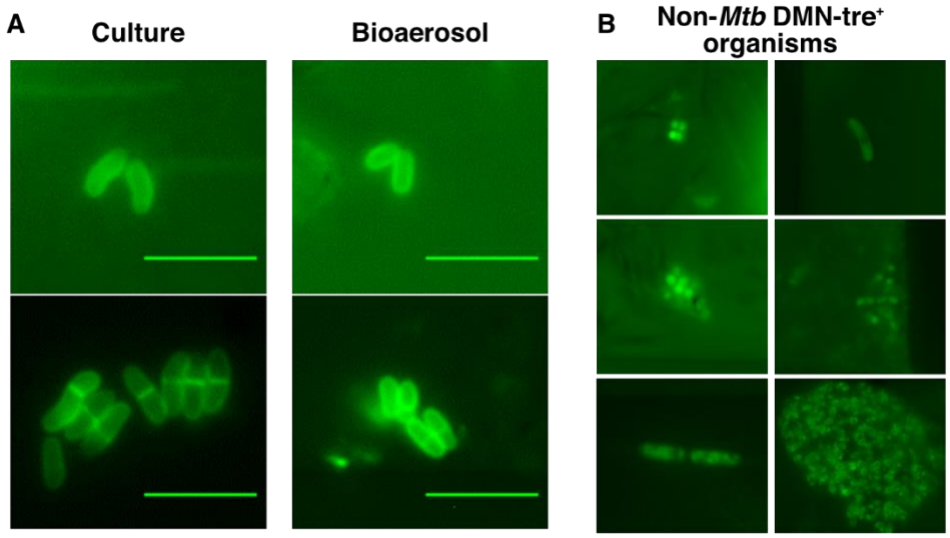

Figure S2.5: Exclusion of non-mycobacterial, DMN-tre-positive organisms detected in bioaerosol samples based on cell morphology. *(**A**) Representative images of (i) C. striatum cultured in LB broth during log-phase and stained with 100 uM DMN-tre for 5 min, and (ii) DMN-tre-positive organisms detected within a bioaerosol sample. (**B**) A panel of non-Mtb, DMN-tre-positive organisms, as determined by our inclusion criteria, identified in various bioaerosol samples. Scale bar, 5 µm.*

Figure S2.6: The Respiratory Aerosol Sampling Chamber (RASC).

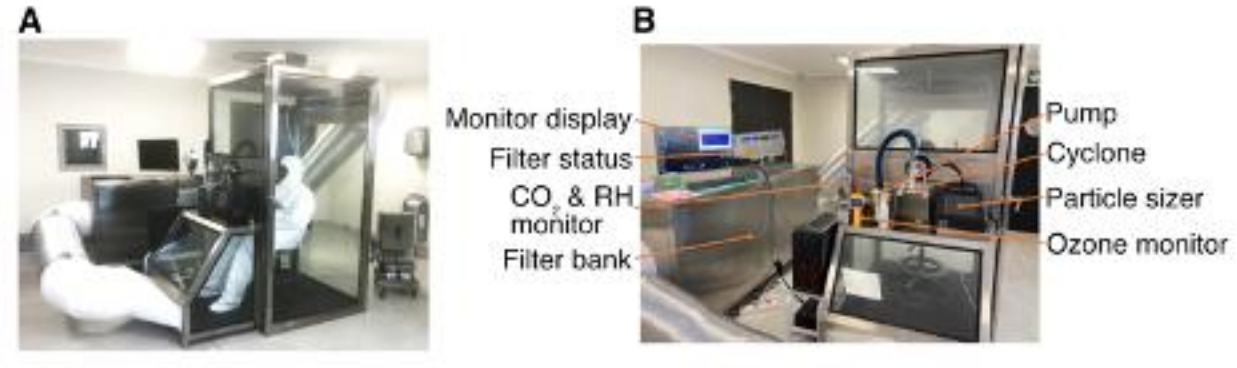

Figure S3.1: Updated Respiratory Aerosol Sampling Chamber (RASC).

SI

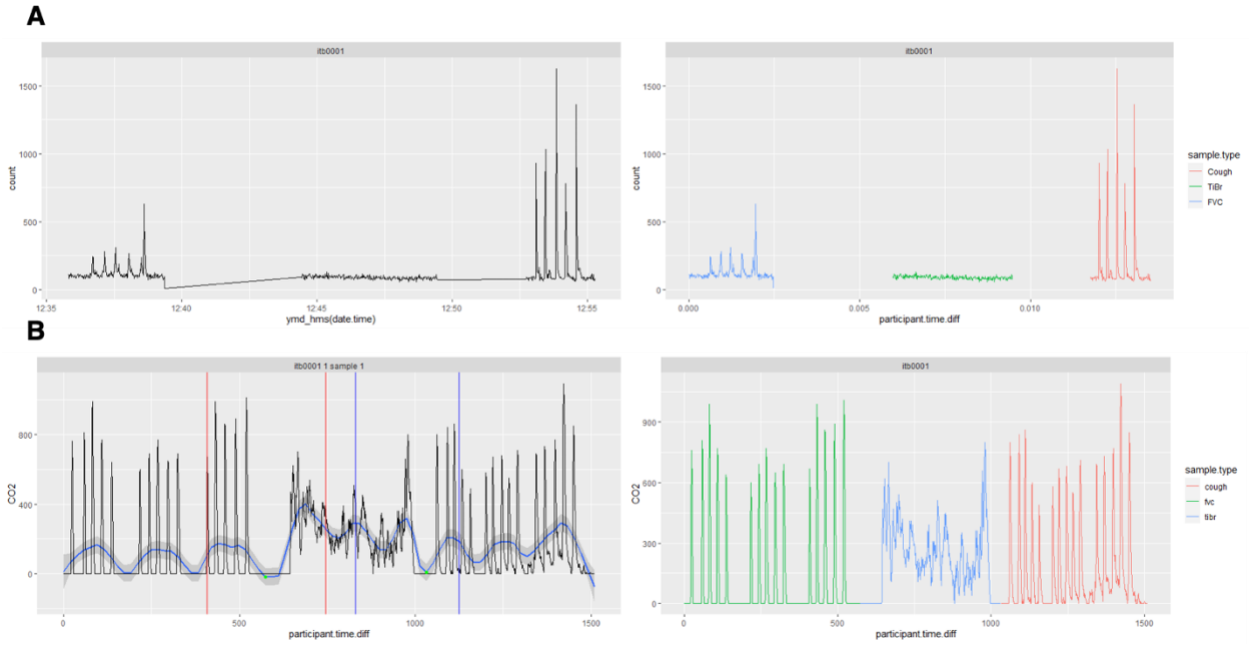

Figure S3.2: Examples of the automated manoeuvre detection algorithms for particle count and CO_2 data. *(**A**) A single particle dataset was captured for each participant during sampling; however, particles were only enumerated periodically during participant sampling. This resulted in large gaps in time, which were detected and used to split the data into the three respiratory manoeuvres. (**B**) CO_2 concentration measurements were captured throughout sampling, leaving no time gaps for splitting manoeuvres. To separate the CO_2 measurements according to respiratory manoeuvre, the data were smoothed and the lowest minima in the regions indicated between the red and blue vertical lines were detected: these positions corresponded to the end of FVC and TiBr sampling, respectively. These positions were readily detectable, as the breaks between manoeuvres were longer then within manoeuvre samples, generating long, contiguous zero measures for CO_2 concentration, thereby lowering the smoothed average detected for these sections.*

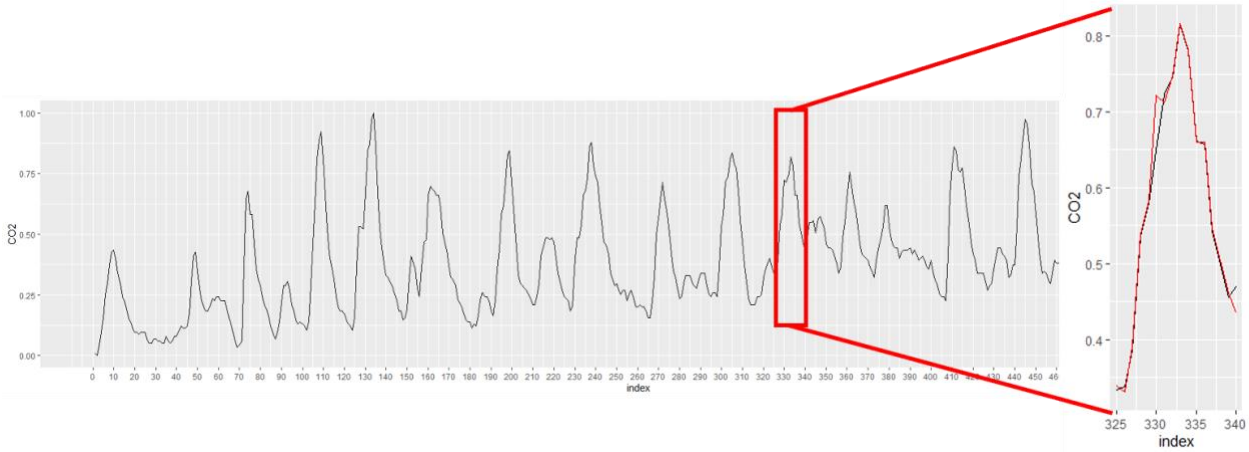

Figure S3.3: Example of the bespoke smoothing algorithm used to facilitate peak detection. *A peak, representing a single manoeuvre, was detected as a maximum flanked by two minima. Prior to smoothing, sharp kinks in the data prevented peak detection through the introduction of several minima and maxima within the peak. This can be seen in the right-hand panel in the ascending red line. A localised smoothing algorithm was written that detected and removed these kinks (black line, right panel) to facilitate the detection of the entire peak.*

SI

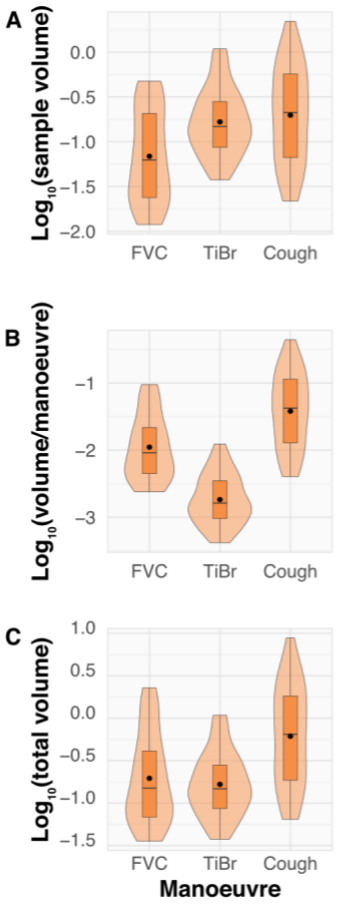

	Level	β	95% CI	Fold change	p
Manoeuvre	FVC	-0.387	-0.615, -0.158	0.41	**0.0015**
	Cough	0.075	-0.144, 0.294	1.19	0.5039

	Level	β	95% CI	Fold change	p
Manoeuvre	FVC	0.777	0.551, 1.004	6.0	**6.5e-09**
	Cough	1.317	1.100, 1.534	20.7	**<2e-16**

	Level	β	95% CI	Fold change	p
Manoeuvre	FVC	0.070	-0.169, 0.308	1.17	0.569
	Cough	0.568	0.340, 0.797	3.70	**8.8e-06**

Figure S3.4: Variation in volume of bioaerosol production by FVC, TiBr and cough. *A comparison of the (**A**) sample volume, (**B**) volume/manoeuvre and (**C**) total volume of particles during sampling. The adjacent tables contain the results of univariate linear mixed models for each. The beta-coefficient (β) and 95% confidence intervals (CI) are presented with fold-change relative to TiBr.*

SI

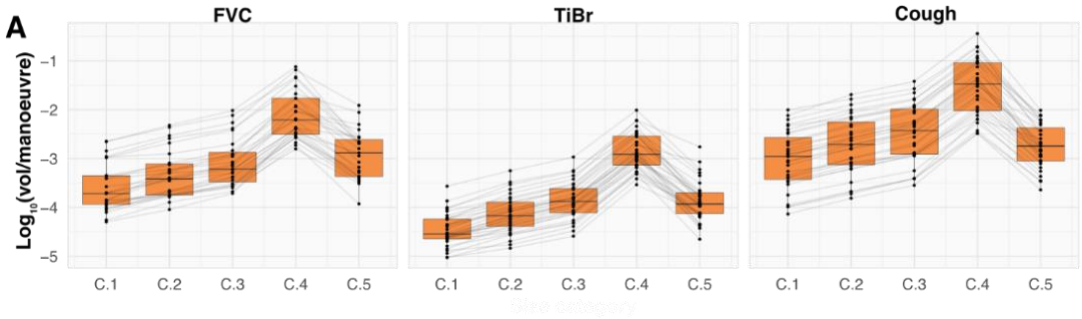

B

	Level	β	95% CI	Percent
Manoeuvre	FVC	**0.820**	0.727, 0.913	560.5
	Cough	**1.338**	1.250, 1.427	2079.5
Size category	C2	**-0.892**	-1.009, -0.776	-83.2
	C3	**-1.069**	-1.186, -0.952	-88.8
	C4	**-0.798**	-0.915, -0.682	-79.2
	C5	**-2.489**	-2.606, -2.372	-99.6
Random effects	PTID			31.3

C

	Level	β	95% CI	Percent
Manoeuvre	FVC	**0.820**	0.727, 0.913	560.5
	Cough	**1.338**	1.250, 1.427	2079.5
Size category	C2	**0.302***	0.185, 0.418	100.2
	C3	**0.563**	0.447, 0.680	265.9
	C4	**1.536**	1.420, 1.653	3337.8
	C5	**0.511**	0.394, 0.628	224.3
Random effects	PTID			31.3

Figure S3.5: The relative volume contribution of particles of various sizes is consistent between FVC, TiBr and cough. *(**A**) A comparison of the average volume per manoeuvre stratified by size category. Grey lines indicate the average volume of particles per manoeuvre stratified by size category and participant ID (PTID). Results of a mixed effects linear regression of average count (**B**) or volume (**C**) per manoeuvre against size category and manoeuvre. The beta-coefficients (β) and 95% confidence intervals (CI) are presented with fold-change relative to TiBr. p < 2e-16 for all coefficients, except where indicated by an asterisk, p = 5.63e-07.*

SI

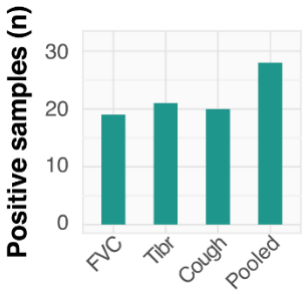

Figure S3.6. The detection of Mtb bacilli within each respiratory manoeuvre sample. *A comparison of the number of samples that were positive for aerosolized Mtb. The "pooled" variable represents the number of individuals who produced at least one positive sample.*

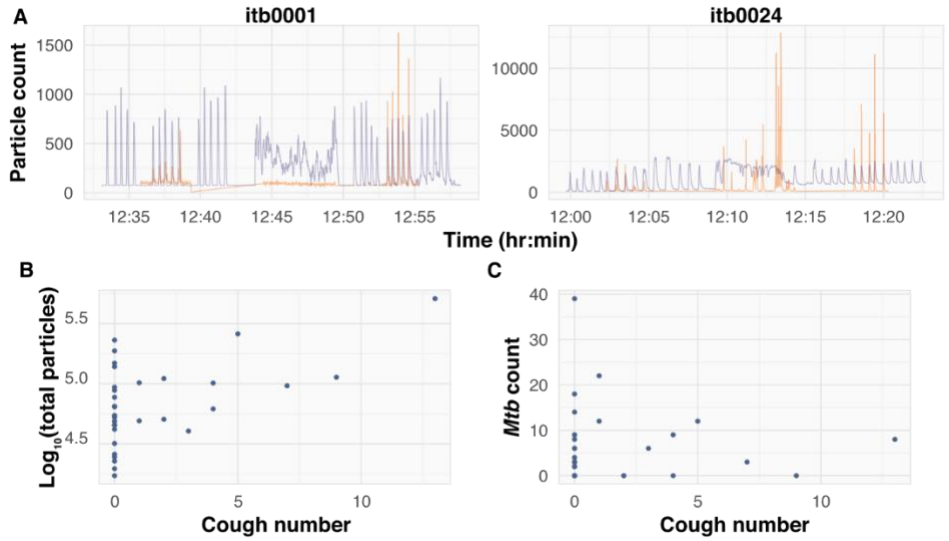

Figure S3.7. No association between spontaneous coughs and the aerosolization of total particles or Mtb during TiBr sampling. *(**A**) CO_2 (purple) and particle count (orange) versus time stratified by participant. Itb0001 represents an ideal sample collection; Itb0024 indicates the occurrence of spontaneous coughing during TiBr sampling. (**B**) Scatter plot of the total number of particles and spontaneous coughs detected during TiBr sampling. (**C**) Scatter plot of the number of putative viable Mtb bacilli and spontaneous coughs detected during TiBr sampling. Spontaneous coughs occurred in 11/33 participants, and the mean number of coughs was 1.55 per five minutes (max = 13).*

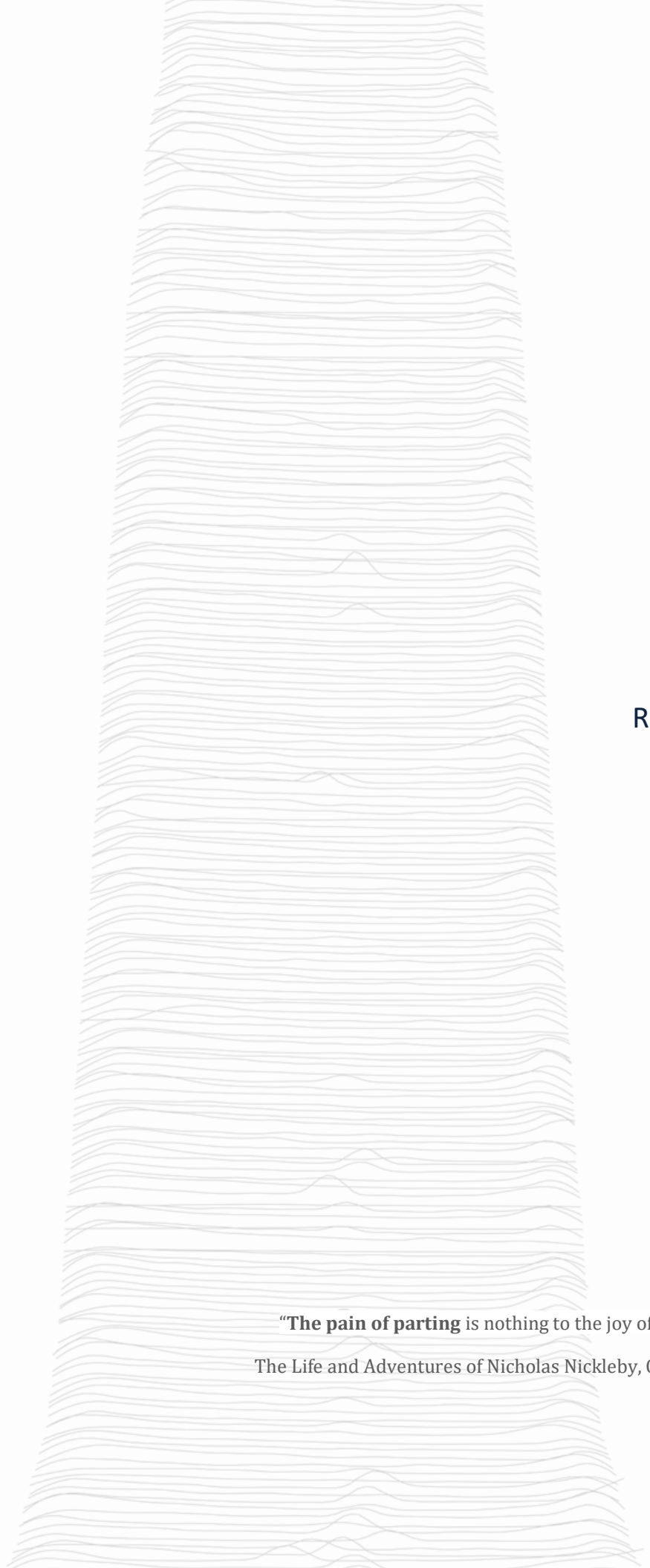

References

"**The pain of parting** is nothing to the joy of meeting again."

The Life and Adventures of Nicholas Nickleby, Charles Dickens[1]

1. Dickens C. *The life and adventures of Nicholas Nickleby*: New York: F.M. Lupton Pub. Co.; 1889.
2. Riley RL, Mills CC, Nyka W, et al. Aerial dissemination of pulmonary tuberculosis: A two-year study of contagion in a tuberculosis ward. *American Journal of Epidemiology* 1959; **142**(1): 3-14.
3. Gagneux S. Ecology and evolution of Mycobacterium tuberculosis. *Nature Reviews Microbiology* 2018; **16**(4): 202-13.
4. Barberis I, Bragazzi NL, Galluzzo L, Martini M. The history of tuberculosis: from the first historical records to the isolation of Koch's bacillus. *J Prev Med Hyg* 2017; **58**(1): E9-E12.
5. Daniel TM. The history of tuberculosis. *Respir Med* 2006; **100**(11): 1862-70.
6. Koch R. Die Aetiologie der Tuberkulose. *Mittheilungen aus dem Kaiserlichen Gesundheitsamte* 1884.
7. Hinshaw C, Feldman WH, Pfuetze KH. Treatment of tuberculosis with streptomycin: a summary of observations on one hundred cases. *Journal of the American Medical Association* 1946; **132**(13): 778-82.
8. Murray JF, Schraufnagel DE, Hopewell PC. Treatment of Tuberculosis. A Historical Perspective. *Annals of the American Thoracic Society* 2015; **12**(12): 1749-59.
9. Kaplan G. Tuberculosis control in crisis-causes and solutions. *Progress in Biophysics and Molecular Biology* 2020; **152**: 6-9.
10. Tiemersma EW, van der Werf MJ, Borgdorff MW, Williams BG, Nagelkerke NJD. Natural History of Tuberculosis: Duration and Fatality of Untreated Pulmonary Tuberculosis in HIV Negative Patients: A Systematic Review. *PLOS ONE* 2011; **6**(4): e17601.
11. Hermans S, Horsburgh Jr CR, Wood R. A Century of Tuberculosis Epidemiology in the Northern and Southern Hemisphere: The Differential Impact of Control Interventions. *PLoS ONE* 2015; **10**(8): e0135179.
12. Wood R, Bekker L-G. An epidemic uncurbed: tuberculosis in Cape Town, South Africa, 1910–2010. *Transactions of the Royal Society of South Africa* 2017; **72**(3): 234-41.
13. Andrews JR, Hatherill M, Mahomed H, et al. The Dynamics of QuantiFERON-TB Gold In-Tube Conversion and Reversion in a Cohort of South African Adolescents. *American Journal of Respiratory and Critical Care Medicine* 2015; **191**(5): 584-91.
14. WHO. Global Tuberculosis Report 2021. Geneva: World Health Organization, 2021.
15. Middelkoop K, Bekker L-G, Liang H, et al. Force of tuberculosis infection among adolescents in a high HIV and TB prevalence community: a cross-sectional observation study. *BMC Infectious Diseases* 2011; **11**(1): 156.
16. Koch A, Cox H. Preventing drug-resistant tuberculosis transmission. *Lancet Infect Dis* 2020; **20**(2): 157-8.
17. O'Garra A, Redford PS, McNab FW, Bloom CI, Wilkinson RJ, Berry MP. The immune response in tuberculosis. *Annu Rev Immunol* 2013; **31**: 475-527.
18. Ernst JD. The immunological life cycle of tuberculosis. *Nature Reviews Immunology* 2012; **12**: 581.
19. Gill WP, Harik NS, Whiddon MR, Liao RP, Mittler JE, Sherman DR. A replication clock for Mycobacterium tuberculosis. *Nat Med* 2009; **15**(2): 211-4.
20. Davis JM, Ramakrishnan L. The role of the granuloma in expansion and dissemination of early tuberculous infection. *Cell* 2009; **136**(1): 37-49.
21. Chackerian AA, Alt JM, Perera TV, Dascher CC, Behar SM. Dissemination of *Mycobacterium tuberculosis* is influenced by host factors and precedes the initiation of T-cell immunity. *Infect Immun* 2002; **70**(8): 4501-9.
22. Cohen SB, Gern BH, Delahaye JL, et al. Alveolar Macrophages Provide an Early *Mycobacterium tuberculosis* Niche and Initiate Dissemination. *Cell Host & Microbe* 2018; **24**(3): 439-46.e4.
23. Stallings CL, Glickman MS. Is *Mycobacterium tuberculosis* stressed out? A critical assessment of the genetic evidence. *Microbes and Infection* 2010; **12**(14): 1091-101.
24. Martin CJ, Cadena AM, Leung VW, et al. Digitally Barcoding *Mycobacterium tuberculosis* Reveals *In Vivo* Infection Dynamics in the Macaque Model of Tuberculosis. *mBio* 2017; **8**(3): e00312-17.
25. Houben RMGJ, Dodd PJ. The Global Burden of Latent Tuberculosis Infection: A Re-estimation Using Mathematical Modelling. *PLOS Medicine* 2016; **13**(10): e1002152.
26. Moyo S, Ismail F, Van der Walt M, et al. Prevalence of bacteriologically confirmed pulmonary tuberculosis in South Africa, 2017-19: a multistage, cluster-based, cross-sectional survey. *The Lancet Infectious Diseases* 2022.
27. Dorman SE, Nahid P, Kurbatova EV, et al. Four-Month Rifapentine Regimens with or without Moxifloxacin for Tuberculosis. *New England Journal of Medicine* 2021; **384**(18): 1705-18.

28. Zumla AI, Gillespie SH, Hoelscher M, et al. New antituberculosis drugs, regimens, and adjunct therapies: needs, advances, and future prospects. *The Lancet Infectious Diseases* 2014; **14**(4): 327-40.
29. Dartois V, Barry CE. A Medicinal Chemists' Guide to Lead Optimization for Tuberculosis. *Bioorganic & medicinal chemistry letters* 2013; **23**(17): 4741-50.
30. Barry CE, Boshoff HI, Dartois V, et al. The spectrum of latent tuberculosis: rethinking the biology and intervention strategies. *Nat Rev Micro* 2009; **7**(12): 845-55.
31. Schwartzman K, Menzies D. How long are TB patients infectious? *CMAJ* 2000; **163**(2): 157-8.
32. Calderwood CJ, Wilson JP, Fielding KL, et al. Dynamics of sputum conversion during effective tuberculosis treatment: A systematic review and meta-analysis. *PLOS Medicine* 2021; **18**(4): e1003566.
33. Dowdy DW, Basu S, Andrews JR. Is passive diagnosis enough? The impact of subclinical disease on diagnostic strategies for tuberculosis. *American journal of respiratory and critical care medicine* 2013; **187**(5): 543-51.
34. Pronyk P M, Makhubele M B, Hargreaves J R, Tollman S M, Hausler H P. Assessing health seeking behaviour among tuberculosis patients in rural South Africa. *The International Journal of Tuberculosis and Lung Disease* 2001; **5**(7): 619-27.
35. de Loureiro Maior M, Leborato Guerra R, Cailleaux-Cezar M, Eric Golub J, Barreto Conde M. Time from symptom onset to the initiation of treatment of pulmonary tuberculosis in a city with a high incidence of the disease. *Jornal brasileiro de pneumologia : publicacao oficial da Sociedade Brasileira de Pneumologia e Tisilogia* 2012; **38**(2): 202-9.
36. Wood R, Middelkoop K, Myer L, et al. Undiagnosed tuberculosis in a community with high HIV prevalence: implications for tuberculosis control. *Am J Respir Crit Care Med* 2007; **175**(1): 87-93.
37. Foster N, Vassall A, Cleary S, Cunnama L, Churchyard G, Sinanovic E. The economic burden of TB diagnosis and treatment in South Africa. *Social Science & Medicine* 2015; **130**: 42-50.
38. Fluegge K, Malone LL, Nsereko M, et al. Impact of geographic distance on appraisal delay for active TB treatment seeking in Uganda: a network analysis of the Kawempe Community Health Cohort Study. *BMC Public Health* 2018; **18**(1): 798.
39. Van der Walt M, Moyo S. The First National TB Prevalence Survey, South Africa 2018: Short report. 2021.
40. Finlay A, Lancaster J, Holtz TH, Weyer K, Miranda A, van der Walt M. Patient- and provider-level risk factors associated with default from tuberculosis treatment, South Africa, 2002: a case-control study. *BMC Public Health* 2012; **12**: 56-.
41. Kaona FAD, Tuba M, Siziya S, Sikaona L. An assessment of factors contributing to treatment adherence and knowledge of TB transmission among patients on TB treatment. *BMC Public Health* 2004; **4**: 68-.
42. Naidoo P, Theron G, Rangaka MX, et al. The South African Tuberculosis Care Cascade: Estimated Losses and Methodological Challenges. *The Journal of Infectious Diseases* 2017; **216**(suppl_7): S702-S13.
43. Schito M, Hanna D, Zumla A. Tuberculosis eradication versus control. *International Journal of Infectious Diseases* 2017; **56**: 10-3.
44. Padayatchi N, Daftary A, Naidu N, Naidoo K, Pai M. Tuberculosis: treatment failure, or failure to treat? Lessons from India and South Africa. *BMJ global health* 2019; **4**(1): e001097.
45. Aldridge BB, Barros-Aguirre D, Barry CE, 3rd, et al. The Tuberculosis Drug Accelerator at year 10: what have we learned? *Nat Med* 2021; **27**(8): 1333-7.
46. Katzir I, Cokol M, Aldridge BB, Alon U. Prediction of ultra-high-order antibiotic combinations based on pairwise interactions. *PLOS Computational Biology* 2019; **15**(1): e1006774.
47. Dartois V. The path of anti-tuberculosis drugs: from blood to lesions to mycobacterial cells. *Nature reviews Microbiology* 2014; **12**(3): 159-67.
48. Prideaux B, Via LE, Zimmerman MD, et al. The association between sterilizing activity and drug distribution into tuberculosis lesions. *Nature Medicine* 2015; **21**(10): 1223-7.
49. Dartois VA, Rubin EJ. Anti-tuberculosis treatment strategies and drug development: challenges and priorities. *Nature Reviews Microbiology* 2022.
50. Zhang Q, Lambert G, Liao D, et al. Acceleration of Emergence of Bacterial Antibiotic Resistance in Connected Microenvironments. *Science* 2011; **333**(6050): 1764-7.
51. Mandal S, Njikan S, Kumar A, Early JV, Parish T. The relevance of persisters in tuberculosis drug discovery. *Microbiology (Reading)* 2019; **165**(5): 492-9.

52. Balaban NQ, Helaine S, Lewis K, et al. Definitions and guidelines for research on antibiotic persistence. *Nature Reviews Microbiology* 2019.
53. Brauner A, Fridman O, Gefen O, Balaban NQ. Distinguishing between resistance, tolerance and persistence to antibiotic treatment. *Nat Rev Micro* 2016; **14**(5): 320-30.
54. Aldridge BB, Fernandez-Suarez M, Heller D, et al. Asymmetry and aging of mycobacterial cells leads to variable growth and antibiotic susceptibility. *Science (New York, Ny)* 2012; **335**(6064): 100-4.
55. Sakatos A, Babunovic GH, Chase MR, et al. Posttranslational modification of a histone-like protein regulates phenotypic resistance to isoniazid in mycobacteria. *Science Advances* 2018; **4**(5): eaao1478.
56. Hicks ND, Yang J, Zhang X, et al. Clinically prevalent mutations in *Mycobacterium tuberculosis* alter propionate metabolism and mediate multidrug tolerance. *Nature Microbiology* 2018; **3**(9): 1032-42.
57. Baym M, Lieberman TD, Kelsic ED, et al. Spatiotemporal microbial evolution on antibiotic landscapes. *Science* 2016; **353**(6304): 1147-51.
58. Levin-Reisman I, Ronin I, Gefen O, Braniss I, Shoresh N, Balaban NQ. Antibiotic tolerance facilitates the evolution of resistance. *Science* 2017; **355**(6327): 826-30.
59. Connolly LE, Edelstein PH, Ramakrishnan L. Why Is Long-Term Therapy Required to Cure Tuberculosis? *PLoS Med* 2007; **4**(3): e120.
60. Sharma A, Hill A, Kurbatova E, et al. Estimating the future burden of multidrug-resistant and extensively drug-resistant tuberculosis in India, the Philippines, Russia, and South Africa: a mathematical modelling study. *Lancet Infect Dis* 2017; **17**(7): 707-15.
61. Edlin BR, Tokars JI, Grieco MH, et al. An Outbreak of Multidrug-Resistant Tuberculosis among Hospitalized Patients with the Acquired Immunodeficiency Syndrome. *New England Journal of Medicine* 1992; **326**(23): 1514-21.
62. Dean AS, Tosas Auguet O, Glaziou P, et al. 25 years of surveillance of drug-resistant tuberculosis: achievements, challenges, and way forward. *The Lancet Infectious Diseases* 2022.
63. Udwadia ZF, Amale RA, Ajbani KK, Rodrigues C. Totally Drug-Resistant Tuberculosis in India. *Clinical Infectious Diseases* 2012; **54**(4): 579-81.
64. Klopper M, Warren RM, Hayes C, et al. Emergence and spread of extensively and totally drug-resistant tuberculosis, South Africa. *Emerg Infect Dis* 2013; **19**(3): 449-55.
65. Supply P, Warren RM, Bañuls A-L, et al. Linkage disequilibrium between minisatellite loci supports clonal evolution of Mycobacterium tuberculosis in a high tuberculosis incidence area. *Molecular Microbiology* 2003; **47**(2): 529-38.
66. Comas I, Chakravartti J, Small PM, et al. Human T cell epitopes of *Mycobacterium tuberculosis* are evolutionarily hyperconserved. *Nature genetics* 2010; **42**(6): 498-503.
67. Sreevatsan S, Pan X, Stockbauer KE, et al. Restricted structural gene polymorphism in the *Mycobacterium tuberculosis* complex indicates evolutionarily recent global dissemination. *Proceedings of the National Academy of Sciences* 1997; **94**(18): 9869-74.
68. Ramaswamy S, Musser JM. Molecular genetic basis of antimicrobial agent resistance in Mycobacterium tuberculosis: 1998 update. *Tubercle and Lung Disease* 1998; **79**(1): 3-29.
69. Reid MJA, Arinaminpathy N, Bloom A, et al. Building a tuberculosis-free world: The Lancet Commission on tuberculosis. *Lancet* 2019; **393**(10178): 1331-84.
70. Donald PR, Diacon AH, Lange C, Demers AM, von Groote-Biddlingmeier F, Nardell E. Droplets, dust and guinea pigs: an historical review of tuberculosis transmission research, 1878 -1940. *Int J Tuberc Lung Dis* 2018; **22**(9): 972-82.
71. Laschtschenko P. Ueber Luftinfektion durch beim Husten, Niessen und Sprechen verspritzte Tröpfchen. *Z Hyg Infekt* 1899; **30**: 125-38.
72. Heymann B. Ueber die Ausstreuung infectioser Tropfchen beim husten der Phthisiker. *Zeitschr Hyg Infectionskr* 1899; **30**: 139-62.
73. Heymann B. Versuche über die Verbreitung der Phthise durch ausgehustete Tröpfchen und durch trockenen Sputumstaub. *Zeitschrift für Hygiene und Infektionskrankheiten* 1901; **38**(1): 21-93.
74. Chaussé P. Nouvelles recherches sur la contagion de la tuberculose par l'air expiré pendant la toux,'. *Ann Inst Pasteur* 1916; **30**: 613-41.
75. Esmail H, Dodd PJ, Houben RMGJ. Tuberculosis transmission during the subclinical period: could unrelated cough play a part? *The Lancet Respiratory Medicine* 2018; **6**(4): 244-6.
76. Turner RD, Bothamley GH. Cough and the transmission of tuberculosis. *J Infect Dis* 2015; **211**(9): 1367-72.

77. Hippke E. Neue Veruche über die Bedeutung der Tropfchenfektion für die Ausbreitung der Lungenchwindsucht. *Zeitschr Hyg Infectionskr* 1921; **93**: 122-46.
78. Wang CC, Prather KA, Sznitman J, et al. Airborne transmission of respiratory viruses. *Science* 2021; **373**(6558): eabd9149.
79. Jimenez JL, Marr LC, Randall K, et al. What were the historical reasons for the resistance to recognizing airborne transmission during the COVID-19 pandemic? *Indoor Air* 2022; **32**(8): e13070.
80. Bourouiba L, Dehandschoewercker E, Bush John WM. Violent expiratory events: on coughing and sneezing. *Journal of Fluid Mechanics* 2014; **745**: 537-63.
81. Riley RL, Mills CC, O'Grady F, Sultan LU, Wittstadt F, Shivpuri DN. Infectiousness of Air from a Tuberculosis Ward. 1961.
82. Wells WF. Airborne Contagion and Air Hygiene. An Ecological Study of Droplet Infections. *Airborne Contagion and Air Hygiene An Ecological Study of Droplet Infections* 1955.
83. Nardell EA. Wells Revisited: Infectious Particles vs. Quanta of *Mycobacterium tuberculosis* Infection-Don't Get Them Confused. *Mycobact Dis* 2016; **6**(5): 1000231.
84. Rudnick S, Milton D. Risk of indoor airborne infection transmission estimated from carbon dioxide concentration. *Indoor air* 2003; **13**(3): 237-45.
85. Riley E, Murphy G, Riley R. Airborne spread of measles in a suburban elementary school. *American journal of epidemiology* 1978; **107**(5): 421-32.
86. Escombe AR, Moore DA, Gilman RH, et al. The infectiousness of tuberculosis patients coinfected with HIV. *PLoS Med* 2008; **5**(9): e188.
87. Escombe AR, Oeser C, Gilman RH, et al. The Detection of Airborne Transmission of Tuberculosis from HIV-Infected Patients, Using an In Vivo Air Sampling Model. *Clinical infectious diseases : an official publication of the Infectious Diseases Society of America* 2007; **44**(10): 1349-57.
88. Dharmadhikari AS, Basaraba RJ, Van Der Walt ML, et al. Natural infection of guinea pigs exposed to patients with highly drug-resistant tuberculosis. *Tuberculosis* 2011; **91**(4): 329-38.
89. Dharmadhikari AS, Mphahlele M, Stoltz A, et al. Surgical Face Masks Worn by Patients with Multidrug-Resistant Tuberculosis. *American Journal of Respiratory and Critical Care Medicine* 2012; **185**(10): 1104-9.
90. Dharmadhikari AS, Mphahlele M, Venter K, et al. Rapid impact of effective treatment on transmission of multidrug-resistant tuberculosis. *The international journal of tuberculosis and lung disease : the official journal of the International Union against Tuberculosis and Lung Disease* 2014; **18**(9): 1019-25.
91. Xu Y, Cancino-Muñoz I, Torres-Puente M, et al. High-resolution mapping of tuberculosis transmission: Whole genome sequencing and phylogenetic modelling of a cohort from Valencia Region, Spain. *PLOS Medicine* 2019; **16**(10): e1002961.
92. Kendall EA, Shrestha S, Dowdy DW. The Epidemiological Importance of Subclinical Tuberculosis. A Critical Reappraisal. *Am J Respir Crit Care Med* 2021; **203**(2): 168-74.
93. Sultan L, Nyka W, Mills C, O'Grady F, Wells W, Riley RL. Tuberculosis Disseminators. *American Review of Respiratory Disease* 1960; **82**(3): 358-69.
94. Issarow CM, Mulder N, Wood R. Modelling the risk of airborne infectious disease using exhaled air. *Journal of Theoretical Biology* 2015; **372**: 100-6.
95. Johnson GR, Morawska L. The mechanism of breath aerosol formation. *Journal of aerosol medicine and pulmonary drug delivery* 2009; **22**(3): 229-37.
96. Morawska L, Johnson G, Ristovski Z, et al. Size distribution and sites of origin of droplets expelled from the human respiratory tract during expiratory activities. *Journal of Aerosol Science* 2009; **40**(3): 256-69.
97. Roy CJ, Milton DK. Airborne transmission of communicable infection-the elusive pathway. 2004.
98. Edwards DA, Man JC, Brand P, et al. Inhaling to mitigate exhaled bioaerosols. *Proceedings of the National Academy of Sciences of the United States of America* 2004; **101**(50): 17383-8.
99. Wood R, Morrow C, Barry CE, 3rd, et al. Real-Time Investigation of Tuberculosis Transmission: Developing the Respiratory Aerosol Sampling Chamber (RASC). *PLoS One* 2016; **11**(1): e0146658.
100. Patterson B, Morrow C, Singh V, et al. Detection of *Mycobacterium tuberculosis* bacilli in bio-aerosols from untreated TB patients *Gates Open Research* 2018; **1**(11).
101. Issarow CM, Mulder N, Wood R. Environmental and social factors impacting on epidemic and endemic tuberculosis: a modelling analysis. *Royal Society Open Science* 2018; **5**(1): 170726.
102. Andrews JR, Morrow C, Walensky RP, Wood R. Integrating social contact and environmental data in evaluating tuberculosis transmission in a South African township. *J Infect Dis* 2014; **210**(4): 597-603.

103. Issarow C, Wood R, Mulder N. Seminal *Mycobacterium tuberculosis* in vivo transmission studies: Reanalysis using probabilistic modelling. *Mycobact Dis* 2016; **6**(217): 2161-1068.1000217.
104. Kleinstreuer C, Zhang Z, Kim CS. Combined inertial and gravitational deposition of microparticles in small model airways of a human respiratory system. *Journal of Aerosol Science* 2007; **38**(10): 1047-61.
105. Lenaerts A, Barry CE, Dartois V. Heterogeneity in tuberculosis pathology, microenvironments and therapeutic responses. *Immunological Reviews* 2015; **264**(1): 288-307.
106. Melsew YA, Gambhir M, Cheng AC, et al. The role of super-spreading events in *Mycobacterium tuberculosis* transmission: evidence from contact tracing. *BMC Infectious Diseases* 2019; **19**(1): 244.
107. Small PM, Hopewell PC, Singh SP, et al. The epidemiology of tuberculosis in San Francisco. A population-based study using conventional and molecular methods. *N Engl J Med* 1994; **330**(24): 1703-9.
108. Auld SC, Kasmar AG, Dowdy DW, et al. Research Roadmap for Tuberculosis Transmission Science: Where Do We Go From Here and How Will We Know When We're There? *The Journal of Infectious Diseases* 2017; **216**(suppl_6): S662-S8.
109. Shah NS, Auld SC, Brust JC, et al. Transmission of Extensively Drug-Resistant Tuberculosis in South Africa. *N Engl J Med* 2017; **376**(3): 243-53.
110. Middelkoop K, Mathema B, Myer L, et al. Transmission of tuberculosis in a South African community with a high prevalence of HIV infection. *J Infect Dis* 2015; **211**(1): 53-61.
111. Glynn JR, Guerra-Assunção JA, Houben RM, et al. Whole genome sequencing shows a low proportion of tuberculosis disease is attributable to known close contacts in rural Malawi. *PloS one* 2015; **10**(7): e0132840.
112. Mastorides SM, Oehler RL, Greene JN, Sinnott IVJT, Kranik M, Sandin RL. THe detection of airborne *Mycobacterium tuberculosis* using micropore membrane air sampling and polymerase chain reaction*. *Chest* 1999; **115**(1): 19-25.
113. Wan G-H, Lu S-C, Tsai Y-H. Polymerase chain reaction used for the detection of airborne Mycobacterium tuberculosis in health care settings. *American Journal of Infection Control* 2004; **32**(1): 17-22.
114. Williams CML, Cheah ESG, Malkin J, et al. Face Mask Sampling for the Detection of Mycobacterium tuberculosis in Expelled Aerosols. *PLOS ONE* 2014; **9**(8): e104921.
115. Tzonev S. Fundamentals of Counting Statistics in Digital PCR: I Just Measured Two Target Copies-What Does It Mean? *Methods Mol Biol* 2018; **1768**: 25-43.
116. Kolia-Diafouka P, Godreuil S, Bourdin A, et al. Optimized Lysis-Extraction Method Combined With IS6110-Amplification for Detection of Mycobacterium tuberculosis in Paucibacillary Sputum Specimens. *Frontiers in Microbiology* 2018; **9**(2224).
117. Lin PL, Ford CB, Coleman MT, et al. Sterilization of granulomas is common in active and latent tuberculosis despite within-host variability in bacterial killing. *Nat Med* 2014; **20**(1): 75-9.
118. Sabiiti W, Azam K, Farmer ECW, et al. Tuberculosis bacillary load, an early marker of disease severity: the utility of tuberculosis Molecular Bacterial Load Assay. *Thorax* 2020; **75**(7): 606-8.
119. Fennelly KP, Martyny JW, Fulton KE, Orme IM, Cave DM, Heifets LB. Cough-generated aerosols of *Mycobacterium tuberculosis*: a new method to study infectiousness. *Am J Respir Crit Care Med* 2004; **169**(5): 604-9.
120. Acuña-Villaorduña C, White LF, Fennelly KP, Jones-López EC. Tuberculosis transmission: sputum vs aerosols. *The Lancet Infectious Diseases* 2016; **16**(7): 770-1.
121. Fennelly KP, Jones-Lopez EC, Ayakaka I, et al. Variability of infectious aerosols produced during coughing by patients with pulmonary tuberculosis. *Am J Respir Crit Care Med* 2012; **186**(5): 450-7.
122. Andersen AA. NEW SAMPLER FOR THE COLLECTION, SIZING, AND ENUMERATION OF VIABLE AIRBORNE PARTICLES. *Journal of Bacteriology* 1958; **76**(5): 471-84.
123. Fennelly KP, Jones-López EC. Quantity and Quality of Inhaled Dose Predicts Immunopathology in Tuberculosis. *Frontiers in Immunology* 2015; **6**(313).
124. Hegland KW, Troche MS, Davenport PW. Cough expired volume and airflow rates during sequential induced cough. *Front Physiol* 2013; **4**: 167.
125. Patterson B, Morrow CD, Kohls D, Deignan C, Ginsburg S, Wood R. Mapping sites of high TB transmission risk: Integrating the shared air and social behaviour of TB cases and adolescents in a South African township. *Science of The Total Environment* 2017; **583**: 97-103.
126. Yam WC, Siu KH. Rapid identification of mycobacteria and rapid detection of drug resistance in Mycobacterium tuberculosis in cultured isolates and in respiratory specimens. *Methods Mol Biol* 2013; **943**: 171-99.

127. Jones-Lopez EC, Acuna-Villaorduna C, Ssebidandi M, et al. Cough Aerosols of *Mycobacterium tuberculosis* in the Prediction of Incident Tuberculosis Disease in Household Contacts. *Clin Infect Dis* 2016; **63**(1): 10-20.
128. Yeager Jr H, Lacy J, Smith LR, Lemaistre CA. Quantitative Studies of Mycobacterial Populations in Sputum and Saliva 1, 2. *American Review of Respiratory Disease* 1967; **95**(6): 998-1004.
129. Chengalroyen MD, Beukes GM, Gordhan BG, et al. Detection and Quantification of Differentially Culturable Tubercle Bacteria in Sputum from Patients with Tuberculosis. *American Journal of Respiratory and Critical Care Medicine* 2016.
130. Chao MC, Rubin EJ. Letting Sleeping dos Lie: Does Dormancy Play a Role in Tuberculosis? *Annual Review of Microbiology* 2010; **64**(1): 293-311.
131. Ramamurthy T, Ghosh A, Pazhani GP, Shinoda S. Current Perspectives on Viable but Non-Culturable (VBNC) Pathogenic Bacteria. *Frontiers in public health* 2014; **2**: 103-.
132. Turapov O, O'Connor BD, Sarybaeva AA, et al. Phenotypically Adapted *Mycobacterium tuberculosis* Populations from Sputum Are Tolerant to First-Line Drugs. *Antimicrobial Agents and Chemotherapy* 2016; **60**(4): 2476-83.
133. Nimmo C, Shaw LP, Doyle R, et al. Whole genome sequencing *Mycobacterium tuberculosis* directly from sputum identifies more genetic diversity than sequencing from culture. *BMC Genomics* 2019; **20**(1): 389.
134. Bowness R, Boeree MJ, Aarnoutse R, et al. The relationship between Mycobacterium tuberculosis MGIT time to positivity and cfu in sputum samples demonstrates changing bacterial phenotypes potentially reflecting the impact of chemotherapy on critical sub-populations. *Journal of Antimicrobial Chemotherapy* 2014; **70**(2): 448-55.
135. Kennedy JA, Baron VO, Hammond RJH, Sloan DJ, Gillespie SH. Centrifugation and decontamination procedures selectively impair recovery of important populations in Mycobacterium smegmatis. *Tuberculosis* 2018; **112**: 79-82.
136. In this issue. *Nature Reviews Microbiology* 2007; **5**(9): 653-.
137. Ruska E. The development of the electron microscope and of electron microscopy. *Reviews of Modern Physics* 1987; **59**(3): 627-38.
138. Betzig E, Patterson GH, Sougrat R, et al. Imaging intracellular fluorescent proteins at nanometer resolution. *Science* 2006; **313**(5793): 1642-5.
139. Zernike F. How I Discovered Phase Contrast. *Science* 1955; **121**(3141): 345-9.
140. Pluta M. Phase contrast microscopy. *Advanced light microscopy* 1993; **2**.
141. Vicar T, Balvan J, Jaros J, et al. Cell segmentation methods for label-free contrast microscopy: review and comprehensive comparison. *BMC Bioinformatics* 2019; **20**(1): 360.
142. Smith AC, Hussey MA. Gram stain protocols. *American Society for Microbiology* 2005; **1**: 14.
143. Coico R. Gram Staining. *Current Protocols in Microbiology* 2006; **00**(1): A.3C.1-A.3C.2.
144. Jackson M. The mycobacterial cell envelope-lipids. *Cold Spring Harbor perspectives in medicine* 2014; **4**(10): a021105.
145. Fu LM, Fu-Liu CS. Is Mycobacterium tuberculosis a closer relative to Gram-positive or Gram-negative bacterial pathogens? *Tuberculosis (Edinb)* 2002; **82**(2-3): 85-90.
146. Bayot ML, Mirza TM, Sharma S. Acid Fast Bacteria. 2019.
147. Reynolds J, Moyes RB, Breakwell DP. Differential Staining of Bacteria: Acid Fast Stain. *Current Protocols in Microbiology* 2009; **15**(1): A.3H.1-A.3H.5.
148. Kivihya-Ndugga LEA, van Cleeff MRA, Githui WA, et al. A comprehensive comparison of Ziehl-Neelsen and fluorescence microscopy for the diagnosis of tuberculosis in a resource-poor urban setting. *The International Journal of Tuberculosis and Lung Disease* 2003; **7**(12): 1163-71.
149. Nyka W. Studies on *Mycobacterium tuberculosis* in lesions of the human lung: a new method of staining tubercle bacilli in tissue sections. *American Review of Respiratory Disease* 1963; **88**(5): 670-9.
150. Garton NJ, Waddell SJ, Sherratt AL, et al. Cytological and Transcript Analyses Reveal Fat and Lazy Persister-Like Bacilli in Tuberculous Sputum. *PLOS Medicine* 2008; **5**(4): e75.
151. Kamariza M, Shieh P, Ealand CS, et al. Rapid detection of *Mycobacterium tuberculosis* in sputum with a solvatochromic trehalose probe. *Science Translational Medicine* 2018; **10**(430).
152. Hooja S, Pal N, Malhotra B, Goyal S, Kumar V, Vyas L. Comparison of Ziehl Neelsen & Auramine O staining methods on direct and concentrated smears in clinical specimens. *Indian J Tuberc* 2011; **58**(2): 72-6.

153. Koch ML, Cote RA. Comparison of Fluorescence Microscopy with Ziehl-Neelsen Stain for Demonstration of Acid-fast Bacilli in Smear Preparations and Tissue Sections. *American Review of Respiratory Disease* 1965; **91**(2): 283-4.
154. Wanger A, Chavez V, Huang RSP, Wahed A, Actor JK, Dasgupta A. Chapter 5 - Biochemical Tests and Staining Techniques for Microbial Identification. In: Wanger A, Chavez V, Huang RSP, Wahed A, Actor JK, Dasgupta A, eds. Microbiology and Molecular Diagnosis in Pathology: Elsevier; 2017: 61-73.
155. Sarathy JP, Via LE, Weiner D, et al. Extreme Drug Tolerance of *Mycobacterium tuberculosis* in Caseum. *Antimicrobial Agents and Chemotherapy* 2018; **62**(2): e02266-17.
156. Eum S-Y, Kong J-H, Hong M-S, et al. Neutrophils Are the Predominant Infected Phagocytic Cells in the Airways of Patients With Active Pulmonary TB. *Chest* 2010; **137**(1): 122-8.
157. Wong C, Ha NP, Pawlowski ME, Graviss EA, Tkaczyk TS. Differentiating between live and dead Mycobacterium smegmatis using autofluorescence. *Tuberculosis (Edinburgh, Scotland)* 2016; **101S**: S119-S23.
158. Hobby GL, Holman AP, Iseman MD, Jones JM. Enumeration of Tubercle Bacilli in Sputum of Patients with Pulmonary Tuberculosis. *Antimicrobial Agents and Chemotherapy* 1973; **4**(2): 94-104.
159. Backus KM, Boshoff HI, Barry CS, et al. Uptake of unnatural trehalose analogs as a reporter for Mycobacterium tuberculosis. *Nat Chem Biol* 2011; **7**(4): 228-35.
160. Loving G, Imperiali B. A Versatile Amino Acid Analogue of the Solvatochromic Fluorophore 4-N,N-Dimethylamino-1,8-naphthalimide: A Powerful Tool for the Study of Dynamic Protein Interactions. *Journal of the American Chemical Society* 2008; **130**(41): 13630-8.
161. Hodges HL, Brown RA, Crooks JA, Weibel DB, Kiessling LL. Imaging mycobacterial growth and division with a fluorogenic probe. *Proceedings of the National Academy of Sciences* 2018.
162. Cheng Y, Xie J, Lee KH, et al. Rapid and specific labeling of single live *Mycobacterium tuberculosis* with a dual-targeting fluorogenic probe. *Sci Transl Med* 2018; **10**(454).
163. Chauhan A, Lofton H, Maloney E, et al. Interference of *Mycobacterium tuberculosis* cell division by Rv2719c, a cell wall hydrolase. *Mol Microbiol* 2006; **62**.
164. de Wet TJ, Winkler KR, Mhlanga M, Mizrahi V, Warner DF. Arrayed CRISPRi and quantitative imaging describe the morphotypic landscape of essential mycobacterial genes. *eLife* 2020; **9**: e60083.
165. Smith TC, Pullen KM, Olson MC, et al. Morphological profiling of tubercle bacilli identifies drug pathways of action. *Proceedings of the National Academy of Sciences* 2020; **117**(31): 18744-53.
166. Wu J, Liu W, He L, et al. Sputum Microbiota Associated with New, Recurrent and Treatment Failure Tuberculosis. *PLOS ONE* 2013; **8**(12): e83445.
167. Alibi S, Ferjani A, Boukadida J, et al. Occurrence of *Corynebacterium striatum* as an emerging antibiotic-resistant nosocomial pathogen in a Tunisian hospital. *Scientific reports* 2017; **7**(1): 9704-.
168. Rodriguez-Rivera FP, Zhou X, Theriot JA, Bertozzi CR. Acute Modulation of Mycobacterial Cell Envelope Biogenesis by Front-Line Tuberculosis Drugs. *Angewandte Chemie International Edition* 2018; **57**(19): 5267-72.
169. Pohane AA, Carr CR, Garhyan J, Swarts BM, Siegrist MS, Hatfull GF. Trehalose Recycling Promotes Energy-Efficient Biosynthesis of the Mycobacterial Cell Envelope. *mBio* 2021; **12**(1): e02801-20.
170. Williams CM, Abdulwhhab M, Birring SS, et al. Exhaled *Mycobacterium tuberculosis* output and detection of subclinical disease by face-mask sampling: prospective observational studies. *The Lancet Infectious Diseases* 2020; **20**(5): 607-17.
171. Jones-López EC, Namugga O, Mumbowa F, et al. Cough Aerosols of *Mycobacterium tuberculosis* Predict New Infection. A Household Contact Study. *American Journal of Respiratory and Critical Care Medicine* 2013; **187**(9): 1007-15.
172. Theron G, Limberis J, Venter R, et al. Bacterial and host determinants of cough aerosol culture positivity in patients with drug-resistant versus drug-susceptible tuberculosis. *Nature Medicine* 2020; **26**(9): 1435-43.
173. Mahamed D, Boulle M, Ganga Y, et al. Intracellular growth of *Mycobacterium tuberculosis* after macrophage cell death leads to serial killing of host cells. *eLife* 2017; **6**: e22028.
174. Michaud JM, Thompson LR, Kaul D, et al. Taxon-specific aerosolization of bacteria and viruses in an experimental ocean-atmosphere mesocosm. *Nat Commun* 2018; **9**(1): 2017.
175. Rodriguez-Rivera FP, Zhou X, Theriot JA, Bertozzi CR. Visualization of mycobacterial membrane dynamics in live cells. *Journal of the American Chemical Society* 2017; **139**(9): 3488-95.
176. Patterson B, Dinkele R, Gessner S, et al. Sensitivity optimisation of tuberculosis bioaerosol sampling. *PLOS ONE* 2020; **15**(9): e0238193.

177. Patterson B, Koch A, Gessner S, et al. Bioaerosol sampling of patients with suspected pulmonary tuberculosis: a study protocol. *BMC infectious diseases* 2020; **20**(1): 587-.
178. Barr DA, Schutz C, Balfour A, et al. Serial measurement of *M. tuberculosis* in blood from critically-ill patients with HIV-associated tuberculosis. *eBioMedicine* 2022; **78**.
179. Goig GA, Cancino-Muñoz I, Torres-Puente M, et al. Whole-genome sequencing of *Mycobacterium tuberculosis* directly from clinical samples for high-resolution genomic epidemiology and drug resistance surveillance: an observational study. *The Lancet Microbe* 2020; **1**(4): e175-e83.
180. Mtafya B, Sabiiti W, Sabi I, et al. Molecular Bacterial Load Assay Concurs with Culture on NaOH-Induced Loss of Mycobacterium tuberculosis Viability. *J Clin Microbiol* 2019; **57**(7).
181. Justice SS, Hunstad DA, Cegelski L, Hultgren SJ. Morphological plasticity as a bacterial survival strategy. *Nat Rev Micro* 2008; **6**(2): 162-8.
182. Priestman M, Thomas P, Robertson BD, Shahrezaei V. Mycobacteria Modify Their Cell Size Control under Sub-Optimal Carbon Sources. *Frontiers in Cell and Developmental Biology* 2017; **5**.
183. Ioerger TR, Feng Y, Ganesula K, et al. Variation among genome sequences of H37Rv strains of Mycobacterium tuberculosis from multiple laboratories. *J Bacteriol* 2010; **192**(14): 3645-53.
184. Ducret A, Quardokus EM, Brun YV. MicrobeJ, a tool for high throughput bacterial cell detection and quantitative analysis. *Nature Microbiology* 2016; **1**(7): 16077.
185. RCoreTeam. R: A language and environment for statistical computing. R Foundation for Statistical Computing, Vienna, Austria.; 2020.
186. Chung KF, Pavord ID. Prevalence, pathogenesis, and causes of chronic cough. *Lancet* 2008; **371**(9621): 1364-74.
187. Canning BJ, Chang AB, Bolser DC, et al. Anatomy and Neurophysiology of Cough: CHEST Guideline and Expert Panel Report. *Chest* 2014; **146**(6): 1633-48.
188. Tostmann A, Kik SV, Kalisvaart NA, et al. Tuberculosis Transmission by Patients with Smear-Negative Pulmonary Tuberculosis in a Large Cohort in The Netherlands. *Clinical Infectious Diseases* 2008; **47**(9): 1135-42.
189. Behr MA, Warren SA, Salamon H, et al. Transmission of Mycobacterium tuberculosis from patients smear-negative for acid-fast bacilli. *The Lancet* 1999; **353**(9151): 444-9.
190. Delogu G, Sali M, Fadda G. The biology of mycobacterium tuberculosis infection. *Mediterr J Hematol Infect Dis* 2013; **5**(1): e2013070.
191. Patterson B, Wood R. Is cough really necessary for TB transmission? *Tuberculosis* 2019; **117**: 31-5.
192. Wurie FB, Lawn SD, Booth H, Sonnenberg P, Hayward AC. Bio-aerosol production by patients with tuberculosis during normal tidal breathing: implications for transmission risk: a cohort study. *The Lancet* 2015; **386**: S81.
193. Dinkele R, Gessner S, McKerry A, et al. Capture and visualization of live *Mycobacterium tuberculosis* bacilli from tuberculosis patient bioaerosols. *PLOS Pathogens* 2021; **17**(2): e1009262.
194. Patterson B, Bryden W, Call C, et al. Cough-independent production of viable Mycobacterium tuberculosis in bioaerosol. *Tuberculosis* 2021; **126**: 102038.
195. Borchers HW. pracma: Practical Numerical Math Functions. R package version 2.3.3; 2021.
196. Douglas B, Martin M, Ben B, Steve W. Fitting Linear Mixed-Effects Models Using lme4. *Journal of Statistical Software* 2015; **67**(1): 1-48.
197. RStudioTeam. RStudio: Integrated Development Environment for R. RStudio, PBC, Boston, MA; 2020.
198. Venables WN, Ripley BD. Modern Applied Statistics with S. New York; 2002.
199. Ruhl CR, Pasko BL, Khan HS, et al. Mycobacterium tuberculosis Sulfolipid-1 Activates Nociceptive Neurons and Induces Cough. *Cell* 2020; **181**(2): 293-305.e11.
200. Gralton J, Tovey E, McLaws M-L, Rawlinson WD. The role of particle size in aerosolised pathogen transmission: A review. *Journal of Infection* 2011; **62**(1): 1-13.
201. Pai M, Behr MA, Dowdy D, et al. Tuberculosis. *Nature Reviews Disease Primers* 2016; **2**: 16076.
202. Haslbeck K, Schwarz K, Hohlfeld JM, Seume JR, Koch W. Submicron droplet formation in the human lung. *Journal of aerosol science* 2010; **41**(5): 429-38.
203. Ioerger TR, Koo S, No E-G, et al. Genome Analysis of Multi- and Extensively-Drug-Resistant Tuberculosis from KwaZulu-Natal, South Africa. *PLOS ONE* 2009; **4**(11): e7778.